2014-03-13

Enhanced Acquisition Techniques for GPS L1C Receivers

Kelly Charles Seals
Worcester Polytechnic Institute

ENHANCED ACQUISITION TECHNIQUES FOR GPS L1C RECEIVERS

A Dissertation
Presented to
The Academic Faculty

By

Kelly Charles Seals

In Partial Fulfillment
of the Requirements for the Degree
Doctor of Philosophy
in
Electrical and Computer Engineering

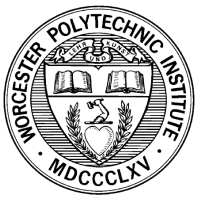

Department of Electrical and Computer Engineering
Worcester Polytechnic Institute
February 2014

ENHANCED ACQUISITION TECHNIQUES

FOR GPS L1C RECEIVERS

Approved by:

Dr. William R. Michalson, Advisor
Professor
Department of Electrical & Computer Engineering
Worcester Polytechnic Institute

Dr. Alexander M. Wyglinski
Associate Professor
Department of Electrical & Computer Engineering
Worcester Polytechnic Institute

Dr. Peter F. Swaszek
Professor
Department of Electrical, Computer & Biomedical Engineering
University of Rhode Island

Date Approved: 13 February 2014

To Nova, Anderson & Dashiell

ABSTRACT

A new, open-access Global Positioning System (GPS) signal, known as L1C, is the most recent of several modernized Global Positioning System (GPS) signals. The first launch of a GPS satellite with this signal is expected to occur within a few years. One of the interesting features of modern Global Navigation Satellite System (GNSS) signals, including GPS L1C, is the presence of data and pilot components. The pilot component is a carrier with a deterministic overlay code but no data symbols; whereas, the data component carries the navigation data symbols used in the receiver processing. A unique aspect of GPS L1C is the asymmetrical power split between the two components, 75% of the power is used for the pilot and the remaining power, or 25%, for the data. In addition, the pilot and the data components are transmitted in phase with orthogonal spreading codes.

Unassisted acquisition of GNSS spread spectrum signals requires a two-dimensional search for the spreading code delay and Doppler frequency. For modern two-component GNSS signals, conventional GNSS acquisition schemes may be used on either component, correlating the received signal with either the pilot or the data spreading code. One obvious disadvantage of this approach is the wasting of power; hence, new techniques for combining, or joint acquisition of the pilot and the data components, have been proposed.

In this dissertation, acquisition of GPS L1C is analyzed and receiver techniques are proposed for improving acquisition sensitivity. Optimal detectors for GPS L1C acquisition in additive white Gaussian noise are derived, based on various scenarios for a GPS receiver. Monte Carlo simulations are used to determine the performance of these optimal detectors, based on detection and false alarm probabilities. After investigating the optimal detectors for GPS L1C acquisition, various sub-optimal detectors that are more efficient to implement are thoroughly investigated and compared. Finally, schemes for joint acquisition of L1C and the legacy GPS C/A code signal are proposed and analyzed.

ACKNOWLEDGMENTS

I greatly appreciate the support of Dr. William Michalson. He welcomed me aboard as a part-time PhD student despite the fact I had a full-time job as an active duty member of the United States Coast Guard. At the time I wasn't even sure that I would be stationed in the area for very long. I am thankful for his support and guidance throughout this voyage.

I would like to thank Dr. Alex Wyglinski for providing valuable feedback in the research process and challenging me. I appreciate his constructive advice and enthusiastic teaching.

Throughout this process I have been mentored by two outstanding professors, Dr. Richard Hartnett and Dr. Peter Swaszek. Their advocacy on my behalf and personal guidance on a great number of issues including academia and this research has been invaluable.

The Institute of Navigation (ION) has provided exceptional networking and learning opportunities through conferences and publications. In particular, I would like to acknowledge the many comments and suggestions regarding my research by Dr. John Betz and Dr. Thomas Stansell, two experts in the GNSS field.

I extend my thanks and sincere appreciation to Colleen Sweeney, the Electrical and Computer Engineering graduate administrative assistant at WPI, and to Lorraine Eichler, from the administrative staff in the Coast Guard Academy Department of Engineering. I appreciate their diligence and professionalism.

I appreciate the support provided by Lucia Maziar, the director of the Coast Guard Academy Library as well as Dr. Kathleen Jernquist, Linda Burrows, and Kathleen O'Reilly-Wild from the Academy's Cadet Writing and Reading Center. Thank you to Dr. Andrea Ackerman for improving the writing in this dissertation. I also appreciate the suggestions and technical advice provided by Dr. Ali Reza.

I would like to acknowledge the support of the current and former Electrical Engineering program chairs at the United States Coast Guard Academy: Commander Joseph Staier,

Commander Robert Oatman and Dr. Keith Gross. Their support and mentorship have been instrumental in getting me to this point. Thanks to Dean Kurt Colella, Captain Richard Sanders, Captain Janet Stevens, and Captain Vincent Wilczynski for their vote of confidence in my selection to the permanent military faculty at the Coast Guard Academy. I am looking forward to getting back in the classroom alongside the talented cadets who make the Academy such an amazing place. I am fortunate to work with many great colleagues and am thankful for their support and friendship.

My family has provided the most encouragement. Thank you to my parents for ensuring I had the opportunity to be where I am today. I am grateful for the amazing love and encouragement from my wife, Nova, and the endless joy provided by my sons, Anderson and Dashiell.

TABLE OF CONTENTS

ABSTRACT iv

ACKNOWLEDGMENTS v

LIST OF FIGURES x

LIST OF TABLES xviii

LIST OF ABBREVIATIONS AND SYMBOLS xix

CHAPTER 1 INTRODUCTION 1
- 1.1 How GNSS Works 2
- 1.2 History of GNSS 4
- 1.3 GPS Modernization 6
- 1.4 Overview of GPS L1C 8
- 1.5 Overview of GNSS Acquisition 10
- 1.6 Motivation and Objectives 11
- 1.7 Contributions 11
  - 1.7.1 Publications 13
- 1.8 Outline 13

CHAPTER 2 THE GPS L1C SIGNAL AND GNSS ACQUISITION 15
- 2.1 Introduction 15
- 2.2 GNSS Signal Structure and Characteristics 15
  - 2.2.1 GNSS Baseband Signal 15
  - 2.2.2 GNSS Bandpass Signal 18
  - 2.2.3 The Legacy GPS L1 C/A Code Signal 19
- 2.3 The GPS L1C Signal 20
  - 2.3.1 Baseband Signal Model for L1C 20
  - 2.3.2 L1C Auto-Correlation Function 23
  - 2.3.3 L1C Power Spectral Density 25
  - 2.3.4 Transmitted Signal Model for L1C 28
  - 2.3.5 L1C Received Signal Model and Output of Correlators 31
- 2.4 Fundamentals of GNSS Signal Acquisition 34
  - 2.4.1 Frequency and Spreading Code Delay Search Space 34
  - 2.4.2 Serial Search 37
  - 2.4.3 Parallel Frequency Space Search 38
  - 2.4.4 Parallel Code Phase Search 38
  - 2.4.5 Acquisition Performance 39
- 2.5 Acquisition of Modern GNSS Signals 41
  - 2.5.1 Sideband Processing 41
  - 2.5.2 Acquisition of Two-Component Signals 42

2.6 Chapter Summary 48

CHAPTER 3 OPTIMAL DETECTORS FOR GPS L1C ACQUISITION . . . 50
3.1 Introduction 50
3.2 Optimal Detection Framework 50
3.3 Unknown Pilot Overlay Code Phase and Data Bits 52
3.3.1 Low SNR Approximation of Optimal Detector 52
3.4 Known Pilot Overlay Code Phase and Unknown Data Bits 55
3.4.1 Low SNR Approximation of Optimal Detector with Known Pilot Overlay Code Phase 55
3.5 Known Pilot Overlay Code Phase and Known Data Bits 57
3.6 Chapter Summary 59

CHAPTER 4 SUB-OPTIMAL DETECTORS FOR GPS L1C ACQUISITION 62
4.1 Introduction 62
4.2 Noncoherent Integration for Signals With Unequal Power 62
4.3 Coherent Channel Combining With Unequal Power Compensation 64
4.4 Semi-Coherent Integration With Unequal Power Compensation 67
4.5 Known Pilot Overlay Code Phase 75
4.5.1 Differentially-Coherent Integration of the Pilot Component 75
4.5.2 Coherent Integration using Relative Pilot/Data Sign Estimation . . 76
4.6 Chapter Summary 80

CHAPTER 5 JOINT ACQUISITION OF GPS C/A AND L1C SIGNALS . . . 81
5.1 Introduction 81
5.2 Received Power and Power Split Parameters 81
5.3 Signal Model for Composite GPS L1C and C/A Signal 83
5.4 Optimal Detector for Acquisition With GPS C/A and L1C 86
5.5 Sub-Optimal Detectors for Joint C/A and L1C Acquisition 88
5.5.1 Noncoherent Combining Detector 88
5.5.2 Coherent Combining 90
5.5.3 Semi-Coherent Integration 94
5.6 Joint L1C Pilot and C/A Acquisition 96
5.6.1 Optimal 96
5.6.2 Noncoherent Combining 99
5.6.3 Coherent Combining 100
5.6.4 Semi-Coherent Integration 102
5.7 Correct C/A Code Phase and Incorrect L1C Code Phase 105
5.8 Chapter Summary 106

CHAPTER 6 CONCLUSIONS AND FUTURE WORK 110
6.1 Optimal Detectors 110
6.2 Sub-Optimal Detectors 111
6.3 Joint Acquisition of L1C and L1 C/A 112
6.4 Recommendations for Future Work 113

APPENDIX A ADDITIONAL INFORMATION ON THE POWER SPECTRA OF GPS L1C 114

APPENDIX B AMBIGUITY FUNCTION AND CORRELATOR OUTPUTS . 115

APPENDIX C DERIVATION OF OPTIMAL DETECTORS FOR L1C ACQUISITION 117
C.1 Unknown Pilot Overlay Code Phase and Data Bits 118
C.2 Known Pilot Overlay Code Phase and Unknown Data Bits 120
C.3 Known Pilot Overlay Code Phase and Known Data Bits 122

APPENDIX D DERIVATION OF OPTIMAL DETECTOR FOR JOINT L1C AND C/A ACQUISITION 123

APPENDIX E JOINT ACQUISITION DETECTION PROBABILITIES REFERENCED TO C/N_O OF L1 C/A CODE SIGNAL 127

APPENDIX F JOINT ACQUISITION DETECTION PROBABILITIES REFERENCED TO C/N_O OF COMPOSITE SIGNAL 136

REFERENCES 145

LIST OF FIGURES

Figure 2.1 BOC(1,1) and C/A code auto-correlation function. 24

Figure 2.2 BOC(6,1) auto-correlation function. 25

Figure 2.3 Power spectral density of the L1C data component. 27

Figure 2.4 Power spectral density of the L1C pilot component, BOC(1,1) spreading symbol, and BOC(6,1) spreading symbol. 29

Figure 2.5 Power spectral density of the L1C signal, L1C data component, and L1C pilot component. 29

Figure 2.6 Power spectral density of L1C and L1 C/A code signals. 30

Figure 2.7 Acquisition search space. 35

Figure 2.8 Block diagram of the serial search algorithm for GNSS acquisition. . . 37

Figure 2.9 Block diagram of the parallel frequency space search algorithm for GNSS acquisition. 38

Figure 2.10 Block diagram of the parallel code phase search algorithm for GNSS acquisition. 39

Figure 2.11 Block diagram of dual-sideband processing for GNSS acquisition. . . . 42

Figure 3.1 Probability of detection for the L1C optimal detector using one spreading code period. 53

Figure 3.2 Probability of detection for the L1C optimal detector using three spreading code periods. 54

Figure 3.3 Probability of detection for the L1C optimal detector using five spreading code periods. 54

Figure 3.4 Probability of detection for the L1C optimal detector with known pilot overlay code phase using one spreading code period. 56

Figure 3.5 Probability of detection for the L1C optimal detector with known pilot overlay code phase using three spreading code periods. 56

Figure 3.6 Probability of detection for the L1C optimal detector with known pilot overlay code phase using five spreading code periods. 57

Figure 3.7 Probability of detection for the low SNR approximation to the L1C optimal detector with known pilot overlay code phase using one spreading code period. 58

Figure 3.8 Probability of detection for the low SNR approximation to the L1C optimal detector with known pilot overlay code phase using three spreading code periods. 58

Figure 3.9 Probability of detection for the low SNR approximation to the L1C optimal detector with known pilot overlay code phase using five spreading code periods. 59

Figure 3.10 Probability of detection for the optimal detector with knowledge of pilot overlay code phase and navigation data using one spreading code period. 60

Figure 3.11 Probability of detection for the optimal detector with knowledge of pilot overlay code phase and navigation data using three spreading code periods. 60

Figure 4.1 Performance of single channel detector (using pilot component) compared to noncoherent combining detector with simulated and analytical results. 65

Figure 4.2 Performance of coherent combining detector compared to coherent combining with weights for unequal power detector. 67

Figure 4.3 Performance of the optimal detector compared to the other channel combining detectors. 68

Figure 4.4 Simulation results that show the detection probability of the noncoherent combining detector using the pilot only, the noncoherent combining detector using the pilot and the data components, and the semi-coherent detector over two (K=2) primary spreading code periods. 70

Figure 4.5 Simulation results that show the detection probability of the noncoherent combining detector using the pilot only, the noncoherent combining detector using the pilot and the data components, and the semi-coherent detector over twenty-five (K=25) primary spreading code periods. . . . 70

Figure 4.6 Simulation results that show the detection probability of semi-coherent integration with and without compensating for the data/pilot power split over two (K=2) primary spreading code periods. 71

Figure 4.7 Simulation results that show the detection probability of various GPS L1C acquisition schemes over one (K=1) primary spreading code period. 72

Figure 4.8 Simulation results that show the detection probability of various GPS L1C acquisition schemes over two (K=2) primary spreading code periods. 72

Figure 4.9 Simulation results that show the detection probability of various GPS L1C acquisition schemes over five (K=5) primary spreading code periods. 73

Figure 4.10 Simulation results that show the detection probability of semi-coherent integration with unequal power compensation and noncoherent combining over 10 primary spreading code periods (K=10). 74

Figure 4.11 Simulation results that show the detection probability of semi-coherent integration with unequal power compensation and noncoherent combining over 20 primary spreading code periods (K=20). 74

Figure 4.12 Simulation results that show the detection probability of the coherent combining detector using the pilot only, the differentially-coherent detector using the real part, the differentially-coherent detector using the magnitude squared and the noncoherent combining detectors for pilot plus data and pilot-only over eight (K=8) primary spreading code periods. 76

Figure 4.13 Simulation results that show the detection probability of the coherent combining detector using the pilot only, the differentially-coherent detector using the real part, the differentially-coherent detector using the magnitude squared and the noncoherent combining detectors for pilot plus data and pilot-only over twenty-five (K=25) primary spreading code periods. 77

Figure 4.14 Simulation results that show the detection probability of coherent integration using relative pilot/data bit estimation and known pilot overlay code phase, semi-coherent integration, and standard coherent integration over two (K=2) primary spreading code periods. 78

Figure 4.15 Simulation results that show the detection probability of coherent integration using relative pilot/data bit estimation and known pilot overlay code phase, semi-coherent integration and standard coherent integration over three (K=3) primary spreading code periods. 79

Figure 4.16 Simulation results that show the detection probability of coherent integration using relative pilot/data bit estimation and known pilot overlay code phase, semi-coherent integration and standard coherent integration over eight (K=8) primary spreading code periods. 79

Figure 5.1 Detection probability of optimal joint L1C and C/A detector compared to optimal L1C detector for acquisition over one L1C spreading code period referenced to L1C signal power. 87

Figure 5.2 Detection probability of optimal joint L1C and C/A detector compared to optimal L1C detector for acquisition over three L1C spreading code periods referenced to L1C signal power. 87

Figure 5.3 Block diagram of noncoherent combining detector for joint acquisition of GPS L1C and C/A. 88

Figure 5.4 Detection probability of noncoherent combining joint L1C and C/A detector for acquisition over one L1C spreading code period referenced to L1C signal power. 89

Figure 5.5 Detection probability of noncoherent combining joint L1C and C/A detector for acquisition over three L1C spreading code periods referenced to L1C signal power. 90

Figure 5.6 Detection probability of coherent combining joint L1C and C/A detector for acquisition over one L1C spreading code period referenced to L1C signal power. 94

Figure 5.7 Detection probability of semi-coherent joint L1C and C/A detector for acquisition over three L1C spreading code periods referenced to L1C signal power. 95

Figure 5.8 Detection probability of semi-coherent joint L1C and C/A detector for acquisition with an extended integration time over twenty-five spreading code periods referenced to L1C signal power. 96

Figure 5.9 Detection probability of optimal joint L1C pilot and C/A detector for acquisition over one L1C spreading code period referenced to L1C signal power. 98

Figure 5.10 Detection probability of optimal joint L1C pilot and C/A detector for acquisition over three L1C spreading code periods referenced to L1C signal power. 98

Figure 5.11 Block diagram of noncoherent combining detector for joint acquisition of GPS L1C Pilot and L1 C/A. 99

Figure 5.12 Detection probability of noncoherent combining joint L1C pilot and C/A detector for acquisition over one L1C spreading code period referenced to L1C signal power. 100

Figure 5.13 Detection probability of noncoherent combining joint L1C pilot and C/A detector for acquisition over three L1C spreading code periods referenced to L1C signal power. 101

Figure 5.14 Detection probability of coherent combining joint L1C pilot and C/A detector for acquisition over one L1C spreading code period referenced to L1C signal power. 103

Figure 5.15 Detection probability of semi-coherent combining joint L1C pilot and C/A detector for acquisition over three L1C spreading code periods referenced to L1C signal power. 104

Figure 5.16 Detection probability of semi-coherent combining joint L1C pilot and C/A detector for acquisition over extended integration time of twenty-five spreading code period referenced to L1C signal power. 104

Figure 5.17 Detection probability of joint L1C and C/A detectors with incorrect L1C code phase estimate but correct C/A code phase estimate for acquisition over one L1C spreading code period referenced to L1C signal power. . 106

Figure 5.18 Detection probability of joint L1C and C/A detectors with incorrect L1C code phase estimate but correct C/A code phase estimate for acquisition over three L1C spreading code periods referenced to L1C signal power. 107

Figure 5.19 Detection probability of joint L1C and C/A detectors with incorrect L1C code phase estimate but correct C/A code phase estimate for acquisition over extended integration time of twenty-five L1C spreading code periods referenced to L1C signal power. 107

Figure 5.20 Detection probability of joint L1C pilot and C/A detectors with incorrect L1C code phase estimate but correct C/A code phase estimate for acquisition over one L1C spreading code period referenced to L1C signal power. 108

Figure 5.21 Detection probability of joint L1C pilot and C/A detectors with incorrect L1C code phase estimate but correct C/A code phase estimate for acquisition over three L1C spreading code periods referenced to L1C signal power. 108

Figure 5.22 Detection probability of joint L1C pilot and C/A detectors with incorrect L1C code phase estimate but correct C/A code phase estimate for acquisition over extended integration time of twenty-five L1C spreading code periods referenced to L1C signal power. 109

Figure E.1 Detection probability of optimal joint L1C and C/A detector compared to optimal L1C detector for acquisition over one L1C spreading code period referenced to L1 C/A signal power. 127

Figure E.2 Detection probability of optimal joint L1C and C/A detector compared to optimal L1C detector for acquisition over three L1C spreading code periods referenced to L1 C/A signal power. 128

Figure E.3 Detection probability of noncoherent combining joint L1C and C/A detector for acquisition over one L1C spreading code period referenced to L1 C/A signal power. 128

Figure E.4 Detection probability of noncoherent combining joint L1C and C/A detector for acquisition over three L1C spreading code periods referenced to L1 C/A signal power. 129

Figure E.5 Detection probability of coherent combining joint L1C and C/A detector for acquisition over one L1C spreading code period referenced to L1 C/A signal power. 129

Figure E.6 Detection probability of semi-coherent joint L1C and C/A detector for acquisition over three L1C spreading code periods referenced to L1 C/A signal power. 130

Figure E.7 Detection probability of optimal joint L1C pilot and C/A detector for acquisition over one L1C spreading code period referenced to L1 C/A signal power. 130

Figure E.8 Detection probability of optimal joint L1C pilot and C/A detector for acquisition over three L1C spreading code periods referenced to L1 C/A signal power. 131

Figure E.9 Detection probability of noncoherent combining joint L1C pilot and C/A detector for acquisition over one L1C spreading code period referenced to L1 C/A signal power. 131

Figure E.10 Detection probability of noncoherent combining joint L1C pilot and C/A detector for acquisition over three L1C spreading code periods referenced to L1 C/A signal power. 132

Figure E.11 Detection probability of coherent combining joint L1C pilot and C/A detector for acquisition over one L1C spreading code period referenced to L1 C/A signal power. 132

Figure E.12 Detection probability of semi-coherent combining joint L1C pilot and C/A detector for acquisition over three L1C spreading code periods referenced to L1 C/A signal power. 133

Figure E.13 Detection probability of joint L1C and C/A detectors with incorrect L1C code phase estimate but correct C/A code phase estimate for acquisition over one L1C spreading code period referenced to L1 C/A signal power. 133

Figure E.14 Detection probability of joint L1C and C/A detectors with incorrect L1C code phase estimate but correct C/A code phase estimate for acquisition over three L1C spreading code periods referenced to L1 C/A signal power. 134

Figure E.15 Detection probability of joint L1C pilot and C/A detectors with incorrect L1C code phase estimate but correct C/A code phase estimate for acquisition over one L1C spreading code period referenced to L1 C/A signal power. 134

Figure E.16 Detection probability of joint L1C pilot and C/A detectors with incorrect L1C code phase estimate but correct C/A code phase estimate for acquisition over three L1C spreading code periods referenced to L1 C/A signal power. 135

Figure F.1 Detection probability of optimal joint L1C and C/A detector compared to optimal L1C detector for acquisition over one L1C spreading code period referenced to the L1C and C/A composite signal power. 136

Figure F.2 Detection probability of optimal joint L1C and C/A detector compared to optimal L1C detector for acquisition over three L1C spreading code periods referenced to the L1C and C/A composite signal power. 137

Figure F.3 Detection probability of noncoherent combining joint L1C and C/A detector for acquisition over one L1C spreading code period referenced to the L1C and C/A composite signal power. 137

Figure F.4 Detection probability of noncoherent combining joint L1C and C/A detector for acquisition over three L1C spreading code periods referenced to the L1C and C/A composite signal power. 138

Figure F.5 Detection probability of coherent combining joint L1C and C/A detector for acquisition over one L1C spreading code period referenced to the L1C and C/A composite signal power. 138

Figure F.6 Detection probability of semi-coherent joint L1C and C/A detector for acquisition over three L1C spreading code periods referenced to the L1C and C/A composite signal power. 139

Figure F.7 Detection probability of optimal joint L1C pilot and C/A detector for acquisition over one L1C spreading code period referenced to the L1C and C/A composite signal power. 139

Figure F.8 Detection probability of optimal joint L1C pilot and C/A detector for acquisition over three L1C spreading code periods referenced to the L1C and C/A composite signal power. 140

Figure F.9 Detection probability of noncoherent combining joint L1C pilot and C/A detector for acquisition over one L1C spreading code period referenced to the L1C and C/A composite signal power. 140

Figure F.10 Detection probability of noncoherent combining joint L1C pilot and C/A detector for acquisition over three L1C spreading code periods referenced to the L1C and C/A composite signal power. 141

Figure F.11 Detection probability of coherent combining joint L1C pilot and C/A detector for acquisition over one L1C spreading code period referenced to the L1C and C/A composite signal power. 141

Figure F.12 Detection probability of semi-coherent combining joint L1C pilot and C/A detector for acquisition over three L1C spreading code periods referenced to the L1C and C/A composite signal power. 142

Figure F.13 Detection probability of joint L1C and C/A detectors with incorrect L1C code phase estimate but correct C/A code phase estimate for acquisition over one L1C spreading code period referenced to the L1C and C/A composite signal power. 142

Figure F.14 Detection probability of joint L1C and C/A detectors with incorrect L1C code phase estimate but correct C/A code phase estimate for acquisition over three L1C spreading code periods referenced to the L1C and C/A composite signal power. 143

Figure F.15 Detection probability of joint L1C pilot and C/A detectors with incorrect L1C code phase estimate but correct C/A code phase estimate for acquisition over one L1C spreading code period referenced to the L1C and C/A composite signal power. 143

Figure F.16 Detection probability of joint L1C pilot and C/A detectors with incorrect L1C code phase estimate but correct C/A code phase estimate for acquisition over three L1C spreading code periods referenced to the L1C and C/A composite signal power. 144

LIST OF TABLES

Table 1.1 Summary of Civil GPS Signals 7

Table 5.1 Nominal Received Power Levels 82

LIST OF ABBREVIATIONS AND SYMBOLS

C/N_o	Carrier Power-to-Noise Power Density (W/Hz)
ARNS	Aeronautical Radionavigation Service ITU Band
BOC	Binary Offset Carrier
bps	Bits-Per-Second
C/A	Coarse Acquisition
CDF	Cumulative Distribution Function
CDMA	Code Division Multiple Access
DFT	Discrete Fourier Transform
DSSS	Direct Sequence Spread Spectrum
FFT	Fast Fourier Transform
GEO	Geostationary Earth Orbit
GNSS	Global Navigation Satellite System
GPS	Global Positioning System
ITU	International Telecommunications Union
L1C	Civil GPS Signal at 1575.42 MHz
L2C	Civil GPS Signal at 1227.60 MHz
L5	Civil GPS Signal at 1176.45 MHz
MEO	Medium Earth Orbit

P(Y)	Military (Encrypted) GPS Signal
PNT	Position, Navigation and Timing
ppm	Parts Per Million
PRN	Pseudo-Random
PSD	Power Spectral Density (W/Hz)
RF	Radio Frequency
RNSS	Radionavigation Satellite Service ITU Band
RTCA	Radio Technical Commission for Aeronautics
SNR	Signal-to-Noise Ratio
TMBOC	Time-Multiplexed Binary Offset Carrier

CHAPTER 1

INTRODUCTION

The Officer of the Deck placed a small piece of cardboard over the display of the ship's Global Positioning System (GPS) once all 22 sails were set and land was safely behind us. By order of the ship's Captain, GPS would not be relied on for navigation for the next several days. After all, this was the Coast Guard tall-ship *Eagle*, the two hundred ninety-five foot sail training vessel for future leaders of the United States Coast Guard. Sextants became commonplace on deck as we became proficient at "swinging the arc" to measure the altitude, the angular distance, from the horizon to various celestial bodies such as the sun, moon, planets, and stars. Earlier in the classroom at the Coast Guard Academy, we learned the details of the altitude-intercept method of plotting a celestial line of position and the nuances of sight reduction tables. Developed in 1875, by Marc St. Hilaire, this method of celestial navigation involves four basic steps [1, 2]:

1. Taking actual measurements,

2. Estimating position at the time of the measurements,

3. Determining the expected measurements for the estimated position, and

4. Updating the estimated position by comparing actual and expected measurements.

I had no idea at the time that the ship's GPS receiver was essentially following the same four steps to find our position.[1] Instead of angles, GPS depends on ranges, and the celestial bodies are satellites placed into orbit around the Earth by the United States Air Force. Since GPS has become ubiquitous, celestial navigation has vanished from use by the navigator. While sextants are still found aboard the tall-ship *Eagle* today, nineteen years after I was a cadet onboard, the theory behind this nautical tradition has sadly been removed from

[1]This similarity between various types of navigation problems was emphasized by Van Diggelen in his book *A-GPS: Assisted GPS, GNSS, and SBAS* [3].

the education that future Coast Guard leaders receive. In its place, however, GPS satellite navigation has allowed for accuracy and applications never before imagined.

The more generic term for a system for navigation by satellite, Global Navigation Satellite System (GNSS), has become widely utilized in the position, navigation, and timing community as other nations are modernizing or developing their own systems (GLONASS in Russia, Galileo in Europe, Beidou in China). GNSS research continues to expand as engineers explore how to use GNSS in challenging radio frequency environments, as they consider it for new applications, and as they seek to mitigate vulnerabilities while exploiting modernized signal structures.

The purpose of this study is to analyze the performance of new acquisition techniques for the most recent of the modernized GPS signals through a cohesive examination of GPS L1C acquisition. The GNSS receiver needs to find, or acquire, the signal before processing begins. Various methods are proposed to increase sensitivity to enable use of L1C in challenging radio frequency environments. This introduction provides a high level overview on how GNSS works, a brief history of GNSS, and a summary of GPS modernization efforts. An overview of the GPS L1C signal is provided. The introduction concludes with the motivation for this research and the contributions of this dissertation.

1.1 How GNSS Works[2]

Navigation with satellites is based on the principle of trilateration; that is, the determining of a position based on known distances from known locations. In GNSS, the satellite positions are predicted by orbit data, and the distance from each is determined by measuring how long a radio signal takes to travel to the user. Once this travel time is multiplied by the speed of

[2]A very brief conceptual introduction to how GNSS works is provided here. Chapter 2 presents more details on GNSS signals and the acquisition process. Three textbooks that have been valuable to many GNSS researchers and that were also used in this research effort are: *Global Positioning System: Theory and Applications* edited by Parkinson and Spilker [4], *Global Positioning System: Signals, Measurements, and Performance* by Misra and Enge [5], and *Understanding GPS: Principles and Applications* edited by Kaplan and Hegarty [6].

light, how fast the signal travels, the distance is known.

Thinking geometrically helps in understanding how GNSS works. If the GNSS receiver can measure its distance from one satellite, then it must be located somewhere on the surface of a sphere, with that satellite at the center, and the measured distance as the radius. If three different but simultaneous distance measurements are found, then the GNSS receiver must be located at the intersection of three spheres. This intersection will give two possible locations of which only one is a reasonable option for the actual receiver position. Increased accuracy in the measurements leads to improved positioning; therefore, satellite and receiver clocks must be synchronized.

GNSS satellites have accurate and expensive atomic clocks onboard. However, the quality of clocks in GNSS receivers is limited by the desire for users to have inexpensive and small receivers. Fortunately, the time bias between GNSS time in the satellites and the receiver clock can be determined by adding a fourth satellite to the observations. This extra observation will give the GNSS receiver four equations from which it can easily solve for the four unknowns: the three dimensions of position offset from the assumed location and the time bias. In reality, more than four measurements are generally utilized when available to give a more accurate and robust position, navigation, and timing (PNT) solution.

For global navigation capability, a GNSS user must receive at least four signals from the satellite constellation, anywhere on Earth. Currently, GPS has 31 healthy satellites orbiting the earth on six different orbital planes at a nominal altitude of 20,000 km, 44 times higher than the International Space Station.[3] On average, a GPS receiver on the Earth, with a clear view of the sky above ten degrees elevation, will be able to receive eight to eleven GPS signals.

This large number of signals sharing the same frequency and time is accomplished by using Code Division Multiple Access (CDMA) where each satellite transmits a unique

[3]GPS had 31 healthy satellites as of February 2014. GPS World magazine has a webpage called "The Almanac" that provides up-to-date information on various GNSS constellations: `http://gpsworld.com/the-almanac`. The United States Coast Guard Navigation Center website provides GPS constellation status and notifications: `http://www.navcen.uscg.gov/?Do=constellationStatus`.

ranging code on the same carrier frequency. Despite transmitting at the same time, and on the same frequency, these unique codes, allow the locating and the distinguishing of a signal. Data is also inserted into each signal. This navigation data contains information needed by the GNSS receiver to complete the PNT solution such as ephemeris, clock corrections, and timing information to specify when the unique code was transmitted. After acquiring the signals, the GNSS receiver then tracks them, reads the navigation data, and computes a PNT solution for the user.

1.2 History of GNSS[4]

The concept of a system based on satellites for navigation was born in the United States in 1958, with the Navy Navigation Satellite System, which later became known as "Transit." One year earlier, the Soviet Union had launched Sputnik I, the first artificial Earth satellite. Doppler shift (change in frequency due to motion) measurements from Sputnik signals were used to determine its orbit; however, the realization that the opposite could work emerged soon thereafter. Thus, Doppler shift measurements could be used to determine a position on Earth, if the orbit of a satellite was known. Transit became operational in 1964 and was utilized by submarines and ships to determine their position. With 10 to 15 minutes of receiver processing of the Doppler shift measurements, Transit receivers could get a position fix every 30 to 110 minutes, depending on their latitude [6]. The significant time between position fixes, however, made Transit impractical for high-dynamic platforms.

A new and improved system that included better clocks and more satellites was soon on the drawing board. By the end of the 1960s, the U.S. Navy and U.S. Air Force were developing programs for new navigation systems. These were eventually combined into NAVSTAR GPS, which became the GPS system in use today. Since advancements in clock technology allowed time synchronization between different satellites, ranging, as opposed

[4] A detailed history of GPS can be found in the article "A History of Satellite Navigation" by Parkinson, Stansell, Beard, and Gromov [7].

to Doppler shift measurements, was selected as the positioning method. Spread spectrum technology allowed the simultaneous transmission of signals from different satellites on the same frequency. A medium earth obit (MEO) for the satellites was selected so that a total constellation of 24 satellites provided global coverage.

The GPS constellation was initially designed to transmit three different signals. Two different center carrier frequencies were selected in the L-band (1 GHz to 2 GHz), with civil and encrypted military signals on L1 (1575.42 MHz), and another encrypted military signal on L2 (1227.60 MHz). The civil signal on L1, called the Coarse Acquisition (C/A) signal, was designed so that military receivers could acquire the encrypted military signal known as P(Y). The United States government also made the commitment to allow the free and open use of L1 C/A by civilians as part of the Standard Positioning Service (SPS); whereas, L1 P(Y) and L2 P(Y) were designed for U.S. Department of Defense authorized personnel as part of the Precise Positioning Service (PPS). The basic GPS architecture was approved in 1973; the first satellite was launched in 1978; and the system was declared fully operational in 1995. There are most likely more than a billion GPS enabled devices around the world that employ GPS L1 C/A.

While the United Sates was developing GPS, the former Soviet Union was developing a system known as GLONASS. The system architecture is very similar to GPS, with one major difference, its reliance on Frequency Division Multiple Access (FDMA), where each satellite has the same ranging code but transmits at a different carrier frequency. The first satellite was launched in 1982, and the system reached full capability in 1996. There was a quick decline in availability, however, as GLONASS had just six working satellites in 2001. Due to reinvestments by Russia, GLONASS is back up to 24 healthy satellites in orbit and is undergoing its own modernization effort which includes incorporating new CDMA signals.

New satellite navigation systems are emerging globally as governments see the need for their institution. Initiated in 1998, by the European Commission and the European Space Agency (ESA), Galileo, Europe's program for its own GNSS, is being developed by the

European GNSS Supervisory Authority (GSA) in Brussels, Belgium. The system is in the In-Orbit Validation phase with two experimental and four operational satellites in space. The first was launched in 2005, with the most recent in 2012. A fully operational system with 30 satellites is expected by 2020. China created a regional navigation system known as Beidou that was completed in 2003 with three geostationary Earth orbit (GEO) satellites. Beidou is currently expanding into a global system known as Beidou-2 or Compass. In 2011, the new system was declared ready for use in China and is expected to be available globally with 37 satellites in various orbits (MEO, GEO, and inclined geosynchronous orbit) by 2020.

1.3 GPS Modernization

Even when GPS became fully operational in 1995, the National Research Council and others were making recommendations for an additional civil signal [8]. The initial GPS modernization plans were announced in 1998 and called for two new civil signals. In addition, the U.S. military wanted improved jam resistance as well as the ability to jam locally in the theater of operations without interfering with their own users. Since 1995, three new civil signals and two new military signals have been designed with significant enhancements over legacy GPS.

The United States federal government announced in 1998 that a new civil signal would be added to L2 (1227.60 MHz). The original plan was to broadcast the same L1 C/A code until a GPS Joint Program Office (JPO) official questioned replicating a legacy signal on a modernized satellite [9]. Changing the original plan led to a compressed design period in which the L2 civil design was completed early in 2001 for inclusion in the first Block-IIR-M satellite that was scheduled for launch in 2003 but was eventually launched in 2005. This signal is known as L2C, and its design is delineated in an Interface Specification document [10].

After several years of studies, the United States federal government announced in 1999

Table 1.1: Summary of Civil GPS Signals

Signal	Center Frequency	# of Operational Satellites	Availability (first/global)
L1 C/A	1575.42 MHz	30	1978/1995
L2C	1227.60 MHz	10	2005/2016*
L5	1176.45 MHz	3	2010/2018*
L1C	1575.42 MHz	0	2015*/2021*

* projected [15]

that the center frequency of the second new civil signal would be at 1176.45 MHz, an International Telecommunication Union (ITU) band designated for aeronautical radionavigation service. As the only signal in the GPS L5 radio frequency link, it is now commonly referred to as L5 and was designed primarily for aviation navigation. The Radio Technical Commission for Aeronautics (RTCA) Special Committee 159 Working Group One developed the specifications [11] which were later converted into the Interface Specification [12].

The design for a new civil GPS signal on the same frequency as L1 C/A was initiated in 2003 and completed in 2006 [13]. As the most recent of the modernized GPS signals, known as L1C, it has acquired and extended many advancements seen in other modern signals including L5 and L2C. L1C was designed to be interoperable and compatible with other GNSS L1 signals. The design for L1C is specified in the Interface Specification document IS-GPS-800A [14]. Since this dissertation focuses on this new signal, a brief overview of the L1C is provided in the next section with a detailed model presented in the next chapter. The first GPS satellite with L1C is expected to launch in 2015. The United States government estimates that there will be a full constellation of 24 satellites transmitting these new signals in 2016, 2018, and 2021 for L2C, L5, and L1C, respectively [15]. A summary is shown in Table 1.1.

With the increasing number of signals in each satellite, various multiplexing techniques are used onboard for transmission. This composite signal needs to have a constant envelope for efficient transmitter operation. Two signals can be combined with quadrature phase shift

keying (QPSK) where two RF carriers with a phase difference of 90 degrees are summed. QPSK is used in legacy GPS; the inphase component is L1 C/A, and the quadraphase component is L1 P(Y) military signal.

Now, more advanced techniques to combine three or more signals on the same carrier frequency are necessary. On the L1 carrier frequency, GPS satellites will soon transmit five different signals: C/A code, P(Y) code, the new military signal known as M-code, and the two components of L1C (pilot and data). More complex multiplexing techniques include interplexing [16], majority vote [17], intervoting [18], and Coherent Adaptive Subcarrier Modulation (CASM) [19]. A relatively new technique called Phase-Optimized Constant-Envelope Transmission (POCET) is a likely candidate for future GPS satellites [20].

1.4 Overview of GPS L1C[5]

The research in this dissertation focuses on acquisition of the most recently-designed GPS signal, L1C. Its carrier frequency of 1575.42 MHz is the same as the legacy L1 C/A code designed thirty years prior; however, many innovative features separate this signal from its counterpart. L1C is split with 75% power in the pilot, or data-less, component and 25% power in the data component. This two-component nature, which is not seen in the legacy GPS, is common to many modern GNSS signals; the unequal power split, however, is a novel feature. L1C will be multiplexed onto the L1 carrier along with the other L1 signals (P(Y) code, M code, and C/A code). The two components of L1C will be transmitted in-phase with each other and in-phase with the P(Y) code [22].

As in all GNSS signals, spreading codes are utilized to produce wider bandwidth and to uniquely identify each satellite, allowing for simultaneous transmission on the same carrier frequency. Spreading codes with a length of 10,230 chips and a duration of 10 ms at a

[5]Details of the L1C signal are published in the Interface Specification IS-GPS-800A [14]. The discussion here is based on L1C descriptions provided by Betz et al. [13] and Stansell, Hudnut, and Keegan [21].

chipping rate of 1.023 Mcps, are based on Weil codes [23]. This is the same rate as L1 C/A code, but 10 times longer. Each satellite has unique spreading codes, and different codes are used for the pilot and the data components. In addition to the spreading code, also referred to as the primary code, the pilot component has an 18 second 1800-bit deterministic overlay code, also referred to as the secondary, or synchronization, code. The overlay code effectively lengthens the short repeating pilot spreading code since it has no data modulation and also simplifies synchronization to the data symbols on the data component. One bit of this overlay code and one bit of the navigation data on the data component each has a duration of 10 ms which corresponds to the duration of the spreading code.

Once the overlay code phase for the pilot component is determined by the receiver, and hence no unknown phase modulation exists, the minimum Carrier Power-to-Noise Power Density (C/N_o in W/Hz) threshold for tracking the pilot component is lowered by 4.75 dB by employing a phase-locked loop (PLL), instead of the traditional Costas loop [21]. More power in the pilot component is attractive for receivers that ignore the data component due to the use of out-of-band data messages such as other radio frequencies or the internet. Low density parity check (LDPC) codes for forward error correction (FEC) are used to mitigate the concerns of users who do not receive out-of-band data messages and depend on the data component, even though it has only 25% of the total transmit power. Despite the reduced power in the data component, the FEC allows for equivalent or better bit error rate (BER) for L1C when compared to the legacy C/A code signal.

In order to achieve spectral shaping and fit L1C in an already crowded GNSS frequency band, the two components of L1C use Binary Offset Carrier (BOC) modulation, originally proposed for GNSS by Betz [24], for a new military signal known as M-code. BOC modulation uses a square-wave subcarrier which splits the spectrum about the carrier frequency. The higher the frequency of this subcarrier, the farther the energy is moved away from the center, allowing GNSS designers to occupy space in the radio frequency spectrum that will cause lower multiple access interference with other systems. A thorough design

process has created a new civil GPS signal with many modern features that provide GPS receiver manufacturers more design flexibility and greater opportunity to improve receiver performance. The detailed model for L1C is presented in section 2.3.

1.5 Overview of GNSS Acquisition

Any GNSS receiver must find the satellite signal through the process of acquisition before it determines position or time. This critical step involves determining whether a desired satellite signal is present, and if it exists, finding the correct frequency and spreading code delay. The receiver can then implement algorithms for tracking, as the frequency and code delay continuously change, while simultaneously decoding the navigation data which is needed to compute the receiver's position.

While the GNSS receiver knows the carrier frequency of the transmitted signal (1575.42 MHz for GPS L1C), the received GNSS signal will have a slightly different frequency caused by Doppler shift due to the motion of the satellite, up to ±800 m/s line-of-sight velocity for a rising or setting satellite, and the motion of the receiver. An additional frequency offset will be caused by the unknown receiver oscillator drift. The range of unknown frequency around the carrier is typically between 10-25 kHz [3].

Even with the correct frequency, the receiver is not able to acquire a particular signal without having the correct delay or phase of the spreading code. This procedure creates a two-dimensional search space in which the GNSS receiver examines all possible frequencies and code delays to find a particular signal. Once the receiver has the frequency and code delay estimates, it can pass that information along to a process known as tracking, which allows the receiver to continuously observe the signal and measure ranges. While tracking a satellite, the receiver will demodulate the data and then compute a position.

1.6 Motivation and Objectives

GPS modernization and development of new satellite navigation systems such as Galileo have spawned significant GNSS research over the past fifteen years. Features of modern GNSS have given receiver manufacturers more flexibility in how they design their receivers to meet the specific requirements of a variety of applications. Modern GNSS signals also provide the potential for better accuracy and improved performance in challenging radio frequency environments such as low signal-to-noise power, multipath, and interference. Some recent research has focused on acquisition of these modern GNSS signals to exploit their new features to improve acquisition sensitivity. Very little of this research, however, has focused on GPS L1C. As the most recently designed GPS signal, L1C will not be available from a satellite in space until 2015 and is not expected to be fully operational until 2021 (as previously shown in Table 1.1).

Despite this timeframe for GPS L1C deployment, and the lack of published research regarding GPS L1C acquisition, GNSS receiver manufacturers are starting to design new multi-signal and multi-constellation GNSS receivers with L1C compatibility. The objective of this dissertation is to provide a comprehensive evaluation of L1C acquisition and to propose techniques to improve acquisition sensitivity. The goal is to provide performance results for various techniques and to propose enhanced acquisition techniques for various receiver scenarios. The findings will assist GNSS engineers in evaluating the cost and benefits of enhanced receiver acquisition schemes for GPS L1C.

1.7 Contributions

The following are the contributions of this dissertation:

- Derivation of the optimal detector for GPS L1C acquisition (Chapter 3).
- Derivation of the optimal detector for GPS L1C acquisition under scenarios when the pilot overlay code phase and the navigation data are known (Chapter 3).

- Approximations to optimal detectors based on the signal-to-noise to simplify detector complexity (Chapter 3).

- Performance analysis of the optimal detectors in term of detection and false alarm probabilities using Monte Carlo computer simulations (Chapter 3).

- Detailed analysis of coherent combining of L1C pilot and data components over a single spreading code period based on relative data bit estimation including derivation of analytical expressions for the detection and false alarm probabilities as well as the probability density function of the decision variable (Chapter 4).

- Detailed analysis of semi-coherent integration for combining L1C pilot and data components over multiple spreading code periods including the threshold when the performance advantage disappears (Chapter 4).

- Proposal and analysis of various acquisition techniques when the L1C pilot overlay code phase is known, including differentially-coherent detection and coherent integration using relative pilot/data sign bit estimation (Chapter 4).

- Derivation of the optimal detector for GPS L1 C/A and L1C joint acquisition and performance analysis of detection and false alarm probabilities using Monte Carlo computer simulations (Chapter 5).

- Detailed analysis of coherent combining of GPS L1 C/A code and L1C signals for joint acquisition including derivation of analytical detection and false alarm probabilities; analysis extended over multiple spreading code periods with semi-coherent integration (Chapter 5).

- Proposal and analysis of joint L1C pilot and L1 C/A acquisition techniques while ignoring the lower power L1C data component (Chapter 5).

1.7.1 Publications

The research detailed in this dissertation has been published within the GNSS community in the following conference proceedings:

- Seals, K., Michalson, W., Swaszek, P., and Hartnett, R. (September 2012) *Analysis of Coherent Combining for GPS L1C Acquisition*. Paper published in the Proceedings of the 25th International Technical Meeting of the Satellite Division of the Institute of Navigation (ION GNSS 2012), Nashville, TN.
- Seals, K., Michalson, W., Swaszek, P., and Hartnett, R. (January 2013) *Analysis of L1C Acquisition by Combining Pilot and Data Components over Multiple Code Periods*. Paper published in the Proceedings of the 2013 International Technical Meeting of The Institute of Navigation (ION ITM Conference), San Diego, CA.
- Seals, K., Michalson, W. (April 2013) *Semi-Coherent and Differentially Coherent Integration for GPS L1C Acquisition*. Paper published in the Proceedings of the Pacific Position, Navigation and Timing Conference of the Institute of Navigation (ION Pacific PNT Conference), Honolulu, HI.
- Seals, K., Michalson, W., Swaszek, P., and Hartnett, R. (September 2013) *Using Both GPS L1 C/A and L1C: Strategies to Improve Acquisition Sensitivity*. Paper published in the Proceedings of the International Technical Meeting of The Satellite Division of the Institute of Navigation (ION GNSS+ 2013), Nashville, TN.

1.8 Outline

The signal model for GPS L1C, the origin and history of the GNSS acquisition problem and state-of-the-art acquisition methods for modern GNSS signals are described in Chapter 2 of this dissertation.

Classical detection and estimation theory is used in Chapter 3 to derive the optimal detector for GPS L1C acquisition in various receiver scenarios. Detector performance is presented based on single trial false alarm and detection probabilities using Monte Carlo computer simulations.

Novel sub-optimal, but more efficient, acquisition techniques for the GPS L1C signal are proposed in Chapter 4. Whenever possible, analytical results are derived for the false alarm and detection probabilities and confirmed with simulation results. Where analytical

results are not obtained, simulation results are used to compare the performance of these proposed detectors to others: optimal, traditional, and state-of-the-art.

Chapter 5 focuses on the most probable scenario in the near future of processing GPS L1C with GPS L1 C/A, when a GPS L1C signal is available, for joint acquisition of a particular satellite. Joint acquisition schemes are proposed and their performance is evaluated.

Conclusions and recommendations for future research are presented in Chapter 6.

CHAPTER 2

THE GPS L1C SIGNAL AND GNSS ACQUISITION

2.1 Introduction

This chapter first presents an overview of a typical GNSS signal, highlighting the important elements of its structure and characteristics. The legacy GPS L1 C/A code signal is then presented as an example. Next, a detailed explanation of L1C is provided along with the signal model used in this dissertation. The development of optimal detectors for acquisition in the next chapter is based on this mathematical model of the L1C signal. Finally, basic acquisition theory is explained and state-of-the-art GNSS acquisition techniques from recent publications are highlighted.

2.2 GNSS Signal Structure and Characteristics

GNSS signals, used primarily for precise ranging instead of communication, generally have a large-bandwidth and low data-rate. The structure allows the receiver to measure time of arrival; whereas, the transmitted data facilitates the determination of the satellite's location. To illustrate the structure and characteristics of GNSS signals, a generic transmitted GNSS signal model is presented here based on information from [25, 26].

2.2.1 GNSS Baseband Signal

GNSS employs Direct Sequence Spread Spectrum (DSSS) to produce wider bandwidth signals. The energy is spread over a much larger frequency band than required by the low data rate. DSSS spreading modulations with larger bandwidths lead to better tracking accuracy and improved resistance to narrowband interference.

GNSS involves many signals, some from the same satellite, some from different satellites in the same system, and some from multiple systems. The majority of GNSSs are classified as Code Division Multiple Access (CDMA) systems since each satellite transmitting the signal has a unique spreading code, also called a pseudo-random or PRN code. CDMA

allows simultaneous transmission of the signal at the same carrier frequency from multiple satellites; it also identifies the satellite. The spreading code is sometimes called the "ranging" code since this feature assists in measuring time of arrival, which is then converted to the range to the satellite.

A typical baseband representation of a DSSS GNSS repeated spreading series is:

$$h(t) = \sum_{k=0}^{L-1} c_k g(t - kT_c), \tag{2.1}$$

where c_k is the spreading code, which is a binary sequence of bits, also called chips; $g(t)$ is the spreading symbol, which is non-zero over the interval $[0, T_c]$; and $1/T_c$ is known as the spreading code rate, or chipping rate; and L is the length of the spreading code in number of bits.

Civil signals use spreading codes that repeat. For efficient operation of the transmitter, satellite navigation systems need $h(t)$ with a constant envelope. This requirement is achieved by selecting $\{c_k\} \in \{-1, +1\}$ and choosing a spreading waveform $g(t)$ that is a real-valued function with constant magnitude. One example of a spreading symbol is the rectangular pulse, $p(t)$, which has unit width, unit height, and is centered at the origin:

$$g(t) = p(t) = \begin{cases} 1 & \text{if } |t| \leq \frac{T_c}{2}, \\ 0 & \text{otherwise.} \end{cases} \tag{2.2}$$

Different spreading waveforms are employed in some modern GNSS signals (including GPS L1C as discussed in section 2.3.1) to provide spectral separation in crowded frequency bands.

Longer codes generally mean improved performance but also increase the complexity of receiver processing. Problems from short or medium-length spreading codes include narrow spectral lines, which interfere with other GNSS signals, and increased susceptibility to narrowband interference. Data modulation acts to effectively lengthen the spreading code. Newer signals generally have data bit durations which are the same length as the spreading

code period to prevent repetition. This technique, however, is not the case in the legacy GPS C/A code signal in which there are twenty repeats of the spreading code during one data bit.

Not all signals carry data, however, since most modern GNSS signals have two components, data and pilot. The former transmits the navigation data; whereas, the latter allows better tracking performance since there are no unknown phase transitions caused by the unknown data symbols. Deterministic overlay codes can also mitigate the effects of shorter spreading codes, especially on the pilot component, by phase-modulating each spreading code period with a sequence of bits that are known to the receiver. These overlay codes are also known as secondary codes or synchronization codes since they simplify the synchronization to data symbols. The spreading time series of this general GNSS signal, now with an overlay code, is:

$$x(t) = \sum_{l=0}^{N-1} b_l h(t - lT_b), \tag{2.3}$$

where T_b is the duration of the overlay code bit and the repeating sub-segment of the spreading time series, $h(t)$, as defined in (2.1); and $\{b_l\} \in \{-1, +1\}$ are the bits of the overlay code which has a length of N bits.

Information needed to calculate satellite positions may be modulated on this spread spectrum signal at a low rate (i.e., many GNSS signals use 50 bps). Referred to as the navigation data or the broadcast ephemeris, this information contains the satellite orbit model, clock offset data, and other information used by the receiver. The baseband representation of the GNSS signal with data is now:

$$s(t) = \sum_{m=-\infty}^{\infty} d_m x(t - mT_d) \tag{2.4}$$

$$= \sum_{m=-\infty}^{\infty} d_m \sum_{l=0}^{N-1} b_l \sum_{k=0}^{L-1} c_k g(t - mT_d - kT_c), \tag{2.5}$$

where $\{d_m\} \in \{-1, +1\}$ are the data symbols with bit duration of T_d seconds. If the signal is a pilot component without data modulation, then without loss of generality, $\{d_m\} = 1$.

The generic baseband GNSS signal, $s(t)$, from (2.4) consists of a single waveform and is considered a biphase keyed signal. Some modernized GNSS signals are represented by multiple waveforms each described by (2.4). GNSS signals with more than one waveform may be time-multiplexed together as in GPS L2C, combined in phase with orthogonal spreading codes as in GPS L1C, or combined in phase quadrature with two biphase keyed signals ninety degrees apart as in GPS L5.

2.2.2 GNSS Bandpass Signal

GNSS signals have carrier frequencies in the portion of radio frequency spectrum known as L-band. The spectrum between 1559 MHz to 1610 MHz is referred to as the "upper L-band" and the spectrum between 1164 MHz and 1300 MHz is referred to as the "lower L-band." All of these frequencies have been designated for Radionavigation Satellite Service (RNSS) by the the International Telecommunications Union (ITU). Parts of these frequencies are also designated for Aeronautical Radionavigation Service (ARNS) by the ITU, which provides protection for safety-critical uses.

In general, the bandpass signal at the satellite transmitter has the form:

$$s_{bp}(t) = \sqrt{2P_I}s_I(t)\cos(2\pi f_c t) - \sqrt{2P_Q}s_Q(t)\sin(2\pi f_c t) \tag{2.6}$$

$$= \sqrt{2P_T}Re\left\{\left[s_I(t) + \mathrm{j}s_Q(t)\right]e^{\mathrm{j}2\pi f_c t}\right\} \tag{2.7}$$

$$= \sqrt{2P_T}Re\left[s(t)e^{\mathrm{j}2\pi f_c t}\right]. \tag{2.8}$$

The L-band carrier frequency is f_c (Hertz) and without loss of generality, the carrier phase is defined to be zero at time of transmission. Here the components are in phase quadrature and $s_I(t)$ and $s_Q(t)$ are the quadrature components of the lowpass or baseband GNSS signal, $s(t)$, also known as the complex-envelope of the radio frequency (RF) signal. The "Re" denotes the real part of the complex-valued quantity in brackets. The signal power of the inphase and quadraphase components are represented by P_I and P_Q (Watts), respectively, and P_T is the total transmitted signal power. Power of GNSS signals is a critical factor. Higher power helps overcome noise, interference, and propagation loss; however, higher power also costs

more and increases multiple access interference. Power levels are controlled by international agreements between systems. The general signal model just presented will now be adjusted to represent the legacy GPS L1 C/A code signal.

2.2.3 The Legacy GPS L1 C/A Code Signal

The original GPS civil signal, L1 C/A, was the first GNSS signal with open access and is now used by numerous GPS enabled devices worldwide. At baseband, the GPS L1 C/A signal may be expressed as:

$$s_{C/A}(t) = \sum_{m=-\infty}^{\infty} d_m x\left(t - mT_d\right), \tag{2.9}$$

where $d_m \in \{-1, +1\}$ are the data symbols with bit duration of $T_d = 0.02$ seconds; and $x(t)$ is the spreading series:

$$x(t) = \sum_{l=0}^{N-1} b_l h\left(t - lT_b\right) \tag{2.10}$$

where, since there is no overlay code, $b_l = 1$ and $T_b = 0.001$ seconds and $N = \frac{T_d}{T_b} = 20$ repetitions of the spreading code during one data symbol. The repeating sub-segment of the spreading time series is:

$$h(t) = \sum_{n=0}^{L-1} c_n p\left(\frac{t - nT_c}{T_c}\right), \tag{2.11}$$

where:

- $c_n \in \{-1, +1\}$ is the spreading code sequence from a family known as Gold codes, with period of $L = 1023$ chips and chip duration of $T_c = \frac{1}{1.023 \times 10^6}$ seconds, so that the period of the spreading code is 0.001 seconds; and
- the spreading symbol is the rectangular pulse, p(t), with unit height and adjusted to have duration of T_c.

The L1 C/A signal has only an in-phase component and the bandpass transmitted signal is:

$$s_{bp,C/A}(t) = \sqrt{2P} s_{C/A}(t) \cos(2\pi f_c t), \tag{2.12}$$

where the carrier frequency is $f_c = 1575.42 \times 10^6$ Hertz. Thirty years after the design of this signal, L1C was created to be a significant improvement over L1 C/A.

2.3 The GPS L1C Signal

As the most recent GPS signal, GPS L1C will become the second civil GPS signal in the upper L-band along with GPS L1 C/A. This section first provides the baseband signal model for L1C. Next the correlation function is discussed. The power spectrum is presented to show how the spreading symbol shapes the spectrum so that it can share space with other GNSS signals. The transmitted and received signal models are then presented. Finally, a model for the correlator outputs in the GPS L1C receiver is developed so that it can be used in deriving optimal detectors for acquisition.

2.3.1 Baseband Signal Model for L1C

This section introduces the baseband waveform model used in this dissertation for the L1C signal. The pilot and the data components are combined in-phase so that the composite waveform is:

$$s(t) = \sum_{m=-\infty}^{\infty} \left[d_{P,m} h_P(t - mT_d) + d_{D,m} h_D(t - mT_d) \right], \tag{2.13}$$

where:

- the $\{d_{D,m}\} \in \{-1, +1\}$ are the data symbols with duration $T_d = .01$ seconds on the data component;
- the $\{d_{P,m}\} \in \{-1, +1\}$ are the deterministic bits of the overlay code on the pilot component and have the same duration as a data symbol on the data component: $T_d = .01$ seconds; the overlay code has a length of 1800 bits and repeats every 18 seconds; and
- $h_D(t)$ and $h_P(t)$ are the spreading time series (defined below) for the data and pilot components, respectively.

The spreading time series for each component, $h_D(t)$ and $h_P(t)$, consists of the unique code with each chip modulating a spreading symbol. GNSS spread spectrum signals have traditionally employed the rectangular spreading symbol. Binary Offset Carrier (BOC) modulation, however, has a square-wave symbol and was proposed for GNSS in [24]. This new technique acts as a square-wave subcarrier that splits the spectrum about the center frequency. The convention of using BOC(m, n) to describe a BOC-modulated symbol for GNSS has become standard where the subcarrier frequency is $f_s = m \times 1.023$ MHz and the spreading code rate is $f_c = n \times 1.023$ MHz. In this work, BOC modulation with a sine-phased subcarrier is assumed and is specified by "BOC" or "BOC_s"; whereas, cosine-phased BOC is denoted by BOC_c.

The spreading symbol for the L1C data component is strictly BOC(1,1): one period of a square wave for each spreading code chip. The L1C pilot component uses a time-multiplexed combination of BOC(6,1) and BOC(1,1) known as TMBOC.

The L1C data component spreading series is described by:

$$h_D(t) = \sum_{n=0}^{N-1} c_{D,n} g_{\text{BOC}(1,1)}(t - nT_c), \tag{2.14}$$

where:

- $\{c_{D,n}\} \in \{-1, +1\}$ is the sequence of spreading code chips for the data component, where each chip has a duration of $T_c = \frac{1}{1.023MHz}$ seconds, or approximately 1 microsecond;
- N=10,230 is the length of the spreading code with a period of 10 milliseconds; and
- $g_{\text{BOC}(1,1)}(t)$ is the BOC(1,1) spreading symbol (one period of a square wave for each spreading code chip).

The L1C pilot component spreading series uses a time-multiplexed combination of BOC(1,1) and BOC(6,1) spreading symbols and is described by:

$$h_P(t) = \sum_{\substack{n=0 \\ n \notin \{0,4,6,29,\ldots\}}}^{N-1} c_{P,n} g_{\text{BOC}(1,1)}(t - nT_c) + \sum_{\substack{n=0 \\ n \in \{0,4,6,29,\ldots\}}}^{N-1} c_{P,n} g_{\text{BOC}(6,1)}(t - nT_c), \tag{2.15}$$

where:

- $\{0, 4, 6, 29, ...\}$ are the indices where $g_{\text{BOC(6,1)}}(t)$ is inserted instead of $g_{\text{BOC(1,1)}}(t)$; the BOC(6,1) spreading symbol is used in 4 out of every 33 chips of the spreading code, with the locations described in the L1C Interface Specification document [14];
- $\{c_{P,n}\} \in \{-1, +1\}$ is the sequence of spreading code chips for the pilot component, where each chip has a duration of $T_c = \frac{1}{1.023MHZ}$ seconds, or approximately 1 microsecond;
- N=10,230 is the length of the spreading code with a period of 10 milliseconds;
- $g_{\text{BOC(1,1)}}(t)$ and $g_{\text{BOC(6,1)}}(t)$ are the spreading symbols with one period and three periods of a square wave for each spreading chip, respectively.

The spreading symbols, $g_{\text{BOC}(m,n)}(t)$, can be described in terms of the rectangular waveform, $p(t)$, which has unit width, unit height and is centered at the origin:

$$g_{\text{BOC(1,1)}}(t) = p\left(\frac{t + \frac{T_s}{2}}{T_s}\right) - p\left(\frac{t - \frac{T_s}{2}}{T_s}\right) \tag{2.16}$$

$$g_{\text{BOC(6,1)}}(t) = \sum_{m=0}^{5} (-1)^m p\left(\frac{t - mT_{s'} + \frac{5T_{s'}}{2}}{T_{s'}}\right), \tag{2.17}$$

where T_s is the duration of the subchip, or the duration of each half-cycle of the square wave subcarrier with frequency f_s, so that $T_s = \frac{1}{2f_s}$. For GPS L1C, the duration of each subchip in the spreading symbols are:

$$T_s = \frac{1}{(2)(1.023\text{MHz})} = 0.48876\ \mu\text{sec}, \tag{2.18}$$

$$T_{s'} = \frac{1}{(2)(6.023\text{MHz})} = 0.081460\ \mu\text{sec}. \tag{2.19}$$

These BOC spreading symbols lead to different auto-correlation functions compared to the conventional rectangular spreading waveform.

2.3.2 L1C Auto-Correlation Function

A GNSS receiver is based on correlation processing. Correlation measures the similarity between two waveforms. The auto-correlation measures the similarity of a waveform and time-shifted versions of itself; whereas, the cross-correlation measures a waveform against the time-shifted versions of another waveform. The spreading codes in GNSS signals were designed to produce good auto-correlation properties, a sharp peak when there is no time shift, and nearly zero at all other time shifts. The spreading codes are nearly orthogonal as well, so that the cross-correlation is close to zero at all time shifts. These exact properties are taken advantage of in acquisition and tracking of GNSS signals.

In general, civil GNSS signals are cyclostationary processes, meaning their auto-correlation function is periodic. To eliminate this time dependence, the time-average auto-correlation function over a single period of the spreading code is used and defined as:

$$R_x(\tau) = \frac{1}{T_{\text{code}}} \int_{T_{\text{code}}/2}^{T_{\text{code}}/2} x(t)x(t-\tau)\,\mathrm{d}t. \tag{2.20}$$

L1C uses BOC(m,n) spreading modulations on the pilot and the data components as described in 2.3.1, where $T_c = 1/f_c$ is the spreading code chip period, $T_s = 1/(2f_s)$ is half the subcarrier (square-wave) period. The number of half-periods of the subcarrier during one spreading code chip is:

$$k = 2m/n = 2f_s/f_c = T_c/T_s. \tag{2.21}$$

This number, k, can also be thought of as the number of sub-chips within each spreading code chip. If q is defined as an integer between $-2k$ and $2k$, then the auto-correlation functions over infinite bandwidth for the (sine-phased) BOC spreading modulation were defined in [26] as:

$$R_{\text{BOC}_s}(\tau = qT_s/2) = \begin{cases} (-1)^{q/2}\left(k - \left|\frac{q}{2}\right|\right)/k, & \text{if } q \text{ even}, \\ (-1)^{(|q|-1)/2}/2k, & \text{if } q \text{ odd}. \end{cases} \tag{2.22}$$

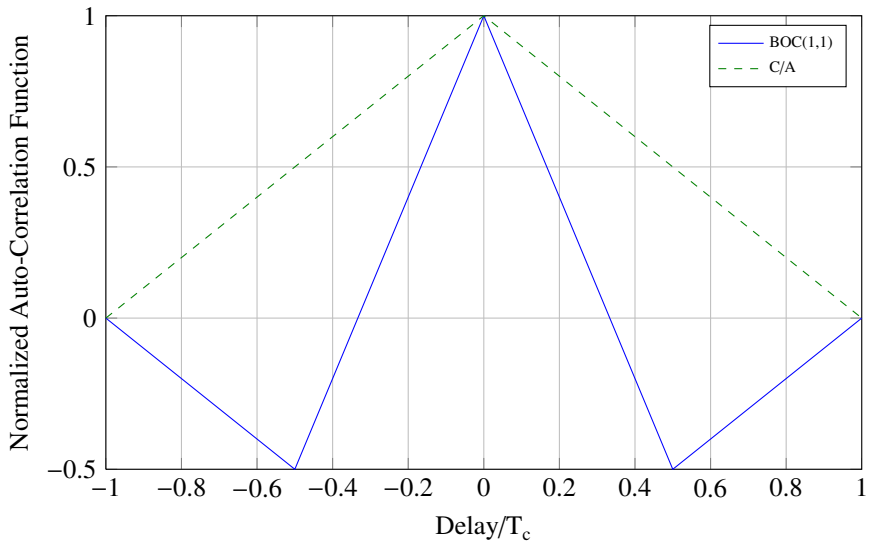

Figure 2.1: BOC spreading modulations provide a narrower correlation peak when compared to the traditional rectangular pulse used in the legacy C/A code signal.

To plot this function at intermediate values of τ, the values at $\tau = qT_s/2$ are connected with a straight line, on account of the BOC spreading modulations containing only rectangular waveforms.

The primary benefit of using the BOC spreading modulation for GNSS signals is the spectral shaping ability since this type of modulation splits the waveform about the center frequency as shown in section 2.3.3. Another benefit is the narrowing of the auto-correlation peak, which improves tracking performance. Fig. 2.1 shows the auto-correlation function for the BOC(1,1) spreading modulation and for the traditional rectangular pulse of the GPS L1C C/A code signal.

One interesting element seen in the BOC auto-correlation function is additional peaks at some non-zero lags. The number of positive and negative peaks in the auto-correlation function is given by $2k - 1$. The BOC(6,1) auto-correlation is shown in Fig. 2.2 with its 23 peaks. These additional peaks do require receiver strategies to avoid acquiring and tracking something other than the peak corresponding to zero-lag. One such strategy is sideband processing as described in 2.5.1.

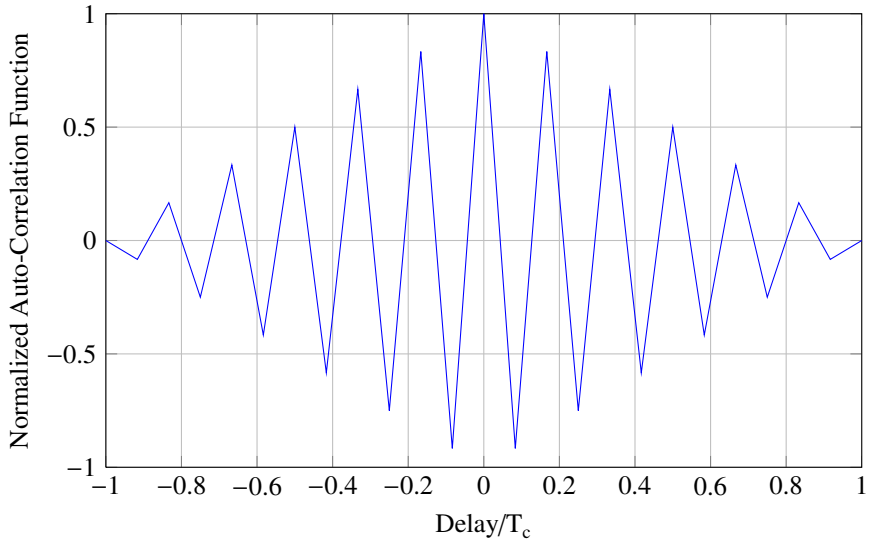

Figure 2.2: The BOC(6,1) auto-correlation function is shown for different offsets of the spreading code chip with duration T_c.

2.3.3 L1C Power Spectral Density

The Fourier Transform of a finite energy signal gives its frequency content. The Fourier series finds the distribution of power at various discrete frequencies for a periodic signal. For random processes, the Fourier Transform of their auto-correlation function is the Power Spectral Density (PSD), which is the *Wiener-Khinchine* relation:

$$\Phi(f) = \mathcal{F}\{R(\tau)\} = \int_{\infty}^{\infty} R(\tau) e^{-j2\pi f\tau}\, \mathrm{d}\tau \tag{2.23}$$

This is the *average* power spectral density of the cyclostationary random process since $R(\tau)$ is the time-average auto-correlation function as defined in (2.20).

Betz showed in [25] that the PSD of the generalized GNSS waveform defined in (2.4) can be factored into four components, after using stationarized statistics from the cyclostationary waveforms:

$$\Phi(f) = P(f)C(f)\Omega(f)D(f), \tag{2.24}$$

where

- $P(f)$ is the factor associated with the spreading symbol;
- $C(f)$ is the factor associated with the spreading code;

- $\Omega(f)$ is the factor associated with the overlay code; and
- $D(f)$ is the factor associated with the data message.

The dependence of the PSD on the spreading code transform is further explored in Appendix A since that provides the most significant contribution to the GNSS PSD. The spreading code transform, $C(f)$, creates a fine structure on top of the PSD [5]; therefore, it is ignored by making the assumption that the pilot and the data components of the GPS L1C signal have ideal repeating spreading codes. Ideal codes have the property that the auto-correlation function is zero, except at lags which correspond to integer multiples of the spreading code length, where the value is unity. When using ideal repeating spreading codes, the associated factor in the PSD is simplified to one: $C(f) = 1$.

The L1C data component has two other factors in the PSD of (2.24) that simplify to one. Since the data message is unknown and treated as random, $D(f) = 1$. With only one repeat of the spreading code within the data symbol, and no overlay code on the data component, the factor associated with the overlay code is one, $\Omega(f) = 1$. Now, the PSD of the L1C data component only depends on the factor associated with the spreading symbol, a simplified result which is commonly used for GNSS signals:

$$\Phi(f) = P(f) = |G(f)|^2 / T_c, \tag{2.25}$$

where T_c is the spreading code chip duration. $G(f)$ is the Fourier Transform of the real-valued spreading symbol, $g(t)$, which is normalized so that:

$$\frac{1}{T_c} \int_{-\infty}^{\infty} |g(t)|^2 \, \mathrm{d}t = 1. \tag{2.26}$$

The spreading symbol transform dominates the spectral shape of all GNSS signals. Determining the Fourier Transform of the BOC(1,1) spreading symbol is the first step in

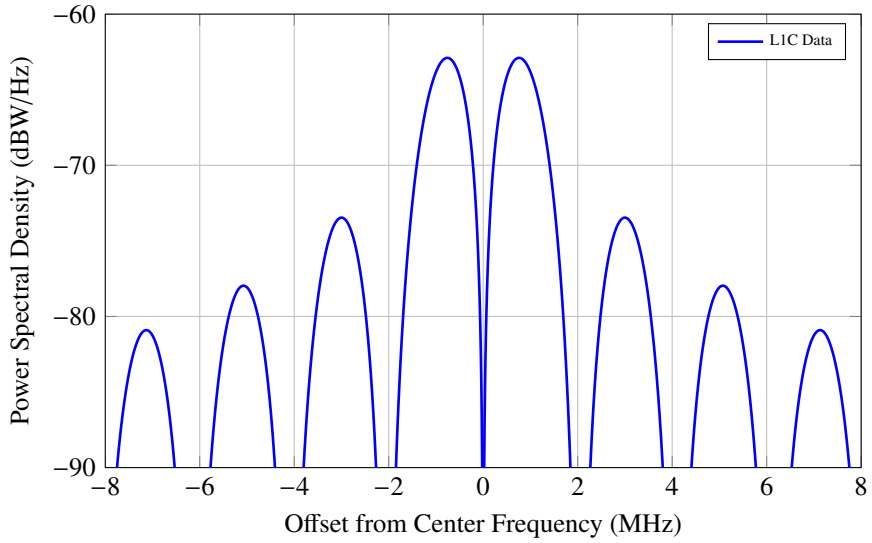

Figure 2.3: Power spectral density of the L1C data component. Under the assumption of repeating ideal spreading codes along with the treading data random, the PSD is the based on the Fourier Transform of the BOC(1,1) spreading symbol. The PSD is normalized to have unit area over an infinite bandwidth.

finding the PSD of the L1C data component:

$$\begin{aligned}
G(f) &= \int_{-\infty}^{\infty} g_{BOC(1,1)}(t) \mathrm{e}^{-\mathrm{j}2\pi f t}\,\mathrm{d}t \\
&= \int_{-\infty}^{\infty} \left[p\left(\frac{t+\frac{T_s}{2}}{T_s}\right) - p\left(\frac{t-\frac{T_s}{2}}{T_s}\right)\right] \mathrm{e}^{-\mathrm{j}2\pi f t}\,\mathrm{d}t \\
&= \int_{-T_s}^{0} \mathrm{e}^{-\mathrm{j}2\pi f t}\,\mathrm{d}t - \int_{0}^{T_s} \mathrm{e}^{-\mathrm{j}2\pi f t}\,\mathrm{d}t \\
&= \mathrm{e}^{-\mathrm{j}2\pi f \frac{T_s}{2}} \int_{-T_s/2}^{T_s/2} \mathrm{e}^{-\mathrm{j}2\pi f t}\,\mathrm{d}t - \mathrm{e}^{+\mathrm{j}2\pi f \frac{T_s}{2}} \int_{-T_s/2}^{T_s/2} \mathrm{e}^{-\mathrm{j}2\pi f t}\,\mathrm{d}t \\
&= \mathrm{e}^{-\mathrm{j}\pi f T_s} \left[\int_{-T_s/2}^{T_s/2} \cos(2\pi f t)\,\mathrm{d}t - \int_{-T_s/2}^{T_s/2} \mathrm{j}\sin(2\pi f t)\,\mathrm{d}t \right] \\
&\quad -\mathrm{e}^{+\mathrm{j}\pi f T_s} \left[\int_{-T_s/2}^{T_s/2} \cos(2\pi f t)\,\mathrm{d}t - \int_{-T_s/2}^{T_s/2} \mathrm{j}\sin(2\pi f t)\,\mathrm{d}t \right] \\
&= T_s \mathrm{sinc}(\pi f T_s) \mathrm{e}^{-\mathrm{j}\pi f T_s} - T_s \mathrm{sinc}(\pi f T_s) \mathrm{e}^{+\mathrm{j}\pi f T_s}
\end{aligned} \tag{2.27}$$

After taking the magnitude-squared of $G(f)$ and dividing by T_c, the PSD of the L1 data component with the distinctive split-spectrum caused by the BOC modulation is shown in Fig. 2.3.

A general formula for the the PSD of $\mathrm{BOC_s}(m,n)$ signals has been provided by Betz

[24, 26]:

$$\Phi_{\mathrm{BOC_s}}(f) = \begin{cases} \frac{1}{f_c}\mathrm{sinc}^2(\pi f/f_c)\tan^2(\pi f/f_c), & \text{if } k \text{ even}, \\ \frac{1}{f_c}\frac{\cos^2(\pi f/f_c)}{(\pi f/f_c)^2}\tan^2(\pi f/f_c), & \text{if } k \text{ odd}, \end{cases} \tag{2.28}$$

where

$$k = 2m/n = 2f_s/f_c = T_c/T_s. \tag{2.29}$$

This number, k, specifies the number of main-lobes plus the number of side-lobes between the main-lobes in the PSD.

The GPS-Galileo Working Group on Interoperability and Compatibility proposed a spectrum for the new civil signals on L1 with 10/11 of the power in a BOC(1,1) spreading modulation and the remaining power in BOC(6,1):

$$\Phi_{L1C}(f) = \tfrac{10}{11}\Phi_{\mathrm{BOC(1,1)}} + \tfrac{1}{11}\Phi_{\mathrm{BOC(6,1)}}. \tag{2.30}$$

The L1C pilot component has time-multiplexed spreading symbols known as TMBOC. To achieve the spectrum requirements, 4 out of every 33 BOC(1,1) spreading symbols are replaced with BOC(6,1). Since the pilot component has 75% of the total L1C signal power, this combination gives $(4/33)\cdot(3/4) = 1/11$ of the total power in the BOC(6,1) component. The result of this combination produces the PSD of the L1C data component as shown in Fig. 2.4. Combining the data and pilot components with their respective relative power ratios,

$$\Phi_{L1C}(f) = \tfrac{3}{4}\Phi_{L1CPilot} + \tfrac{1}{4}\Phi_{L1CData}, \tag{2.31}$$

gives the PSD of the complete L1C signal shown in Fig. 2.5.

The L1C spectrum was carefully selected to provide minimal multiple access interference to other GNSS signals in the upper L-band. As seen in Fig. 2.6, the peaks in the PSD occur at the nulls in the legacy L1 C/A code signal.

2.3.4 Transmitted Signal Model for L1C

The transmitted L1C signal is:

$$s_{tmt}(t) = \left[\sqrt{\tfrac{3}{2}P_{tmt}}d_P(t)\bar{h}_P(t) + \sqrt{\tfrac{1}{2}P_{tmt}}d_D(t)\bar{h}_D(t)\right]\cos(2\pi f_{L1} + \theta_{tmt}), \tag{2.32}$$

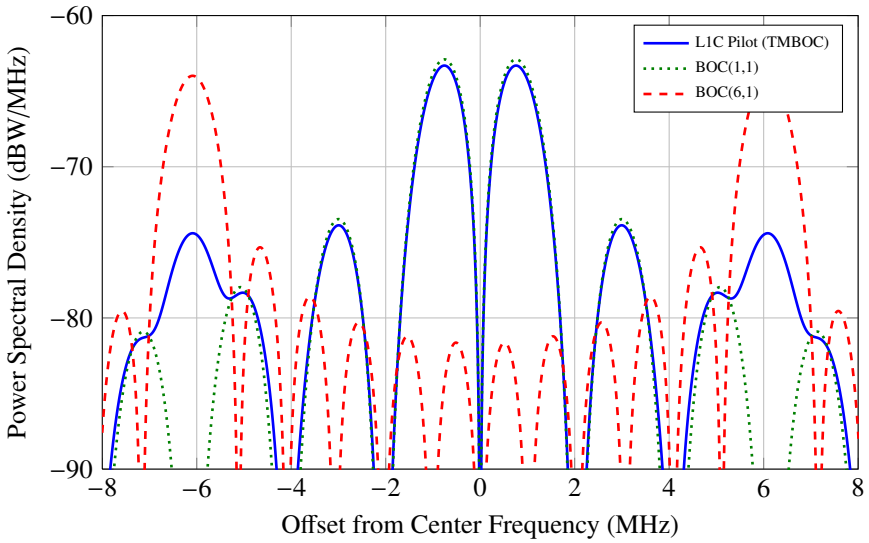

Figure 2.4: Power spectral density of the L1C pilot component, BOC(1,1), and BOC(6,1) spreading symbols. The L1C pilot uses two time-multiplexed spreading symbols known as TMBOC. The BOC(1,1) spreading symbol is primarily used; however, the BOC(6,1) spreading symbol is used in 4 out of every 33 chips of the spreading code, as shown in (2.15). The PSDs are normalized to have unit area over an infinite bandwidth.

.

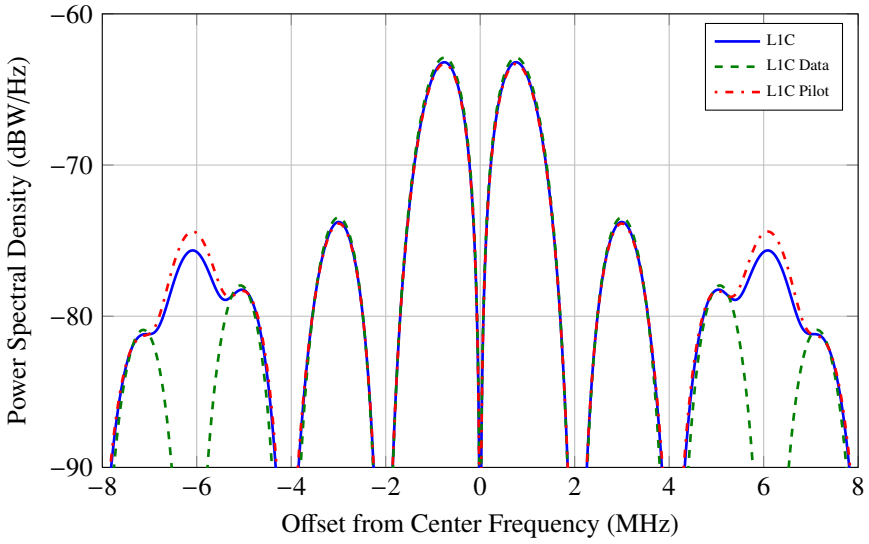

Figure 2.5: Power spectral density of the L1C signal, L1C data component, and L1C pilot component. The L1C signal has 75% of its power in the pilot component, the time-multiplexed spreading symbols BOC(1,1) and BOC(6,1). The remaining 25% of the power is in the data component which uses the single BOC(1,1) spreading symbol. The PSDs are normalized to have unit area over an infinite bandwidth.

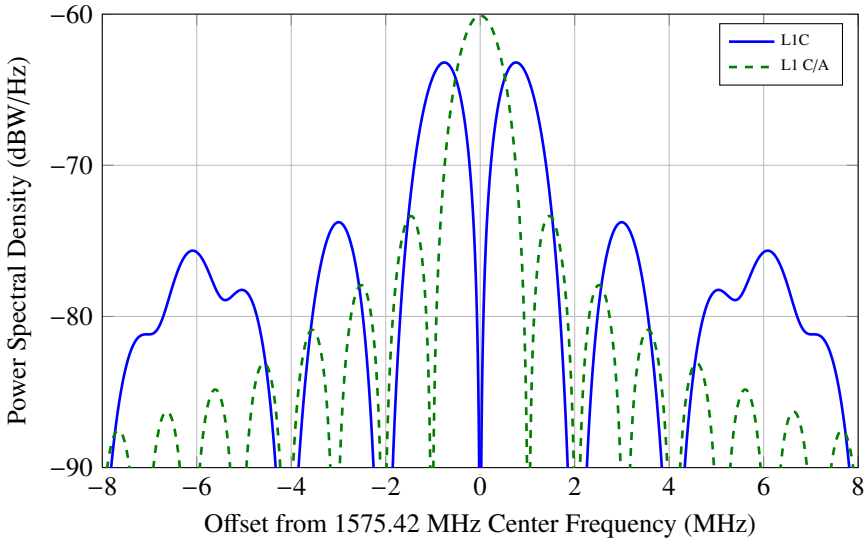

Figure 2.6: Power spectral density of L1C and L1 C/A code signals. The L1C uses BOC modulation to split the spectrum about the center frequency. The peaks in the L1C PSD occur at the nulls of the L1 C/A PSD. A little extra power was provided at higher frequencies by using the BOC(6,1) spreading symbol to allow for better receiver performance. This spectrum was selected and approved jointly between GPS and Galileo so that L1C will be interoperable with the Galileo L1 signal. The PSDs are normalized to have unit area over an infinite bandwidth.

where:

- the unequal amplitudes in each component account for the 75%/25% power split between the pilot and the data components;
- $d_D(t)$ and $d_P(t)$ are the series of data bits on the data component and overlay code bits on the pilot component;
- $\bar{h}_D(t)$ and $\bar{h}_P(t)$ are the periodic repetition of the spreading time series for the data and pilot components defined in equations (2.14) and (2.15), for example:

$$\bar{h}_D(t) = \sum_{m=-\infty}^{+\infty} h_D\left(t - mT_{code}\right),$$

  where the period of the code is $T_{code} = 10$ ms;
- f_{L1} is the L1 carrier frequency of 1575.42 MHz;
- θ_{tmt} is the phase of the transmitted signal.

The average power transmitted is found by the time average of the signal squared (here the average is over T seconds with $T >> 1/f_{L1}$ and the cross term is not included due to the orthogonal spreading codes):

$$\begin{aligned}
\frac{1}{T}\int_0^T s_{tmt}^2(t)\,\mathrm{d}t &= \frac{1}{T}\int_0^T \left[\frac{3}{2}P_{tmt}d_P^2(t)\bar{h}_P^2(t) + \frac{1}{2}P_{tmt}d_D^2(t)\bar{h}_D^2(t)\right]\cos^2(2\pi f_{L1}t + \theta_{tmt})\,\mathrm{d}t \\
&= \left[\frac{3}{2}P_{tmt} + \frac{1}{2}P_{tmt}\right]\frac{1}{T}\int_0^T \cos^2(2\pi f_{L1}t + \theta_{tmt})\,\mathrm{d}t \\
&= 2P_{tmt}\left(\frac{1}{T}\right)\int_0^T \left(\frac{1}{2} + \frac{\cos(4\pi f_{L1}t + 2\theta_{tmt})}{2}\right)\,\mathrm{d}t \\
&= 2P_{tmt}\left(\frac{1}{T}\right)\left(\frac{T}{2}\right) \\
&= P_{tmt}
\end{aligned} \tag{2.33}$$

Equation (2.33) relies on the navigation data, overlay code, and the spreading series being sequences of +1s and -1s.

2.3.5 L1C Received Signal Model and Output of Correlators

The signal at the input of a GNSS receiver can be modeled as a sum of signals from observed satellites along with additive Gaussian noise:

$$s(t) = \sum_{i=1}^{K} \sqrt{P_{rcv}}y_i(t) + n(t), \tag{2.34}$$

where there are K satellites and $n(t)$ is Gaussian noise. The received power, P_{rcv} is much less than the transmitted power. The two components of L1C are transmitted with the same phase, but with 75% of the power in the pilot component, and 25% of the power in the data component so that:

$$\begin{aligned}
y_i(t) = {} & \sqrt{\tfrac{3}{2}}d_{P,i}(t-\tau_i)c_{P,i}(t-\tau_i)g_{P,i}(t-\tau_i)\cos(2\pi(f_{L1}+f_{d,i})t + \theta_{rcv,i}) \\
& + \sqrt{\tfrac{1}{2}}d_{D,i}(t-\tau_i)c_{D,i}(t-\tau_i)g_{D,i}(t-\tau_i)\cos(2\pi(f_{L1}+f_{d,i})t + \theta_{rcv,i}),
\end{aligned} \tag{2.35}$$

where:

- $d_D(t)$ and $d_P(t)$ are the series of data and overlay code bits;

- $c_D(t)$ and $c_P(t)$ are the periodic repetition of the spreading code series for the data and pilot components;
- $g_D(t)$ and $g_P(t)$ are the periodic repetition of the spreading symbols, also called the subcarrier, for the data and pilot components;
- τ, f_d and θ_{rcv} are the unknown delay, Doppler frequency, and received phase of the signal; and
- f_{L1} is the L1 carrier frequency of 1575.42 MHz.

Unless specifically needed, the satellite term i is dropped due to orthogonality of the spreading codes. After signal conditioning in the front end of the GNSS receiver, the L1C signal from one satellite is

$$\begin{aligned} s(t) = & \sqrt{\tfrac{3}{2}C}d_P(t-\tau)c_P(t-\tau)g_P(t-\tau)\cos(2\pi(f_{IF}+f_d)t+\theta) \\ & + \sqrt{\tfrac{1}{2}C}d_D(t-\tau)c_D(t-\tau)g_D(t-\tau)\cos(2\pi(f_{IF}+f_d)t+\theta) + n(t), \end{aligned} \tag{2.36}$$

where:

- the signal power is now denoted as C (Watts), which includes any antenna gain and receiver implementation losses;
- the signal is now at an intermediate frequency f_{IF} (Hertz); and,
- θ is the unknown phase term.

Despite being a discrete-time signal at this point in the receiver, continuous-time signals are used here to provide insight under the assumption that the sample-rate has been selected fast enough to accurately represent the signal.

After multiplication by two reference signals that are in phase quadrature and subsequent low-pass filtering, the inphase and quadrature channels are:

$$\begin{aligned} \text{I} - \text{Channel} = & \sqrt{\tfrac{3}{4}C}d_P(t-\tau)c_P(t-\tau)g_P(t-\tau)\cos(2\pi\Delta f_d t+\Delta\theta) \\ & + \sqrt{\tfrac{1}{4}C}d_D(t-\tau)c_D(t-\tau)g_D(t-\tau)\cos(2\pi\Delta f_d t+\Delta\theta) + n_I(t) \end{aligned} \tag{2.37}$$

and

$$\begin{aligned}\text{Q} - \text{Channel} = &\sqrt{\tfrac{3}{4}C}d_P(t-\tau)c_P(t-\tau)g_P(t-\tau)\sin(2\pi\Delta f_d t + \Delta\theta) \\ &+ \sqrt{\tfrac{1}{4}C}d_D(t-\tau)c_D(t-\tau)g_D(t-\tau)\sin(2\pi\Delta f_d t + \Delta\theta) + n_Q(t), \quad (2.38)\end{aligned}$$

where $\Delta f_d = f_d - \hat{f}_d$ is the error in Doppler estimate, and $\Delta\theta = \theta - \hat{\theta}$ is the carrier phase offset between the local replica and the received signal.

The inphase and quadrature channels are coherently-integrated after each is multiplied by the local code and spreading symbol replicas. Each coherent integration gives a scalar output every integer multiple, k, of the coherent integration time, kT_{coh}:

$$\begin{aligned}
I_{P,k} &= \frac{\sqrt{\frac{3}{4}C}\, d_{P,k}}{T_{coh}} \int_{kT_{coh}}^{kT_{coh}+T_{coh}} c_P(t-\tau)c_P(t-\hat{\tau})g_P(t-\tau)g_P(t-\hat{\tau})\cos(2\pi\Delta f_d t+\Delta\theta)\,\mathrm{d}t + \eta_{P,I,k} \\
Q_{P,k} &= \frac{\sqrt{\frac{3}{4}C}\, d_{P,k}}{T_{coh}} \int_{kT_{coh}}^{kT_{coh}+T_{coh}} c_P(t-\tau)c_P(t-\hat{\tau})g_P(t-\tau)g_P(t-\hat{\tau})\sin(2\pi\Delta f_d t+\Delta\theta)\,\mathrm{d}t + \eta_{P,Q,k} \\
I_{D,k} &= \frac{\sqrt{\frac{1}{4}C}\, d_{D,k}}{T_{coh}} \int_{kT_{coh}}^{kT_{coh}+T_{coh}} c_D(t-\tau)c_D(t-\hat{\tau})g_D(t-\tau)g_D(t-\hat{\tau})\cos(2\pi\Delta f_d t+\Delta\theta)\,\mathrm{d}t + \eta_{D,I,k} \\
Q_{D,k} &= \frac{\sqrt{\frac{1}{4}C}\, d_{D,k}}{T_{coh}} \int_{kT_{coh}}^{kT_{coh}+T_{coh}} c_D(t-\tau)c_D(t-\hat{\tau})g_D(t-\tau)g_D(t-\hat{\tau})\sin(2\pi\Delta f_d t+\Delta\theta)\,\mathrm{d}t + \eta_{D,Q,k}, \quad (2.39)
\end{aligned}$$

where T_{coh} is the coherent integration time, $\hat{\tau}$ is the estimated delay and η are the uncorrelated noise terms that each have the same variance [5]:

$$\sigma^2 = N_0/2T_{coh}. \quad (2.40)$$

Two assumptions are applied herein: that the coherent integration time is the length of the spreading code period, which is the same as an overlay or data code bit; and that bit transitions are avoided. When the signal from the satellite is present, and correct delay

($\hat{\tau} = \tau$) and Doppler estimates are used, the output of the correlators are now:

$$\begin{aligned} I_{P,k} &= \sqrt{\tfrac{3}{4}C}\, d_{P,k} \cos(\Delta\theta) + \eta_{P,I,k} \\ Q_{P,k} &= \sqrt{\tfrac{3}{4}C}\, d_{P,k} \sin(\Delta\theta) + \eta_{P,Q,k} \\ I_{D,k} &= \sqrt{\tfrac{1}{4}C}\, d_{D,k} \cos(\Delta\theta) + \eta_{D,I,k} \\ Q_{D,k} &= \sqrt{\tfrac{1}{4}C}\, d_{D,k} \sin(\Delta\theta) + \eta_{D,Q,k}. \end{aligned} \tag{2.41}$$

Due to the autocorrelation properties of the spreading code, the correlator outputs contain the noise terms only when incorrect delay estimates ($\hat{\tau} \neq \tau$) are used. Employing complex notation to highlight the ambiguity function is shown in Appendix B, along with the resulting correlator outputs.

2.4 Fundamentals of GNSS Signal Acquisition

Any GNSS receiver must acquire the satellite signal before it may process it to determine position or time. This critical step of initial synchronization, called acquisition, determines whether a desired satellite signal is present and then finds rough estimates of frequency and spreading code delay. Once the signal is acquired, the receiver can implement algorithms to track it as the frequency and code delay change and can decode the navigation data. In this section, the frequency/code-delay search performed by the receiver is introduced. Three different procedures for performing the search are then discussed: serial search, parallel frequency space search, and parallel code phase search. A common method using detection and false alarm probabilities to analyze performance of GNSS acquisition schemes is then presented.

2.4.1 Frequency and Spreading Code Delay Search Space

The two-dimensional search space for GNSS acquisition is shown in Fig. 2.7, where the receiver is searching for the one cell that has the correct frequency and code delay for the signal. The initial frequency uncertainty is bounded by Doppler and receiver oscillator drift. The initial time uncertainty is due to the difference in time between the satellite and receiver

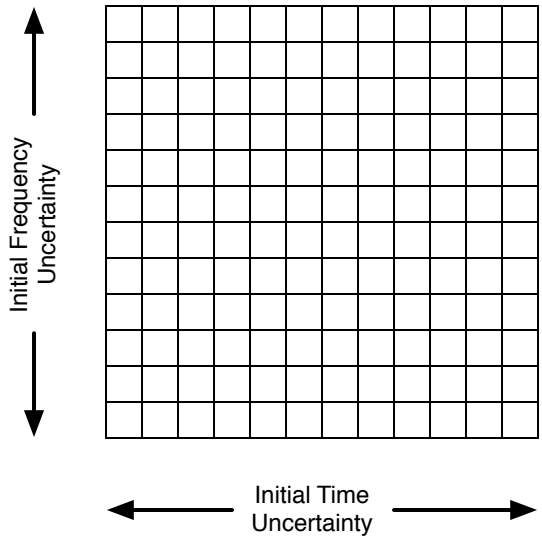

Figure 2.7: Acquisition search space. Initial synchronization to a GNSS signal involves a two-dimensional search through various frequencies and code delays that are bounded by the initial frequency and time uncertainties.

clocks as well as to the unknown distance between them. For L1C and other GNSS signals that use repeating spreading codes, the initial time uncertainty is bounded by the the length of the spreading code period. The actual integer multiple of spreading code periods between the satellite and receiver is determined in later processing using information transmitted in the data component.

While each satellite will transmit at the same frequency, each signal at the receiver is observed at a different frequency, due to Doppler shift caused by the satellite and receiver motion. The receiver, therefore, needs to search all possible frequencies. The greatest contribution to this frequency shift comes from the satellite motion, the receiver oscillator center frequency error, and the receiver oscillator drift rate. Satellites have a maximum line-of-sight velocity of approximately ±900 m/s when rising or setting, a phenomenon which leads to a received Doppler shift of almost ±5 kHz. An additional 1.5 kHz unknown frequency offset is caused by each 1 ppm (parts per million) unknown receiver oscillator drift, which can be anywhere from 2-5 ppm for consumer GPS receivers [3]. Finally, a small Doppler effect of 1.5 Hz is caused by each 1km/h of receiver speed. Each of these

contributing factors leads to an overall range of 10-25 kHz of unknown frequencies to search.

The frequency search is split up into discrete frequency bins in which the frequency at the center of each bin is searched. The size of the bins is determined by the acceptable mistuning loss. The sought-after correlation peak varies with frequency as a sinc function:

$$|\sin(\pi f T_{coh})/(\pi f T_{coh})|\,, \tag{2.42}$$

where f is the frequency error and T_{coh} is the coherent integration time. For the legacy GPS L1 C/A code signal, it is common to search in steps of 500 Hz since a frequency bin width of ± 250 Hz would cause a maximum loss of 1 dB:

$$10\log_{10}|\sin(\pi \cdot 250 \cdot 0.001)/(\pi \cdot 250 \cdot 0.001)| \approx 1 \text{ dB}. \tag{2.43}$$

To have a similar mistuning loss in L1C acquisition, however, search steps of 25 Hz are necessary, due to the longer spreading code and 10 ms coherent integration time:

$$10\log_{10}|\sin(\pi \cdot 25 \cdot 0.01)/(\pi \cdot 25 \cdot 0.01)| \approx 1 \text{ dB}. \tag{2.44}$$

The longer spreading code of L1C increases the number of frequency bins in the search by a factor of ten, compared to L1 C/A.

Even if the correct frequency bin is determined, the correlation peak cannot be found unless the receiver also has the correct spreading code phase which allows it to de-spread the signal. The longer length of the L1C spreading code, with 10230 chips, means 10 times the number of code phases to search when compared to L1 C/A. The narrower central peak and additional peaks in the auto-correlation function caused by the BOC modulation in L1C mean the code phase search will need a resolution of 1/5 or 1/10 of a chip, thus increasing the size of the code phase search. To avoid some of the increased receiver complexity needed to process the BOC modulated signal, sideband processing has been proposed and is explained in section 2.5.1.

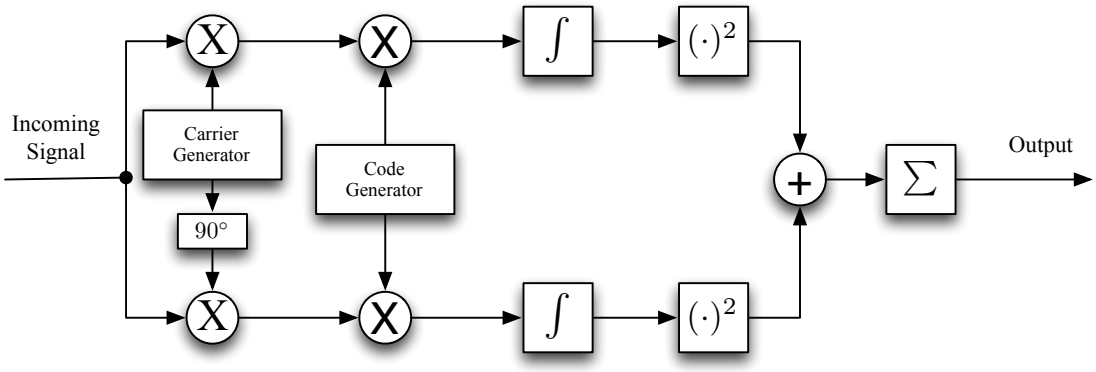

Figure 2.8: Block diagram of the serial search algorithm for GNSS acquisition.

A serial search implemented in hardware is generally used to find the correlation peak. With increased capability to implement more receiver functions in software, two techniques to make this search parallel, using the Fourier Transform, also exist: parallel frequency space search and parallel code phase search.

2.4.2 Serial Search

The common serial search acquisition method used in CDMA systems is shown in Fig. 2.8. Multiplication by a locally generated carrier signal generates the in-phase, or I, channel; and multiplication by a 90° shifted version of the carrier generates the quadrature, or Q, channel. Multiplication by a locally generated spreading code attempts to de-spread the spread spectrum signal. The I and Q signals are then coherently integrated, squared, and added. Further non-coherent integration may be performed by adding subsequent coherent integration results.

The serial search must process all possible carrier frequencies and code delays until a predetermined threshold is exceeded. Multiple correlators are used in hardware to parallelize the search. The search may instead be implemented in parallel with the Fourier Transform in a software receiver.

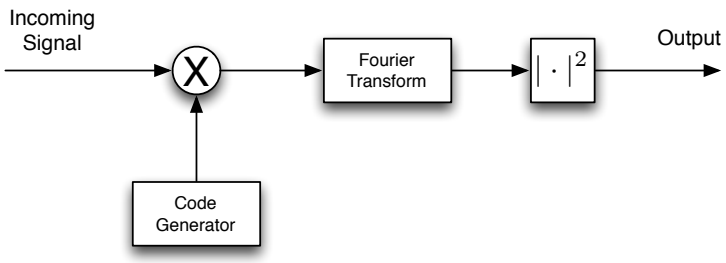

Figure 2.9: Block diagram of the parallel frequency space search algorithm for GNSS acquisition.

2.4.3 Parallel Frequency Space Search

A procedure that parallelizes the search for frequency is shown in Fig. 2.9. After the incoming signal is multiplied by the local copy of the spreading code, a Fourier Transform is implemented as a Discrete Fourier Transform (DFT) or Fast Fourier Transform (FFT) to put the signal into the frequency domain. When the correct code phase is selected, the magnitude of the Fourier Transform will show a distinct peak at the correct frequency.

Accuracy of the frequency at the peak depends on the length of the DFT (N). The frequency resolution is the sample frequency, f_s, divided by the size of the DFT: f_s/N. This procedure still needs to search through all possible code phases.

2.4.4 Parallel Code Phase Search

Since the number of search steps in the code phase is significantly larger than frequency steps, a procedure to parallelize the search for the code phase is shown in Fig. 2.10. The parallel code phase search implements circular correlation in the frequency domain by multiplying the Fourier Transform of the incoming signal by the complex conjugate of the local code transform. After taking the inverse Fourier Transform, a peak will exist at the code phase of the incoming signal if the correct frequency estimate was used. This procedure, therefore, only needs to step through each of the possible frequency bins in the search space.

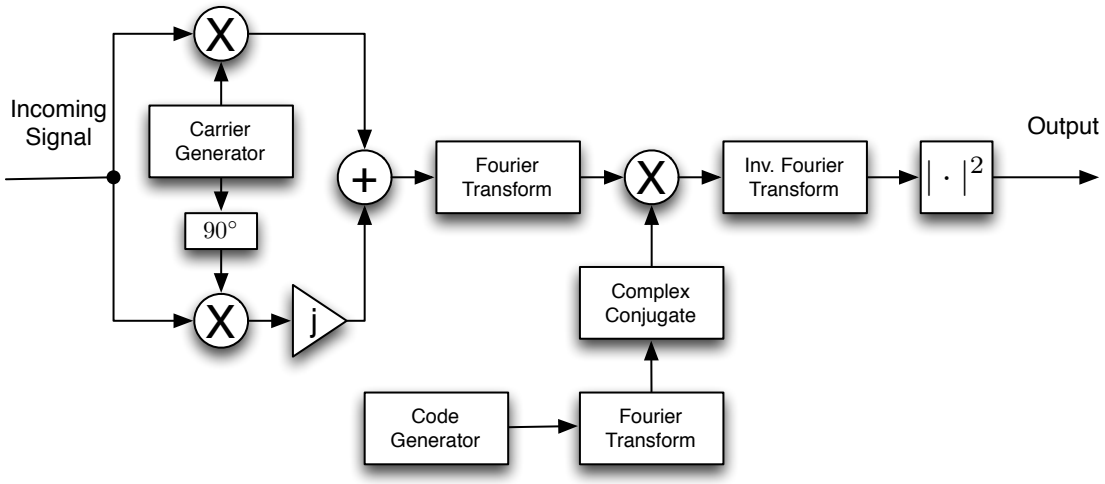

Figure 2.10: Block diagram of the parallel code phase search algorithm for GNSS acquisition.

2.4.5 Acquisition Performance

During acquisition, the GNSS receiver generates a decision statistic for each pair of frequency/code delay values during the two-dimensional search. If this statistic exceeds a pre-determined threshold, then the the signal is declared present with the corresponding frequency and code delay values. Since the phase of the carrier is unknown, the conventional noncoherent detection algorithm squares the output of the correlators and adds them together to get the initial decision variable. Subsequent noncoherent combining may be implemented when necessary to bring the correlation peak out of the noise floor:

$$Z = \sum_{k=1}^{K} \left(I_k^2 + Q_k^2 \right), \tag{2.45}$$

where Z is used to denote an acquisition decision statistic, and I_k and Q_k are the correlator outputs after each coherent integration, every T_{coh} seconds. The number of noncoherent combinations are denoted by K, and KT_{coh} is the total integration time.

Since the output of the correlators (I_k, Q_k) are Gaussian random variables, the decision variable Z is a chi-square random variable with $2K$ degrees of freedom. When incorrect delay and Doppler estimates are selected, the correlator outputs are zero mean so that Z has a central chi-square distribution. However, when correct delay and Doppler values are used,

Z is a noncentral chi-square random variable with noncentrality parameter:

$$a^2 = KC, \tag{2.46}$$

where C is the signal power.

When the value of the decision variable Z is above a threshold λ, the signal is declared present. In the acquisition process, two hypotheses, formally defined as H_1 when the satellite signal is present, and H_0 when it is not, describe the two possible situations in which probability densities of the acquisition statistic are found. Performance of the acquisition scheme can be determined by the frequency in which a signal is declared present when it is not, the false alarm probability (P_{fa}); and, by the frequency in which the signal is correctly declared present, the detection probability (P_d).

Since Z is a chi-square random variable for the conventional acquisition statistic in (2.45), the false alarm and detection probabilities are well known for the case when $K = 1$:

$$\begin{aligned} P_{fa}(\lambda) &= P(Z > \lambda \mid H_0) \\ &= 1 - P(Z < \lambda \mid H_0) \\ &= \exp\left(\frac{-\lambda}{2\sigma^2}\right), \end{aligned} \tag{2.47}$$

and

$$\begin{aligned} P_d(\lambda) &= P(Z > \lambda \mid H_1) \\ &= 1 - P(Z < \lambda \mid H_1) = Q_1\left(\frac{a}{\sigma}, \frac{\sqrt{\lambda}}{\sigma}\right) \\ &= Q_1\left(\frac{\sqrt{C}}{\sigma}, \frac{\sqrt{\lambda}}{\sigma}\right), \end{aligned} \tag{2.48}$$

where σ^2 is the noise power and Q_1 is the first-order Marcum's Q function [27].

The threshold for acquisition is selected by specifying a desired false alarm rate. Solving for the threshold in (2.47) yields:

$$\lambda = -2\sigma^2 \ln\left(P_{fa}\right), \tag{2.49}$$

where ln is the natural logarithm.

Throughout this work, performance of various acquisition schemes will be analyzed by comparing the detection probabilities at a fixed false alarm rate.

2.5 Acquisition of Modern GNSS Signals

Modern GNSS signals have given receiver designers more options for implementing acquisition schemes, depending on desired complexity. With little research published specifically for GPS L1C, many acquisition techniques have been proposed for other modern GNSS signals. This section describes the state-of-the art in GNSS acquisition schemes from recent publications that are applicable to L1C.

2.5.1 Sideband Processing

Some new GNSS signals, including L1C, are implementing BOC modulation to move signal energy away from the center of the band. As shown in section 2.3.2, this type of modulation also produces a narrower peak in the auto-correlation function, an advantage which allows more accurate code tracking. The disadvantages, however, are that the code delay space needs smaller search steps and that consideration must be given to avoiding acquisition of the peaks at non-zero lags in the auto-correlation function.

One possibility to avoid these challenges is to process only one sideband of the signal in a technique known as single sideband processing which was proposed for GNSS in [28]. Processing each sideband individually is similar to processing legacy GNSS signals with the rectangular spreading symbol and conventional single-peak auto-correlation function. If desired, the upper and lower sidebands can be processed separately and noncoherently combined as shown in Fig. 2.11. Each sideband of the GNSS signal contains all of the information, but at a lower signal-to-noise ratio (SNR). Processing only one sideband loses 3 dB of SNR, while noncoherent combining of the sidebands loses 0.5 dB of SNR [28].

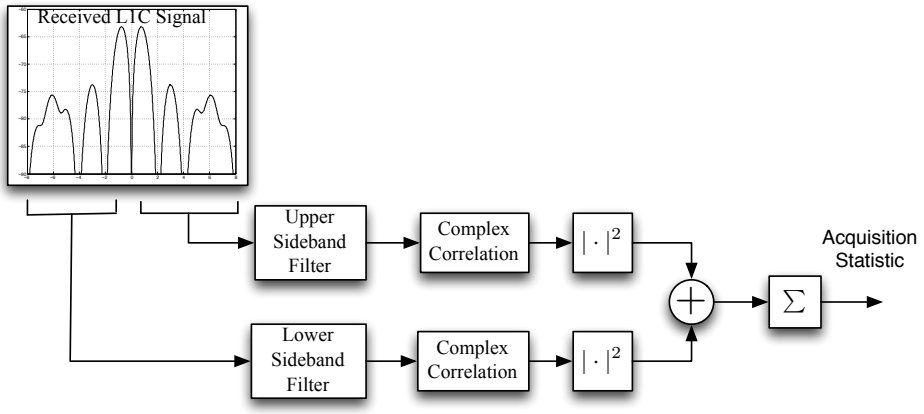

Figure 2.11: Block diagram of dual-sideband processing for GNSS acquisition.

2.5.2 Acquisition of Two-Component Signals

New acquisition schemes have been proposed with the advent of modern GNSS signals with pilot and data components. This section introduces the various acquisition techniques that are applicable to L1C. From acquisition of a single component to various combining techniques, expressions for detection and false alarm probabilities are presented when possible for GPS L1C, based on the received signal model developed in section 2.3.5. Performance of novel techniques developed later in this dissertation are compared to these state-of-the-art schemes.

2.5.2.1 Single Channel Acquisition

Either the pilot or the data component may be used for acquisition of two-component GNSS signals [29, 30, 31], with preference given to the component with the highest power, if applicable, as in GPS L1C. Since the phase of the carrier is unknown, the conventional noncoherent detection algorithm squares the output of the correlators and adds them together to get the decision variable, which in the case of acquisition of the pilot component is:

$$Z_{\text{scp}} = \sum_{k=1}^{K} \left(I_{P,k}^2 + Q_{P,k}^2 \right), \tag{2.50}$$

where the *scp* in the subscript stands for *single channel pilot*. Since each output of the correlators (I_P, Q_P) are Gaussian random variables, the decision variable Z is a chi-square

random variable with 2K degrees of freedom. The underlying Gaussian random variables have a variance of σ^2. With incorrect delay and Doppler estimates, the correlator outputs are zero mean so that Z has a central chi-square distribution. However, when correct delay and Doppler values are used, Z is a noncentral chi-square random variable with noncentrality parameter:

$$a_{scp}^2 = \tfrac{3}{4}KC. \tag{2.51}$$

When the value of the decision variable Z is above a threshold λ, the signal is considered present. Performance of the acquisition scheme can be determined by how often a signal is declared present when it is not, known as the false alarm probability (P_{fa}), and how often the signal is declared present correctly, the detection probability (P_d). Since Z is a chi-square random variable, these two probabilities are:

$$\begin{aligned} P_{fa}^{scp}(\lambda) &= P(Z > \lambda \mid H_0) \\ &= 1 - P(Z < \lambda \mid H_0) \\ &= \exp\left(\frac{-\lambda}{2\sigma^2}\right) \sum_{k=0}^{K-1} \frac{1}{k!} \left(\frac{\lambda}{2\sigma^2}\right)^k \end{aligned} \tag{2.52}$$

and

$$\begin{aligned} P_d^{scp}(\lambda) &= P(Z > \lambda \mid H_1) \\ &= 1 - P(Z < \lambda \mid H_1) = Q_K\left(\frac{a_{scp}}{\sigma}, \frac{\sqrt{\lambda}}{\sigma}\right) \\ &= Q_K\left(\frac{\sqrt{\frac{3}{4}KC}}{\sigma}, \frac{\sqrt{\lambda}}{\sigma}\right), \end{aligned} \tag{2.53}$$

where Q_K is the generalized (Kth-order) Marcum's Q function [27].

In the case of signals with an equal power split between components, the disadvantage of single channel acquisition rises because half the power is wasted; therefore, various techniques have been proposed for combining the pilot and the data components.

2.5.2.2 *Noncoherent Channel Combining*

Noncoherent combining is the separate acquisition of each component and the subsequent combination of the correlator powers; this technique was proposed for GNSS in [32] and has been analyzed in various papers [33, 31].

In order to avoid wasting power during acquisition, the incoming signal can be correlated separately with a local replica of the pilot and the data spreading codes. Noncoherent channel combining is the squaring and summing of correlator outputs to obtain the decision variable:

$$Z_{\text{nc}} = \sum_{k=1}^{K} \left(I_{P,k}^2 + Q_{P,k}^2 + I_{D,k}^2 + Q_{D,k}^2 \right). \tag{2.54}$$

where the *nc* in the subscript stands for *noncoherent* channel combining.

Similar to the single channel acquisition, Z, is a chi-square random variable, but now with $4K$ degrees of freedom. When the signal is not present, or when incorrect delay and Doppler estimates are used, Z has a central chi-square distribution. When the delay and Doppler estimates are correct, Z is a non-central chi-square random variable with noncentrality parameter:

$$a_{nc}^2 = \tfrac{3}{4}KC + \tfrac{1}{4}KC = KC. \tag{2.55}$$

This decision statistic leads to the following false alarm and detection probabilities:

$$\begin{aligned} P_{fa}^{nc}(\lambda) &= P(Z > \lambda \mid H_0) \\ &= \exp\left(\frac{-\lambda}{2\sigma^2}\right) \sum_{k=0}^{2K-1} \frac{1}{k!} \left(\frac{\lambda}{2\sigma^2}\right)^k \end{aligned} \tag{2.56}$$

and

$$\begin{aligned} P_{d}^{nc}(\lambda) &= P(Z > \lambda \mid H_1) = Q_{2K}\left(\frac{a_{nc}}{\sigma}, \frac{\sqrt{\lambda}}{\sigma}\right) \\ &= Q_{2K}\left(\frac{\sqrt{KC}}{\sigma}, \frac{\sqrt{\lambda}}{\sigma}\right), \end{aligned} \tag{2.57}$$

where Q_{2K} is the generalized ($2K$th-order) Marcum's Q function [27]. If the relative sign between the data bit and overlay code bit is known, then the pilot and the data components can be coherently combined to avoid some of the losses caused by the noncoherent combining.

2.5.2.3 *Coherent Channel Combining*

A technique known as coherent channel combining with sign recovery estimates the relative sign between the data and pilot components by correlating the received signal with two different composite codes, the pilot spreading code plus the data spreading code, and the pilot spreading code minus the data spreading code [34, 35, 36, 33, 31]. Borio provided single trial false alarm and detection probabilities, for a single code period, in [31] for the specific case of two-component GNSS signals transmitted in phase quadrature with equal power split.

The pilot and the data components can be combined coherently over one spreading code period by using a local composite spreading code that has the correct relative sign between the data and pilot components:

$$c_P(t)g_P(t) + c_D(t)g_D(t) \quad \text{if } d_P d_D = 1 \tag{2.58a}$$

or

$$c_P(t)g_P(t) - c_D(t)g_D(t) \quad \text{if } d_P d_D = -1. \tag{2.58b}$$

Since this relative sign is unknown to the receiver, these codes are used in coherent channel combining with sign recovery and the estimate of the relative sign given by the correlation with the highest power:

$$Z_{\text{ch}} = \max\left\{|z^+|^2, |z^-|^2\right\}, \tag{2.59}$$

where the *ch* in the subscript stands for *coherent* channel combining, and

$$z^+ = I_P + \mathrm{j}Q_P + I_D + \mathrm{j}Q_D \tag{2.60a}$$

$$z^- = I_P + \mathrm{j}Q_P - I_D - \mathrm{j}Q_D, \tag{2.60b}$$

and

$$|z^+|^2 = (I_P + I_D)^2 + (Q_P + Q_D)^2 \tag{2.61a}$$

$$|z^-|^2 = (I_P - I_D)^2 + (Q_P - Q_D)^2\,. \tag{2.61b}$$

As shown in [31], the false alarm and detection probabilities can be found by noting that:

$$\begin{aligned} P(Z > \lambda) &= P\left(\max\left\{|z^+|^2, |z^-|^2\right\} > \lambda\right) \\ &= 1 - P\left(\max\left\{|z^+|^2, |z^-|^2\right\} < \lambda\right) \\ &= 1 - P\left(|z^+|^2 < \lambda, |z^-|^2 < \lambda\right) \\ &= 1 - P\left(|z^+|^2 < \lambda\right) P\left(|z^-|^2 < \lambda\right). \end{aligned} \tag{2.62}$$

The squared magnitude terms, $|z^+|^2$ and $|z^-|^2$, are chi-square random variables with two degrees of freedom, where the underlying Gaussian random variables now have variance $2\sigma^2$. As in previous detection schemes, when no signal is present or incorrect delay and Doppler estimates are used, $|z^+|^2$ and $|z^-|^2$ have central chi-square distributions. When correct estimates are selected, $|z^+|^2$ and $|z^-|^2$ are non-central chi-square random variables. In this case, the noncentrality parameter for $|z^+|^2$ is:

$$\begin{aligned} a_{+,ch}^2 &= \left(\sqrt{\tfrac{3}{4}C}d_P\cos(\Delta\theta) + \sqrt{\tfrac{1}{4}C}d_D\cos(\Delta\theta)\right)^2 \\ &\quad + \left(\sqrt{\tfrac{3}{4}C}d_P\sin(\Delta\theta) + \sqrt{\tfrac{1}{4}C}d_D\sin(\Delta\theta)\right)^2 \\ &= \left(C + \tfrac{\sqrt{3}}{2}d_Pd_D\right)\cos^2(\Delta\theta) + \left(C + \tfrac{\sqrt{3}}{2}Cd_Pd_D\right)\sin^2(\Delta\theta) \\ &= \left(1 + \tfrac{\sqrt{3}}{2}d_Pd_D\right)C \\ &= \begin{cases} \left(1 + \frac{\sqrt{3}}{2}\right)C, & \text{correct rel. sign } (d_Pd_D = 1) \\ \left(1 - \frac{\sqrt{3}}{2}\right)C, & \text{incorrect rel. sign } (d_Pd_D = -1). \end{cases} \end{aligned} \tag{2.63}$$

The noncentrality parameter for $|z^-|^2$ is:

$$\begin{aligned} a_{-,ch}^2 &= \left(\sqrt{\tfrac{3}{4}C}d_P\cos(\Delta\theta) - \sqrt{\tfrac{1}{4}C}d_D\cos(\Delta\theta)\right)^2 \\ &\quad + \left(\sqrt{\tfrac{3}{4}C}d_P\sin(\Delta\theta) - \sqrt{\tfrac{1}{4}C}d_D\sin(\Delta\theta)\right)^2 \\ &= \left(C + \tfrac{\sqrt{3}}{2}d_Pd_D\right)\cos^2(\Delta\theta) + \left(C + \tfrac{\sqrt{3}}{2}Cd_Pd_D\right)\sin^2(\Delta\theta) \\ &= \left(1 - \tfrac{\sqrt{3}}{2}d_Pd_D\right)C \\ &= \begin{cases} \left(1 + \frac{\sqrt{3}}{2}\right)C, & \text{correct rel. sign } (d_Pd_D = -1) \\ \left(1 - \frac{\sqrt{3}}{2}\right)C, & \text{incorrect rel. sign } (d_Pd_D = 1). \end{cases} \end{aligned} \tag{2.64}$$

This leads to the following false alarm and detection probabilities using (2.62):

$$\begin{aligned} P_{fa}^{ch}(\lambda) &= 1 - P\left(|z^+|^2 < \lambda \mid H_0\right) P\left(|z^-|^2 < \lambda \mid H_0\right) \\ &= 1 - \left[1 - \exp\left(\frac{-\lambda}{4\sigma^2}\right)\right]^2 \end{aligned} \tag{2.65}$$

and

$$\begin{aligned} P_{d}^{ch}(\lambda) &= 1 - P\left(|z^+|^2 < \lambda \mid H_1\right) P\left(|z^-|^2 < \lambda \mid H_1\right) \\ &= 1 - \left[1 - Q_1\left(\frac{\sqrt{\left(1 + \sqrt{3}/2\right)C}}{\sqrt{2}\sigma}, \frac{\sqrt{\lambda}}{\sqrt{2}\sigma}\right)\right] \\ &\quad \cdot \left[1 - Q_1\left(\frac{\sqrt{\left(1 - \sqrt{3}/2\right)C}}{\sqrt{2}\sigma}, \frac{\sqrt{\lambda}}{\sqrt{2}\sigma}\right)\right]. \end{aligned} \tag{2.66}$$

Results were extended for multiple code periods in a technique called semi-coherent integration in [37, 38].

2.5.2.4 Semi-Coherent Channel Combining

Semi-coherent integration refers to the noncoherent combination of the single spreading code period coherent combinations of the data and pilot components by using a local composite spreading code that has the correct relative sign between the data and pilot components as explained in the previous section. Subsequent noncoherent combining leads to:

$$Z_{\text{sch}} = \sum_{k=1}^{K} \max\left\{|z_k^+|^2, |z_k^-|^2\right\}, \tag{2.67}$$

where the *sch* in the subscript stands for *semi-coherent* channel combining, and

$$z_k^+ = I_{P,k} + \mathrm{j}Q_{P,k} + I_{D,k} + \mathrm{j}Q_{D,k} \tag{2.68a}$$

$$z_k^- = I_{P,k} + \mathrm{j}Q_{P,k} - I_{D,k} - \mathrm{j}Q_{D,k}, \tag{2.68b}$$

and

$$|z_k^+|^2 = \left(I_{P,k} + I_{D,k}\right)^2 + \left(Q_{P,k} + Q_{D,k}\right)^2 \tag{2.69a}$$

$$|z_k^-|^2 = \left(I_{P,k} - I_{D,k}\right)^2 + \left(Q_{P,k} - Q_{D,k}\right)^2. \tag{2.69b}$$

For the $K = 1$ case, false alarm and detection probabilities were shown in equations (2.65) and (2.66) but for the generic K case, analytical expressions have not been found. The characteristic function was found in [37] for the decision variable under H_1 using an equal power split assumption. The characteristic function can then be raised to the power K to find the characteristic function for the decision statistic for specific value of K.

2.5.2.5 Differentially Coherent Channel Combining

A detector that maintains the differential phase information between successive correlator outputs uses differentially-coherent integration. This consists of the product of the current correlator output and the complex conjugate of the previous correlator output. Differentially-coherent integration was originally proposed for the acquisition of DSSS signals in [39] and has been considered for GNSS acquisition in [40, 41, 42] with a good summary and more analysis regarding weak signal GNSS acquisition in [43].

2.5.2.6 Joint Acquisition of GPS L1 C/A and L1C

With two civil signals in the future for GPS L1, using both L1C and C/A is a method to improve acquisition sensitivity. Separate correlations and noncoherent combining of these signals serves as a baseline for potential improvement in acquisition performance. Coherent combining of C/A, L1C Pilot, and L1C Data is possible if the relative signs between the corresponding navigation or overlay code bits are known. An acquisition technique that uses a parallel code phase search and checks all four possibilities of the relative signs between the three components was proposed by Macchi-Gernot [44, 45]. Simulation results in that research verified the increased acquisition sensitivity and noted potential issues with secondary peaks at lower C/No caused by the shorter C/A code. Detection and false alarm probabilities were not evaluated.

2.6 Chapter Summary

This chapter described the general structure and characteristics of GNSS signals. The model for L1C along with its unique features was presented. Fundamentals of GNSS acquisition,

along with the state-of-the art acquisition techniques, were also explained. This background will be used throughout this dissertation to evaluate and propose enhanced acquisition techniques for GPS L1C.

CHAPTER 3

OPTIMAL DETECTORS FOR GPS L1C ACQUISITION

3.1 Introduction

In this chapter, optimal detectors for acquisition of GPS L1C in additive white Gaussian noise are presented, with complete derivations provided in Appendix C. Three scenarios are considered. First, the common situation for an unassisted GPS receiver, in which it has no *a priori* information regarding the pilot overlay code phase or the navigation data, is explored. Next, the scenario in which a receiver has sufficient time accuracy to know the phase of the overlay code, but still has no knowledge of the navigation data, is considered. Finally, the optimal detector for the assisted receiver, which has knowledge of the pilot overlay code phase and the navigation data, is shown. Performance of these optimal detectors in terms of their detection probabilities at a fixed false alarm rate of 0.001 are found, using Monte Carlo simulations. For each value of the Carrier-to-Noise ratio, 10^6 trials are performed to find the probability of detection.

3.2 Optimal Detection Framework

Classical detection theory is used to derive the optimal detector for an arbitrary integer number of primary spreading code periods of the GPS L1C signal, and in general, any two-component GNSS signal in which the components are in-phase but have an unequal power split. All the results presented here are new. A similar procedure to find the optimal detector for GPS L5 acquisition was used in [33].

The outputs of the correlators are sufficient statistics for detecting the signal in an additive white Gaussian noise channel [27, 46]. These are derived in (2.39) and given in (2.41) for correct estimation of code delay and Doppler. Due to auto-correlation properties of the codes, it is assumed here that the correlator outputs contain noise only if an incorrect delay estimate is used. The observation vectors at the output of the correlators are the

following two hypotheses, which correspond to when the signal is present and when it is not:

$$H_1 : \ \mathbf{r} = \begin{bmatrix} \mathbf{I}_P \\ \mathbf{Q}_P \\ \mathbf{I}_D \\ \mathbf{Q}_D \end{bmatrix} + \mathbf{n} = \begin{bmatrix} \sqrt{\alpha C}\mathbf{d}_P \cos(\Delta\theta) \\ \sqrt{\alpha C}\mathbf{d}_P \sin(\Delta\theta) \\ \sqrt{\beta C}\mathbf{d}_D \cos(\Delta\theta) \\ \sqrt{\beta C}\mathbf{d}_D \sin(\Delta\theta) \end{bmatrix} + \mathbf{n}$$

$$H_0 : \ \mathbf{r} = \mathbf{n}. \tag{3.1}$$

This observation is over integer K spreading code periods. Under H_1, the observation is the $4K \times 1$ vector of correlator outputs from the $K \times 10$ ms observation. The $4K \times 1$ noise vector, $\mathbf{n}$, is white and Gaussian with covariance $\sigma^2\mathbf{I}$, where $\mathbf{I}$ is the identity matrix, and $\sigma^2 = N_0/(2T_{coh})$ [5], with T_{coh} being the coherent integration time. The received signal power is C, with the parameters α and β describing the power split between the two components, so that $\alpha + \beta = 1$. For the GPS L1C signal, $\alpha = 3/4$ and $\beta = 1/4$. The carrier phase residual, or phase offset between the local replica and the received signal, is $\Delta\theta$. Each component may have data, d_P or d_D, which represents any navigation data, overlay code, or a combination of these two items that may be present. These data vectors, $\mathbf{d}_P$ or $\mathbf{d}_D$, are each $K \times 1$ vectors which represent the data bit during each code period.

Since the *a priori* probabilities of a signal's presence are unknown, the Neyman-Pearson criterion maximizes the probability of detection, P_d, under a particular probability of false alarm constraint, P_f. The optimum test consists of using the observation $\mathbf{r}$, to find the likelihood ratio $\Lambda(\mathbf{r})$, and then comparing this result to a threshold to make a decision [46]. The likelihood ratio is a ratio of conditional joint probabilities, and is, therefore, a scalar:

$$\Lambda(\mathbf{r}) \triangleq \frac{p(\mathbf{r} \mid H_1)}{p(\mathbf{r} \mid H_0)}. \tag{3.2}$$

The likelihood ratio test is:

$$\Lambda(\mathbf{r}) \underset{H_0}{\overset{H_1}{\gtrless}} \lambda, \tag{3.3}$$

where the threshold, λ, is determined by a fixed P_f:

$$P_f = \int_{\lambda}^{\infty} p(\Lambda \mid H_0)\, \mathrm{d}\Lambda. \tag{3.4}$$

The subseuqent development of optimal detectors for L1C acquisition consists of finding the likelihood ratio in (3.2) for each scenario.

3.3 Unknown Pilot Overlay Code Phase and Data Bits

Under the condition that the navigation data bits and the pilot overlay code phase are unknown, the optimal detector as derived in Appendix C is:

$$\sum_{\mathbf{d_P},\mathbf{d_D}\in\{B\}} I_0\left(\frac{\sqrt{C}}{\sigma^2}\sqrt{x^2+y^2}\right) \underset{H_0}{\overset{H_1}{\gtrless}} \lambda', \tag{3.5}$$

where the sum is over the set of all possible pilot and data bit combinations $\{B\}$, I_0 is the modified Bessel function of zeroth order, and

$$\begin{aligned} x &= \sum_{k=1}^{K}\Big(\sqrt{\alpha}I_{P,k}d_{P,k} + \sqrt{\beta}I_{D,k}d_{D,k}\Big), \\ y &= \sum_{k=1}^{K}\Big(\sqrt{\alpha}Q_{P,k}d_{P,k} + \sqrt{\beta}Q_{D,k}d_{D,k}\Big). \end{aligned} \tag{3.6}$$

This optimal detector in has two primary disadvantages. First, this detector requires knowledge of the Carrier-to-Noise ratio. Second, it requires multiple computationally intensive Bessel functions. Approximations to the Bessel function do exist, however, to simplify this detector.

3.3.1 Low SNR Approximation of Optimal Detector

A low SNR version of the optimal detector is found by using an approximation for the modified Bessel function [46]:

$$I_0(x) \simeq 1 + \frac{x^2}{4}, \quad x \ll 1. \tag{3.7}$$

After using 3.7, the likelihood function is now:

$$\Lambda'(\mathbf{r}) = \sum_{\mathbf{d_P},\mathbf{d_D}\in\{B\}}\left[\sum_{k=1}^{K}\Big(\sqrt{\alpha}I_{P,k}d_{P,k}+\sqrt{\beta}I_{D,k}d_{D,k}\Big)\right]^2 + \left[\sum_{k=1}^{K}\Big(\sqrt{\alpha}Q_{P,k}d_{P,k}+\sqrt{\beta}Q_{D,k}d_{D,k}\Big)\right]^2. \tag{3.8}$$

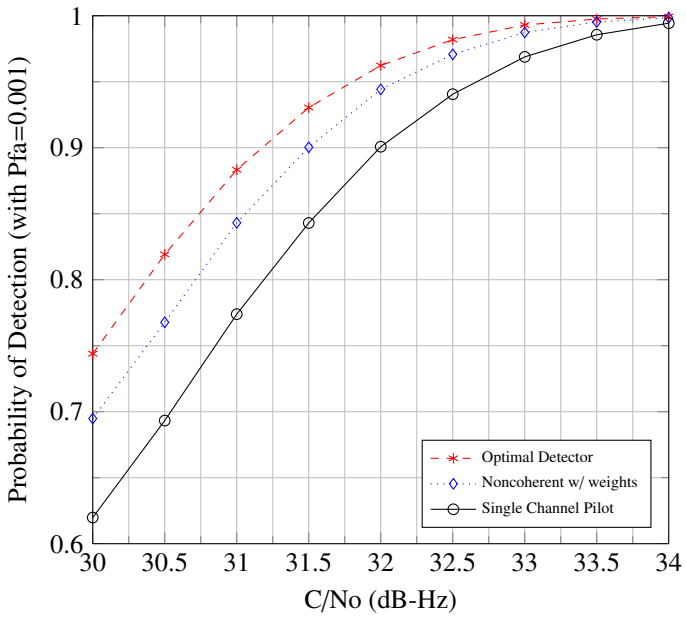

Figure 3.1: Probability of detection for the L1C optimal detector using one spreading code period at a fixed false alarm rate of 0.001. Simulation results compare the performance of the optimal detector to noncoherent combining with unequal power compensation and to the single channel detector that uses the pilot component only.

By modeling the pilot and the data bits as random and equally probable, all of the cross terms of (3.8) cancel after summing over all possible bit combinations. The low SNR approximation of the optimal detector (3.8) reduces to a non-coherent combining detector with scale factors for unequal power compensation:

$$\Lambda'(\mathbf{r}) = \sum_{k=1}^{K} \left(\alpha I_{P,k}^2 + \alpha Q_{P,k}^2 + \beta I_{D,k}^2 + \beta Q_{D,k}^2 \right). \tag{3.9}$$

Simulation results showing the detection probabilities at a fixed false alarm rate are shown in Fig. 3.1 for acquisition over one spreading code period. The results show that the optimal detector has a 1.5 dB sensitivity improvement over the single channel pilot detector at a false alarm rate of 0.9. The noncoherent detector also has an advantage over the single channel detector and is about 0.5 dB less sensitive than the optimal detector. Figs. 3.2 and 3.3 illustrate, however, that the gap between the optimal and noncoherent detectors increases when the total integration time is extended out to three and five spreading code periods.

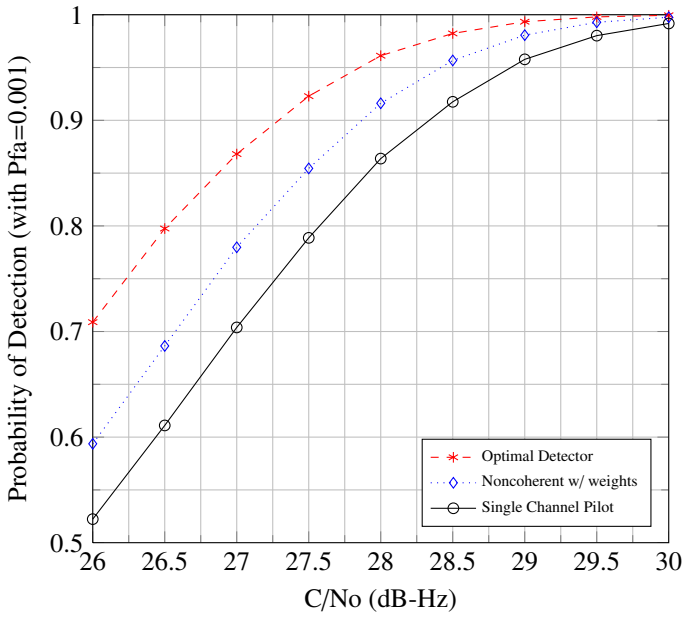

Figure 3.2: Probability of detection for the L1C optimal detector using three spreading code periods at a fixed false alarm rate of 0.001. Simulation results compare the performance of the optimal detector to noncoherent combining with unequal power compensation and to the single channel detector that uses the pilot component only.

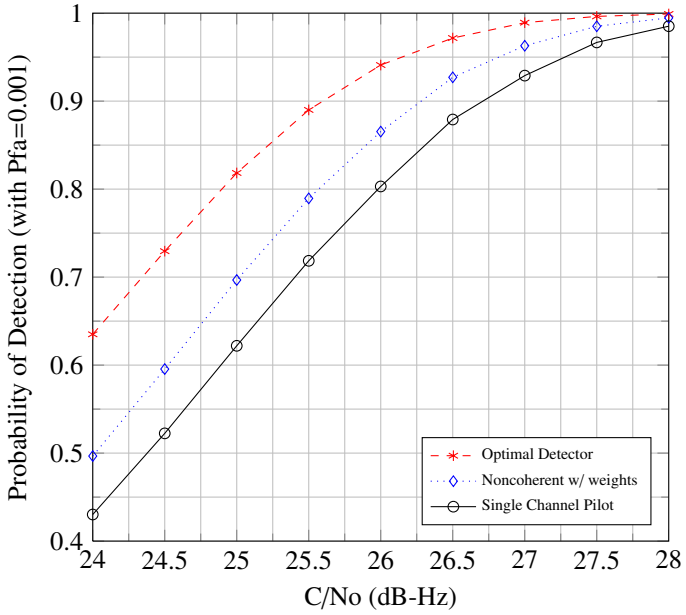

Figure 3.3: Probability of detection for the L1C optimal detector using five spreading code periods at a fixed false alarm rate of 0.001. Simulation results compare the performance of the optimal detector to noncoherent combining with unequal power compensation and to the single channel detector that uses the pilot component only.

3.4 Known Pilot Overlay Code Phase and Unknown Data Bits

The overlay code on the pilot component is a deterministic 1800 bit sequence. The scenario in which the receiver has sufficient time accuracy to use these known bits in the acquisition process is now investigated. As derived in Appendix C, the likelihood ratio for the optimal detector from (C.17) is:

$$\Lambda'(\mathbf{r}) = \sum_{\mathbf{d_D}\in\{B\}} I_0\left(\frac{\sqrt{C}}{\sigma^2}\sqrt{x^2+y^2}\right), \tag{3.10}$$

where:

$$\begin{aligned} x &= \sum_{k=1}^{K}\left(\sqrt{\alpha}I_{P,k}d_{P,k} + \sqrt{\beta}I_{D,k}d_{D,k}\right), \\ y &= \sum_{k=1}^{K}\left(\sqrt{\alpha}Q_{P,k}d_{P,k} + \sqrt{\beta}Q_{D,k}d_{D,k}\right). \end{aligned} \tag{3.11}$$

Simulation results showing the detection probabilities at a fixed false alarm rate when the data overlay code phase is known are shown in Fig. 3.4 for acquisition over one spreading code period. The optimal detector with known pilot code phase has the same performance in terms of detection probability as the optimal detector with no *a priori* knowledge. The optimal detector over one spreading code period depends on the relative sign between the data and pilot overlay code bits so that knowledge the overlay code bit doesn't actually help. Figs. 3.5 and 3.6 illustrate that the optimal detector for the known pilot starts to have an increasing performance improvement over the optimal detector with no knowledge as the total integration time is extended out to three and five spreading code periods.

3.4.1 Low SNR Approximation of Optimal Detector with Known Pilot Overlay Code Phase

Using (3.7), a low SNR approximation for the optimal detector with known pilot overlay code phase is:

$$\Lambda'(\mathbf{r}) = \sum_{\mathbf{d_D}\in\{B\}}\left[\sum_{k=1}^{K}\left(\sqrt{\alpha}I_{P,k}d_{P,k}+\sqrt{\beta}I_{D,k}d_{D,k}\right)\right]^2 + \left[\sum_{k=1}^{K}\left(\sqrt{\alpha}Q_{P,k}d_{P,k}+\sqrt{\beta}Q_{D,k}d_{D,k}\right)\right]^2. \tag{3.12}$$

The averaging is only over the data bits, and not over the known pilot bits; hence, not all the cross terms cancel here after summing over all possible bit combinations when $K > 1$. Once

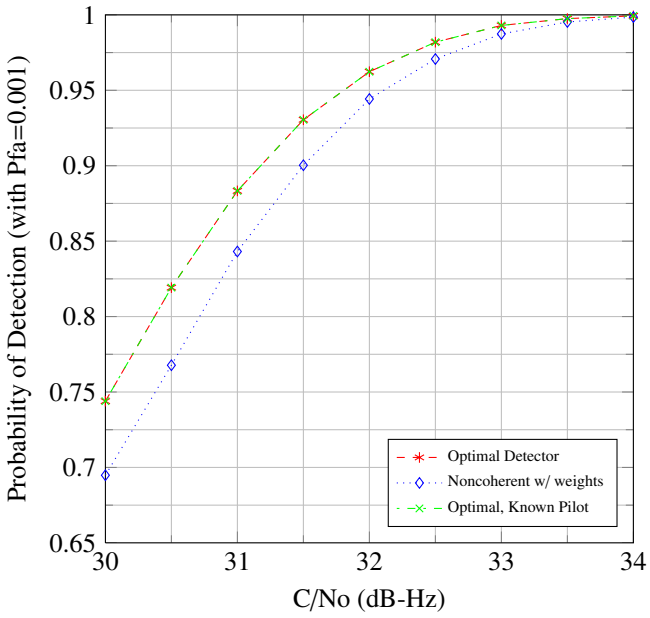

Figure 3.4: Probability of detection for the L1C optimal detector with known pilot overlay code phase using one spreading code period at a fixed false alarm rate of 0.001. Simulation results compare the performance to the optimal detector with *a priori* knowledge and to the noncoherent combining detector with unequal power compensation.

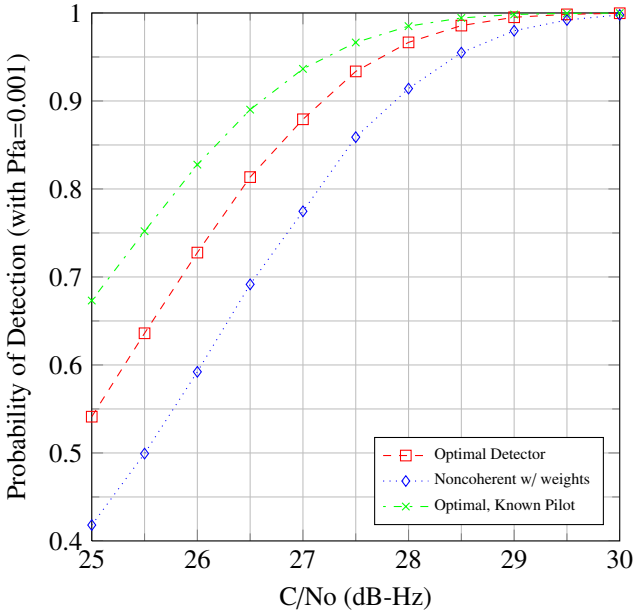

Figure 3.5: Probability of detection for the L1C optimal detector with known pilot overlay code phase using three spreading code periods at a fixed false alarm rate of 0.001. Simulation results compare the performance to the optimal detector with *a priori* knowledge and to the noncoherent combining detector with unequal power compensation.

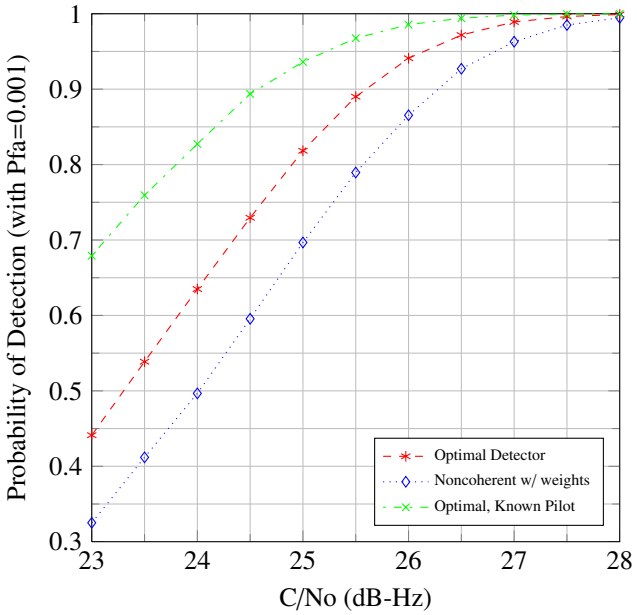

Figure 3.6: Probability of detection for the L1C optimal detector with known pilot overlay code phase using five spreading code periods at a fixed false alarm rate of 0.001. Simulation results compare the performance to the optimal detector with *a priori* knowledge and to the noncoherent combining detector with unequal power compensation.

again, this low SNR approximation will reduce to the non-coherent combining detector when observing only one code period, $K = 1$, but will have additional terms:

$$\Lambda'(\mathbf{r}) = \begin{cases} \sum_{k=1}^{K} \left(\alpha I_{P,k}^2 + \alpha Q_{P,k}^2 + \beta I_{D,k}^2 + \beta Q_{D,k}^2\right) & K = 1, \\ \left[\left(\alpha I_{P,1}^2 + \alpha Q_{P,1}^2 + \beta I_{D,1}^2 + \beta Q_{D,1}^2\right)\right. & \\ \left. + \sum_{k=1}^{K} \left(\alpha I_{P,k}^2 + \alpha Q_{P,k}^2 + \beta I_{D,k}^2 + \beta Q_{D,k}^2 + 2\alpha I_{P,k} d_{P,k} \sum_{m=1}^{K-1} I_{P,m} d_{P,m}\right)\right] & K > 1. \end{cases} \tag{3.13}$$

Simulation results showing the detection probabilities at a fixed false alarm rate for the low SNR approximation, when the data overlay code phase is known, are shown in Figs. 3.7, 3.8 and 3.9. These plots show that the low SNR approximation is within 0.5 dB of the optimal detector for SNR levels that give a detection probability of 0.9.

3.5 Known Pilot Overlay Code Phase and Known Data Bits

In some assisted situations, the overlay code phase and navigation data may be known by the receiver. As derived in Appendix C, the optimal detector in this situation from (C.21)

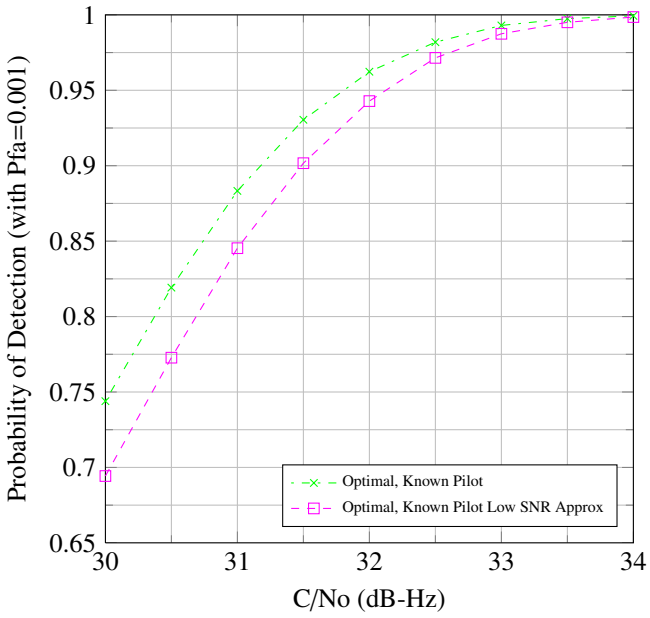

Figure 3.7: Probability of detection for the low SNR approximation to the L1C optimal detector with known pilot overlay code phase using one spreading code period at a fixed false alarm rate of 0.001. Simulation results compare the performance to the optimal detector with knowledge of the pilot overlay code phase.

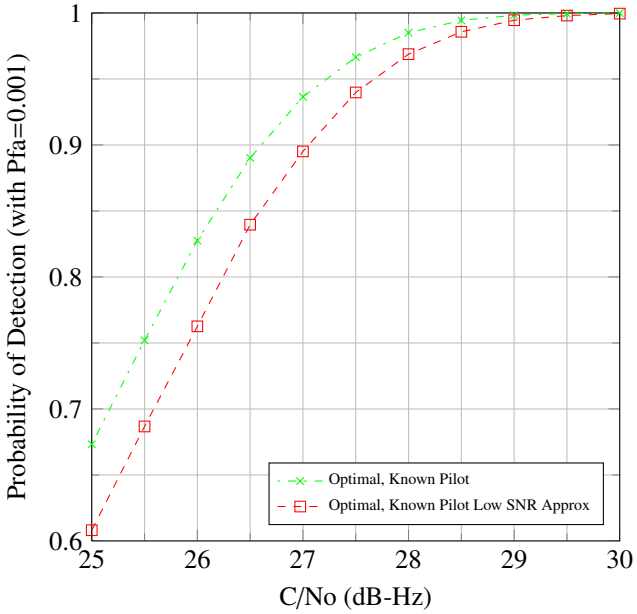

Figure 3.8: Probability of detection for the low SNR approximation to the L1C optimal detector with known pilot overlay code phase using three spreading code periods at a fixed false alarm rate of 0.001. Simulation results compare the performance to the optimal detector with knowledge of the pilot overlay code phase.

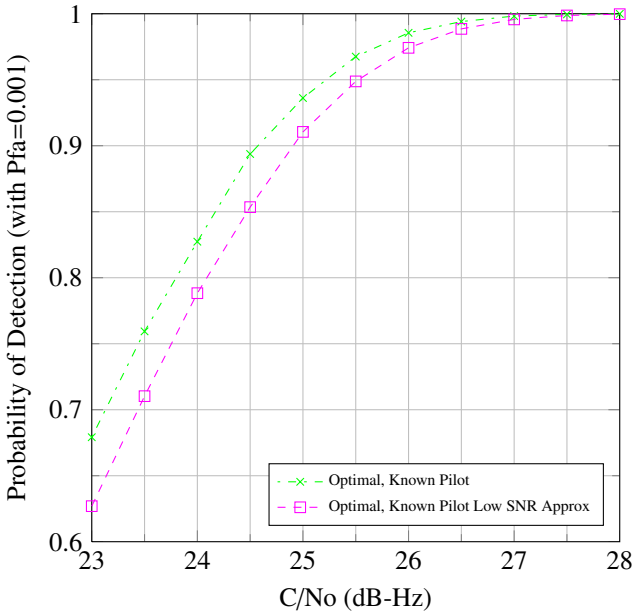

Figure 3.9: Probability of detection for the low SNR approximation to the L1C optimal detector with known pilot overlay code phase using five spreading code periods at a fixed false alarm rate of 0.001. Simulation results compare the performance to the optimal detector with knowledge of the pilot overlay code phase.

simplifies to:

$$\Lambda'(\mathbf{r}) = \left[\sum_{k=1}^{K}\left(\sqrt{\alpha}I_{P,k}d_{P,k}+\sqrt{\beta}I_{D,k}d_{D,k}\right)\right]^2 + \left[\sum_{k=1}^{K}\left(\sqrt{\alpha}Q_{P,k}d_{P,k}+\sqrt{\beta}Q_{D,k}d_{D,k}\right)\right]^2. \quad (3.14)$$

The additional *a priori* knowledge of this detector improves its performance over each of the other optimal detectors in different receiver scenarios as seen in Figs. 3.10 and 3.11. These figures show the best detector performance possible by using knowledge of the data bits and pilot overlay code phase.

3.6 Chapter Summary

Optimal detectors for GPS L1C acquisition in additive white Gaussian noise were derived herein based on three different levels of *a priori* receiver knowledge: no knowledge of pilot overlay code phase or navigation data, knowledge of pilot overlay code phase, and knowledge of each. Performance based on detection probabilities at a fixed false alarm rate was determined using Monte Carlo simulations. These optimal detectors can be used as

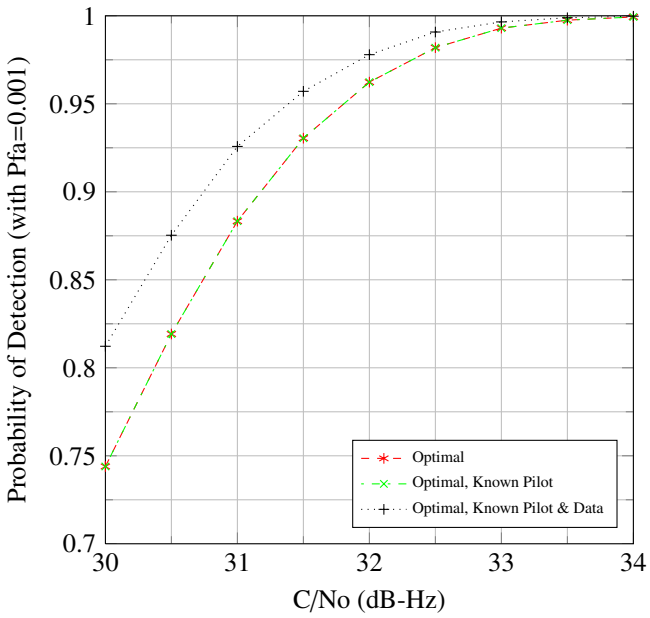

Figure 3.10: Probability of detection for the optimal detector with knowledge of pilot overlay code phase and navigation data using one spreading code period at a fixed false alarm rate of 0.001. Simulation results compare the performance to the optimal detector with knowledge of the pilot overlay code phase and the optimal detector with no *a priori* knowledge.

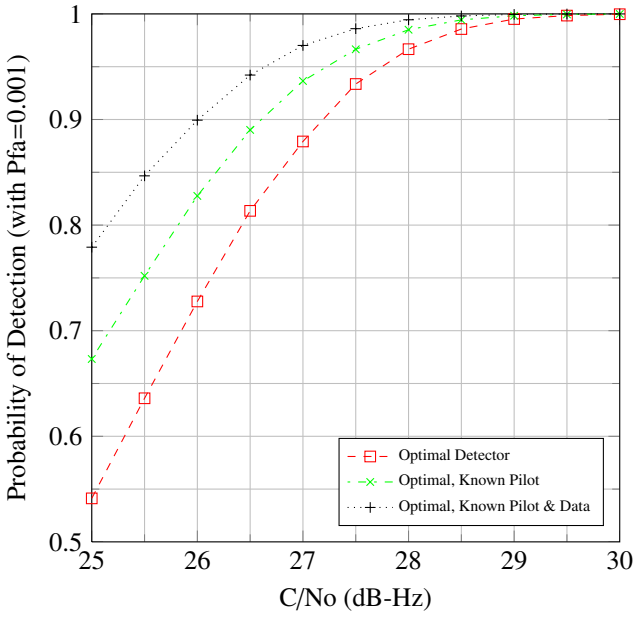

Figure 3.11: Probability of detection for the optimal detector with knowledge of pilot overlay code phase and navigation data using three spreading code periods at a fixed false alarm rate of 0.001. Simulation results compare the performance to the optimal detector with knowledge of the pilot overlay code phase and the optimal detector with no *a priori* knowledge.

a benchmark to compare various acquisition schemes. Implementation of these optimal detectors when any of the data or overlay code bits are unknown, however, presents a computational burden and depends on knowledge of the SNR; thus, Chapter 4 proposes various sub-optimal detectors and compares their performance to that of the optimal detectors.

CHAPTER 4

SUB-OPTIMAL DETECTORS FOR GPS L1C ACQUISITION

4.1 Introduction

This chapter proposes various sub-optimal detectors for GPS L1C acquisition that are more efficient to implement than the optimal detectors derived in Chapter 3. The probability of detection is used to compare performance. Analytical expressions for detection and false alarm probabilities are derived when possible and verified by simulation results. Once again, Monte Carlo simulations are performed with 10^6 trials to determine the probability of detection at each Carrier-to-Noise ratio for a fixed false alarm probability of 10^{-3}.

Techniques to combine the L1C pilot and data components are first proposed and evaluated. Noncoherent integration for signals with unequal power is presented. Coherent channel combining and semi-coherent integration schemes, each with unequal power compensation, are explored. Finally, detectors to use when the the receiver has knowledge of the pilot overlay code phase, inlcluding differentially coherent integration are shown.

4.2 Noncoherent Integration for Signals With Unequal Power

Either the pilot or the data component may be used for acquisition of two-component GNSS signals [29, 30, 31] with preference given to the component with the highest power, if applicable, as in GPS L1C. Since the phase of the carrier is unknown, the conventional noncoherent detection algorithm squares the output of the correlators and adds them together to get the decision variable, which in the case of acquisition of the pilot component, is:

$$Z_{\text{scp}} = \sum_{k=1}^{K} \left(I_{P,k}^2 + Q_{P,k}^2 \right), \tag{4.1}$$

where *scp* in the subscript stands for single channel pilot. Analytical expressions for the false alarm and detection probabilities are well known and shown in (2.52) and (2.53).

To avoid wasting power during acquisition, the incoming signal may be separately correlated with a local replica of the pilot and the data spreading codes [32]. Noncoherent

channel combining results when these correlator outputs are squared and then summed to obtain the decision variable, shown in (2.54). However, the low SNR approximation of the optimal detector in (3.9) highlighted the need to compensate for unequal power split between the different signal components. Noncoherent channel combining for L1C acquisition should scale the squared correlator outputs to obtain the decision variable:

$$Z_{\text{ncw}} = \sum_{k=1}^{K} \left(\alpha I_{P,k}^2 + \alpha Q_{P,k}^2 + \beta I_{D,k}^2 + \beta Q_{D,k}^2 \right), \tag{4.2}$$

where α and β represent the power split between the pilot and the data components. For GPS L1C:

$$\alpha = \frac{3}{4} \quad \text{and} \quad \beta = \frac{1}{4}.$$

Noncoherent channel combining of two-component GNSS signals with equal power leads to a chi-square random variable with $4K$ degrees of freedom. Now that we have scaled each component according to the relative power split, the underlying Gaussian random variables will have different variances. The decision statistic, Z_{ncw}, is therefore a sum of two chi-square random variables, each with $2K$ degrees of freedom. When the signal is not present, or when incorrect delay and Doppler estimates are used these random variables will have a central chi-square distribution. When the delay and Doppler estimates are correct, Z is a sum of two non-central chi-square random variables with noncentrality parameters:

$$a_P^2 = \alpha^2 KC \quad \text{and} \quad a_D^2 = \beta^2 KC \tag{4.3}$$

The Gaussian random variables that are squared and summed have the following varainces due to the unequal power compensation:

$$\sigma_P^2 = \alpha\sigma^2 \quad \text{and} \quad \sigma_D^2 = \beta\sigma^2, \tag{4.4}$$

where σ^2 is the noise power in correlator outputs as defined in (2.40).

The false alarm and detection probabilities are found directly from the cumulative distribution functions (CDF) of the decision statistic under each hypothesis:

$$P_{fa}^{ncw}(\lambda) = P(Z > \lambda \mid H_0) = 1 - P(Z < \lambda \mid H_0) \tag{4.5}$$

and

$$P_d^{ncw}(\lambda) = P(Z > \lambda \mid H_1) = 1 - P(Z < \lambda \mid H_1). \tag{4.6}$$

Using the CDFs of the sum the two independent chi square random variables provided by Simon in [47], the false alarm and detection probabilities of noncoherent combining for L1C acquisition using K spreading code periods are:

$$\begin{aligned} P_{fa}^{ncw}(\lambda) = \exp\left(\frac{\lambda}{2\alpha\sigma^2}\right)\frac{1}{(K-1)!}\left(\frac{\alpha}{\alpha-\beta}\right)^K \sum_{i=0}^{K-1}\sum_{l=0}^{i}\frac{(2(K-1)-i)!}{(i-l)!\,(K-1-i)!} \\ \cdot\left(\frac{\beta}{\beta-\alpha}\right)^{K-1-i}\left(\frac{\lambda}{2\alpha\sigma^2}\right)^{i-l} \\ -\exp\left(\frac{\lambda}{2\beta\sigma^2}\right)\frac{1}{(K-1)!}\left(\frac{\beta}{\beta-\alpha}\right)^K \sum_{i=0}^{K-1}\sum_{l=0}^{i}\frac{(2(K-1)-i)!}{(i-l)!\,(K-1-i)!} \\ \cdot\left(\frac{\alpha}{\alpha-\beta}\right)^{K-1-i}\left(\frac{\lambda}{2\beta\sigma^2}\right)^{i-l} \end{aligned} \tag{4.7}$$

and

$$\begin{aligned} P_d^{ncw}(\lambda) = \left(\frac{\alpha}{\beta}\right)^{2K}\exp\left(-\frac{\beta KC}{2\sigma^2}\right)\sum_{i=0}^{\infty}\sum_{l=0}^{\infty}\frac{\Gamma(K+i+l)}{i!l!\Gamma(K+l)}\left(\frac{\alpha\beta KC}{2}\right)^l\left(\frac{\beta-\alpha}{\beta}\right)^i \\ \cdot\left[1 - Q_{2K+i+l}\left(\frac{\sqrt{\alpha KC}}{\sigma}, \frac{\sqrt{\lambda}}{\sqrt{\alpha}\sigma}\right)\right] \end{aligned} \tag{4.8}$$

Fig. 4.1 compares the performance of a single channel detector using the pilot component only with the performance of the noncoherent combining detector using both the analytical results as well as results from Monte Carlo simulations. As seen in this figure, the simulation results match the analytical results, and, as expected, the noncoherent combining detector outperforms acquisition on a single channel.

4.3 Coherent Channel Combining With Unequal Power Compensation

The coherent channel combining technique proposed for two-component GNSS signals with equal power may be altered to compensate for two-component GNSS signals with unequal power splits. The decision variable now incorporates a weighting of each correlator output:

$$Z_{\text{chw}} = \max\left\{|z^+|^2, |z^-|^2\right\}, \tag{4.9}$$

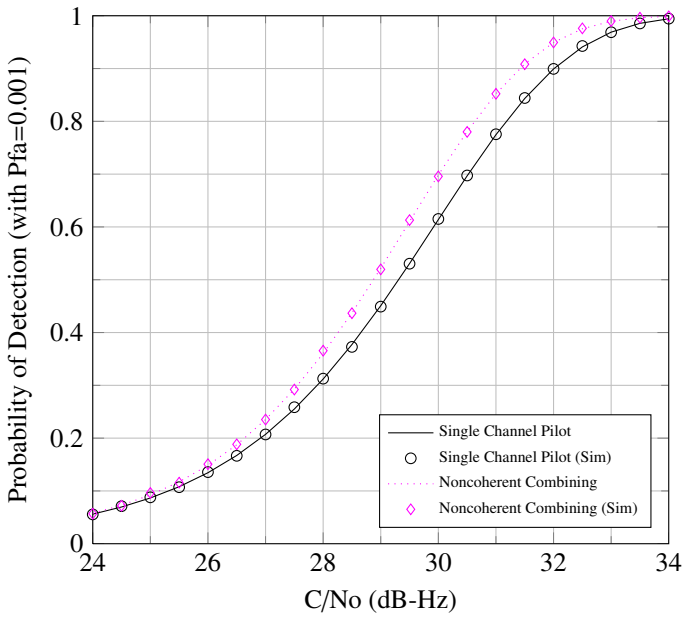

Figure 4.1: Performance of single channel detector (using pilot component) compared to noncoherent combining detector with simulated and analytical results.

where:

$$z^+ = \sqrt{\alpha} I_P + \mathrm{j}\sqrt{\alpha} Q_P + \sqrt{\beta} I_D + \mathrm{j}\sqrt{\beta} Q_D, \tag{4.10a}$$

$$z^- = \sqrt{\alpha} I_P + \mathrm{j}\sqrt{\alpha} Q_P - \sqrt{\beta} I_D - \mathrm{j}\sqrt{\beta} Q_D, \tag{4.10b}$$

and

$$|z^+|^2 = \left(\sqrt{\alpha} I_P + \sqrt{\beta} I_D\right)^2 + \left(\sqrt{\alpha} Q_P + \sqrt{\beta} Q_D\right)^2, \tag{4.11a}$$

$$|z^-|^2 = \left(\sqrt{\alpha} I_P - \sqrt{\beta} I_D\right)^2 + \left(\sqrt{\alpha} Q_P - \sqrt{\beta} Q_D\right)^2, \tag{4.11b}$$

with the following weights for GPS L1C:

$$\alpha = \frac{3}{4} \quad \text{and} \quad \beta = \frac{1}{4}.$$

As in the case of coherent channel combining without compensation for unequal power, $|z^+|^2$ and $|z^-|^2$ are chi-square random variables with two degrees of freedom. However, because of the weights applied, the underlying Gaussian random variables have a variance of σ^2, instead of $2\sigma^2$. When the signal is present with correct estimates of delay and Doppler,

the noncentrality parameter for $|z^+|^2$ is:

$$\begin{aligned}
a^2_{+,chw} &= \left(\tfrac{3}{4}\sqrt{C}d_P\cos(\Delta\theta) + \tfrac{1}{4}\sqrt{C}d_D\cos(\Delta\theta)\right)^2 + \left(\tfrac{3}{4}\sqrt{C}d_P\sin(\Delta\theta) + \tfrac{1}{4}\sqrt{C}d_D\sin(\Delta\theta)\right)^2 \\
&= \left(\tfrac{5}{8} + \tfrac{3}{8}d_Pd_D\right)C\cos^2(\Delta\theta) + \left(\tfrac{5}{8} + \tfrac{3}{8}d_Pd_D\right)C\sin^2(\Delta\theta) \\
&= \left(\tfrac{5}{8} + \tfrac{3}{8}d_Pd_D\right)C \\
&= \begin{cases} C, \text{ correct rel. sign } (d_Pd_D = 1) \\ \\ \tfrac{1}{4}C, \text{ incorrect rel. sign } (d_Pd_D = -1). \end{cases}
\end{aligned} \tag{4.12}$$

The noncentrality parameter for $|z^-|^2$ is:

$$\begin{aligned}
a^2_{-,chw} &= \left(\tfrac{3}{4}\sqrt{C}d_P\cos(\Delta\theta) - \tfrac{1}{4}\sqrt{C}d_D\cos(\Delta\theta)\right)^2 + \left(\tfrac{3}{4}\sqrt{C}d_P\sin(\Delta\theta) - \tfrac{1}{4}\sqrt{C}d_D\sin(\Delta\theta)\right)^2 \\
&= \left(\tfrac{5}{8} - \tfrac{3}{8}d_Pd_D\right)C\cos^2(\Delta\theta) + \left(\tfrac{5}{8} - \tfrac{3}{8}d_Pd_D\right)C\sin^2(\Delta\theta) \\
&= \left(\tfrac{5}{8} - \tfrac{3}{8}d_Pd_D\right)C \\
&= \begin{cases} C, \text{ correct rel. sign } (d_Pd_D = -1) \\ \\ \tfrac{1}{4}C, \text{ incorrect rel. sign } (d_Pd_D = 1). \end{cases}
\end{aligned} \tag{4.13}$$

Using the technique from (2.62) which noted that

$$\begin{aligned}
P\left(\max\left\{|z^+|^2, |z^-|^2\right\} > \lambda\right) &= 1 - P\left(\max\left\{|z^+|^2, |z^-|^2\right\} < \lambda\right) \\
&= 1 - P\left(|z^+|^2 < \lambda, |z^-|^2 < \lambda\right) \\
&= 1 - P\left(|z^+|^2 < \lambda\right)P\left(|z^-|^2 < \lambda\right),
\end{aligned} \tag{4.14}$$

the noncentrality parameters lead to the following false alarm and detection probabilities:

$$\begin{aligned}
P^{chw}_{fa}(\lambda) &= 1 - P\left(|z^+|^2 < \lambda \mid H_0\right)P\left(|z^-|^2 < \lambda \mid H_0\right) \\
&= 1 - \left[1 - \exp\left(\frac{-\lambda}{2\sigma^2}\right)\right]^2,
\end{aligned} \tag{4.15}$$

and

$$\begin{aligned}
P^{chw}_{d}(\lambda) &= 1 - P\left(|z^+|^2 < \lambda \mid H_1\right)P\left(|z^-|^2 < \lambda \mid H_1\right) \\
&= 1 - \left[1 - Q_1\left(\frac{\sqrt{C}}{\sigma}, \frac{\sqrt{\lambda}}{\sigma}\right)\right]\left[1 - Q_1\left(\frac{\sqrt{\frac{1}{4}C}}{\sigma}, \frac{\sqrt{\lambda}}{\sigma}\right)\right].
\end{aligned} \tag{4.16}$$

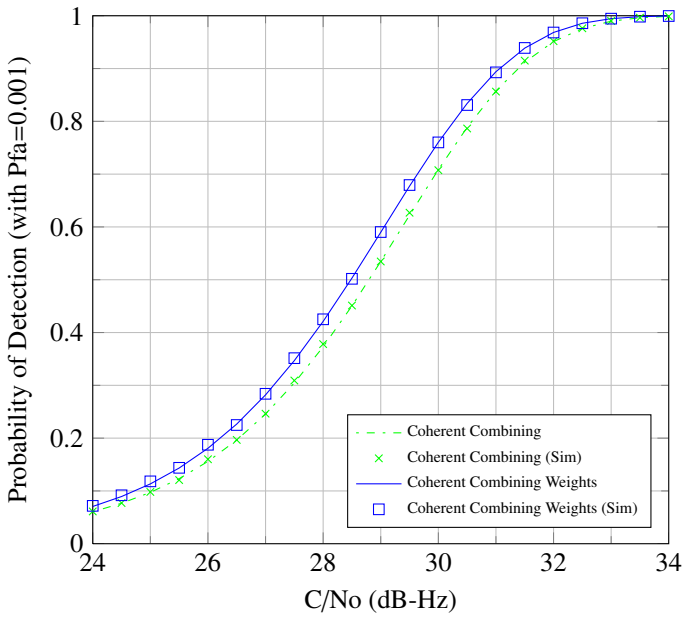

Figure 4.2: Performance of coherent combining detector compared to coherent combining with weights for unequal power detector.

These GPS L1C detectors were evaluated using Monte-Carlo computer simulations to confirm the analytical results. Fig. 4.2 compares the two coherent combining detectors, with and without weights for unequal power compensation. Once again, the simulation results verify the analytically-derived results. The performance of coherent channel combining is improved by compensating for the unequal power.

The performance of the optimal detector is compared to the other detectors in Fig. 4.3. The optimal and coherent combining detectors, with unequal power compensation, have similar performance and provide about a 1 dB advantage over single channel acquisition. Coherent channel combining without compensation for the unequal power in the pilot and the data components leads to performance similar to that of the noncoherent combining detector.

4.4 Semi-Coherent Integration With Unequal Power Compensation

The semi-coherent channel combining technique proposed for two component GNSS signals with equal power may be altered to compensate for two-component GNSS signals with

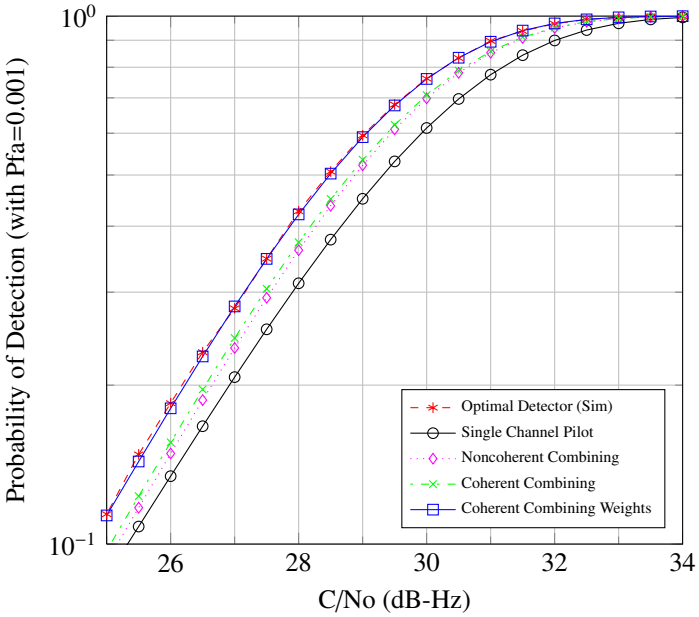

Figure 4.3: Performance of the optimal detector compared to the other channel combining detectors.

unequal power split. The decision variable now incorporates a weighting of each correlator output:

$$Z_{\text{semi}} = \sum_{k=1}^{K} \max\left\{|z_k^+|^2, |z_k^-|^2\right\}, \tag{4.17}$$

where:

$$z_k^+ = \sqrt{\alpha} I_{P,k} + \mathrm{j}\sqrt{\alpha} Q_{P,k} + \sqrt{\beta} I_{D,k} + \mathrm{j}\sqrt{\beta} Q_{D,k}, \tag{4.18a}$$

$$z_k^- = \sqrt{\alpha} I_{P,k} + \mathrm{j}\sqrt{\alpha} Q_{P,k} - \sqrt{\beta} I_{D,k} - \mathrm{j}\sqrt{\beta} Q_{D,k}, \tag{4.18b}$$

and

$$|z_k^+|^2 = \left(\sqrt{\alpha} I_{P,k} + \sqrt{\beta} I_{D,k}\right)^2 + \left(\sqrt{\alpha} Q_{P,k} + \sqrt{\beta} Q_{D,k}\right)^2, \tag{4.19a}$$

$$|z_k^-|^2 = \left(\sqrt{\alpha} I_{P,k} - \sqrt{\beta} I_{D,k}\right)^2 + \left(\sqrt{\alpha} Q_{P,k} - \sqrt{\beta} Q_{D,k}\right)^2, \tag{4.19b}$$

with the following weights for GPS L1C:

$$\alpha = \frac{3}{4} \quad \text{and} \quad \beta = \frac{1}{4}.$$

Analytical expressions for the detection and false alarm probabilities are intractable. The probability density functions of the decision statistic for $K = 1$, however, are easily found

by taking the derivative of the CDF. The CDF's of the decision statistics come directly by subtracting the false alarm or detection probabilities in (4.15) and (4.16) from one. The probability density functions of the decision statistic for $K = 1$ under the noise-only and signal present cases are:

$$f_Z^{K=1}(z; H_0) = \frac{1}{\sigma^2}\exp\left(\frac{-z}{\sigma^2}\right) - \frac{1}{\sigma^2}\exp\left(\frac{-z}{\sigma^2}\right), \tag{4.20}$$

$$\begin{aligned} f_Z^{K=1}(z; H_1) = {} & \frac{1}{4\sigma^2}\exp\left(\frac{-(1-\sqrt{3}/2)C - z}{4\sigma^2}\right) I_0\left(\frac{\sqrt{(1-\sqrt{3}/2)Cz}}{2\sigma^2}\right) \\ & \cdot\left[1 - Q_1\left(\frac{\sqrt{(1+\sqrt{3}/2)C}}{\sqrt{2}\sigma}, \frac{\sqrt{z}}{\sqrt{2}\sigma}\right)\right] \\ & + \frac{1}{4\sigma^2}\exp\left(\frac{-(1+\sqrt{3}/2)C - z}{4\sigma^2}\right) I_0\left(\frac{\sqrt{(1+\sqrt{3}/2)Cz}}{2\sigma^2}\right) \\ & \cdot\left[1 - Q_1\left(\frac{\sqrt{(1-\sqrt{3}/2)C}}{\sqrt{2}\sigma}, \frac{\sqrt{z}}{\sqrt{2}\sigma}\right)\right]. \end{aligned} \tag{4.21}$$

Numerical techniques may be used to find the detection and false alarm probabilities for a particular $K > 1$ from (4.20) and (4.21). For example, the Fourier transform of the density functions can be raised to the power of a particular value of K to find the characteristic functions of the decision statistics. The inverse Fourier transform can then be used to find the density functions. The detection and false alarm probabilities are found by integrating the density functions starting at the threshold.

Figs. 4.4 and 4.5 compare the performance of semi-coherent integration with noncoherent integration, using either the pilot or the two components, for various total integration times. Semi-coherent integration slightly outperforms the noncoherent integration when two spreading code periods are used (20 ms total integration time) but provides similar performance when 25 spreading code periods are used (C/N_0 of approximately 22 dB-Hz). The estimate of the relative sign between the pilot and the data bits is less reliable in lower SNR. At this point, noncoherent integration outperforms semi-coherent integration.

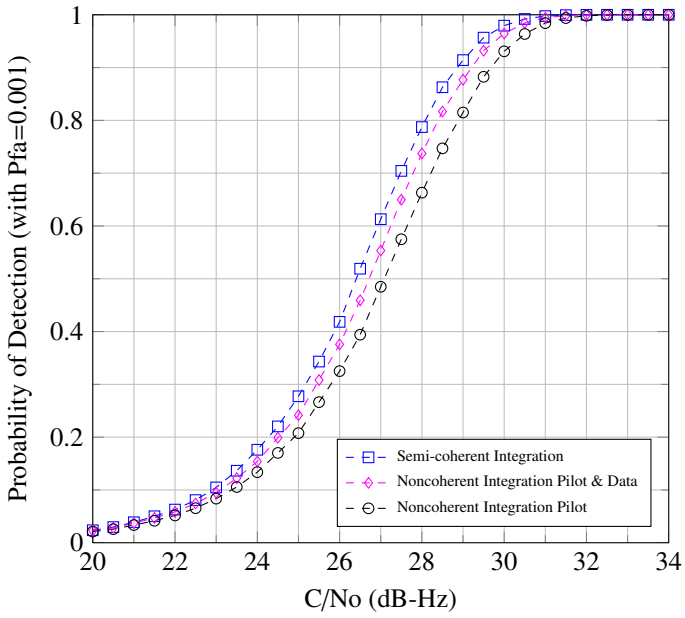

Figure 4.4: Simulation results that show the detection probability of the noncoherent combining detector using the pilot only, the noncoherent combining detector using the pilot and the data components, and the semi-coherent detector over two (K=2) primary spreading code periods at a fixed false alarm rate of 0.001.

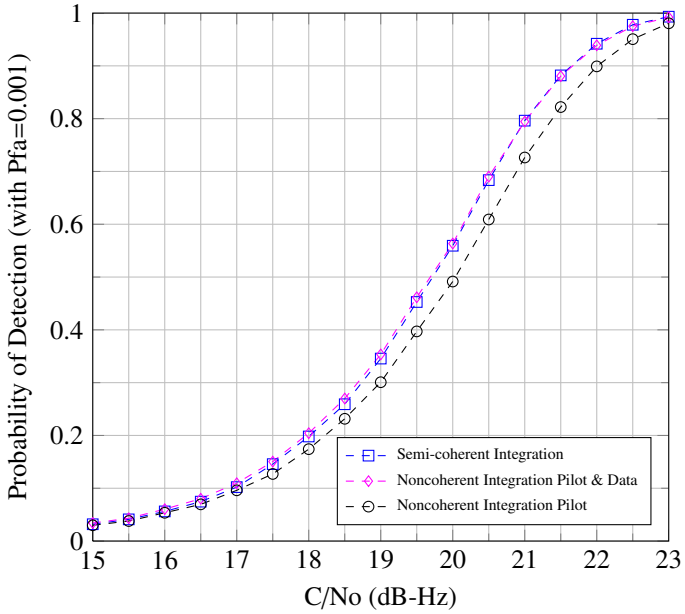

Figure 4.5: Simulation results that show the detection probability of the noncoherent combining detector using the pilot only, the noncoherent combining detector using the pilot and the data components, and the semi-coherent detector over twenty-five (K=25) primary spreading code periods at a fixed false alarm rate of 0.001.

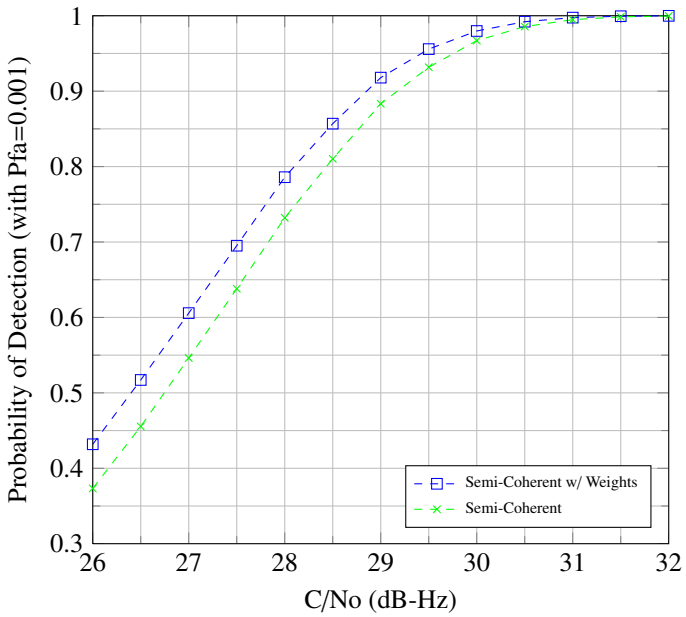

Figure 4.6: Simulation results that show the detection probability of semi-coherent integration with and without compensating for the data/pilot power split over two (K=2) primary spreading code periods.

An improvement of about 0.5 dB in detection performance of semi-coherent integration when compensated for the unequal power split between the data and pilot components is shown in Fig. 4.6. A unique feature of the L1C signal is this unequal power split between the data and pilot components. Receivers can easily implement the scale factor to achieve better performance.

In this section, results from various simulations are presented. In specific, the focus is on the detection probabilities of the various acquisition schemes discussed at a fixed false alarm rate of 0.001. As shown in Fig. 4.7, and also discussed in [48], performance of semi-coherent integration with unequal power compensation is equal to the optimal detector over one spreading code period, $K = 1$, where no noncoherent combinations are used.

Once multiple spreading code periods are used ($K > 1$), semi-coherent integration with unequal power compensation no longer matches the optimal detector, but it still outperforms the noncoherent combining detector, shown in Fig. 4.8 and Fig. 4.9.

Figs. 4.10 and 4.11 show the detection probabilities for K=10 and K=20, illustrating

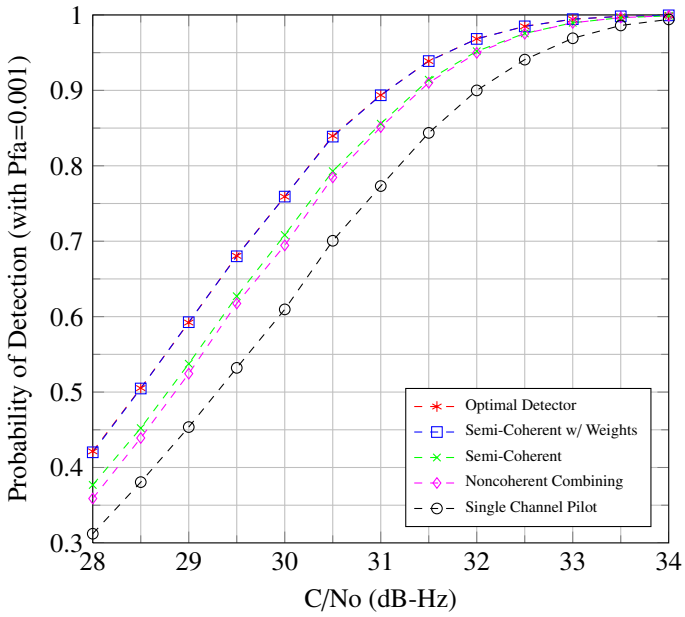

Figure 4.7: Simulation results that show the detection probability of various GPS L1C acquisition schemes over one (K=1) primary spreading code period.

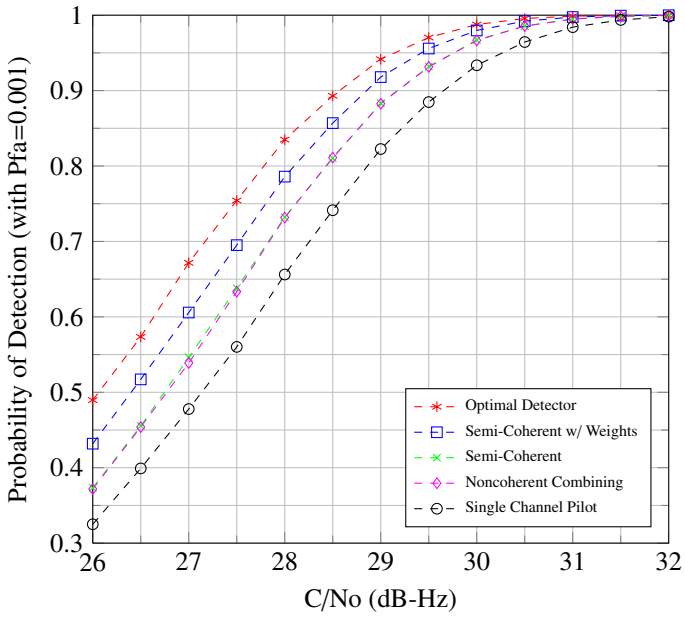

Figure 4.8: Simulation results that show the detection probability of various GPS L1C acquisition schemes over two (K=2) primary spreading code periods.

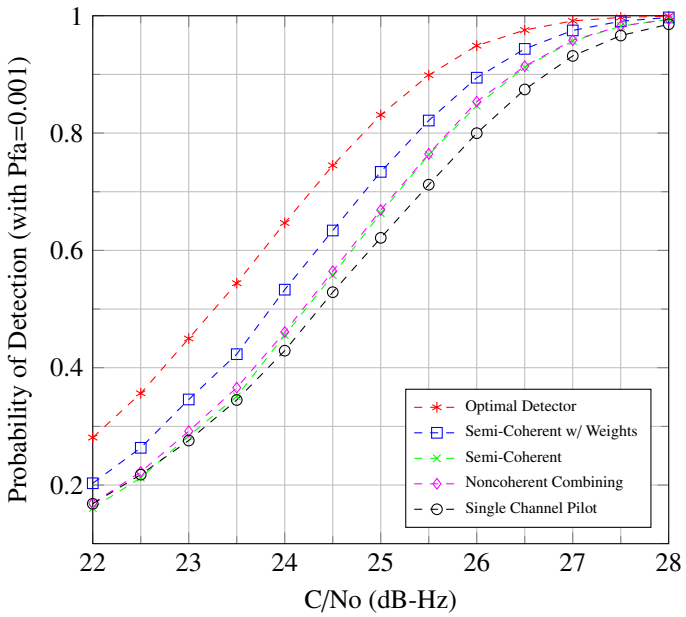

Figure 4.9: Simulation results that show the detection probability of various GPS L1C acquisition schemes over five (K=5) primary spreading code periods.

that semi-coherent integration with unequal power compensation does not provide the performance improvement over noncoherent combining at extended total integration times. This performance advantage disappears when approaching twenty spreading code periods, or a Carrier-to-Noise ratio of 23 dB-Hz.

The GPS L1C signal, like most modern GNSS signals, has a pilot and a data component, but with the unique aspect of an unequal power split between the two components. The optimal detector for GPS L1C acquisition over multiple spreading code periods, without knowledge of the navigation data and overlay code phase, was derived. In addition, noncoherently adding the coherent combinations of the pilot and the data components, or semi-coherent integration, was investigated. Semi-coherent integration was shown to provide a detection performance improvement, about 0.4 dB, over noncoherent combining when compensated for the unequal power split between the data and pilot components. Simulations show the performance of semi-coherent integration compared to the optimal detector, noncoherent combining, and pilot channel only acquisition.

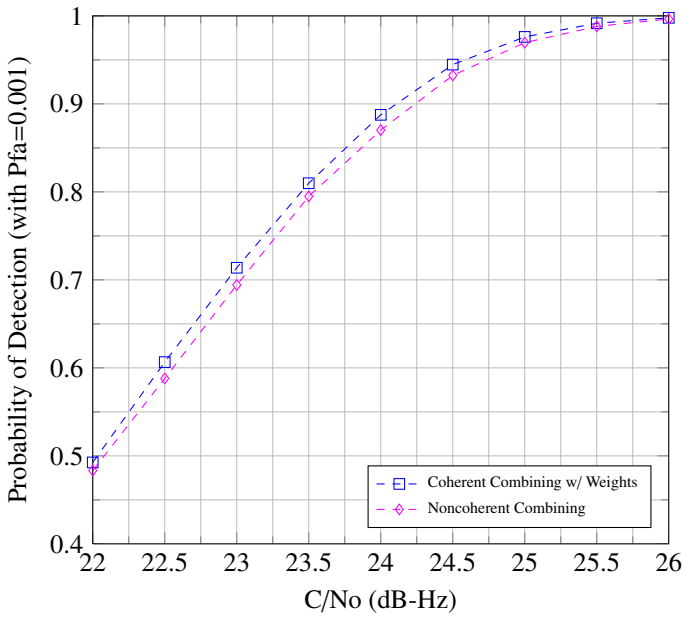

Figure 4.10: Simulation results that show the detection probability of semi-coherent integration with unequal power compensation and noncoherent combining over 10 primary spreading code periods (K=10).

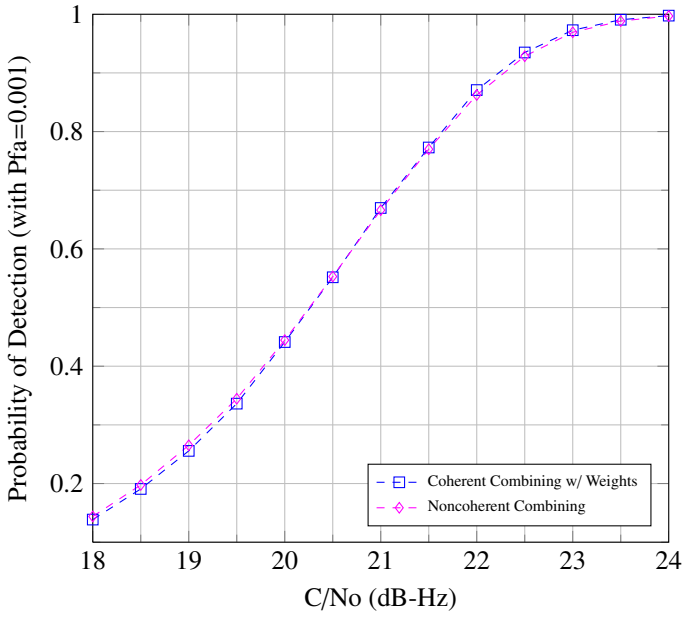

Figure 4.11: Simulation results that show the detection probability of semi-coherent integration with unequal power compensation and noncoherent combining over 20 primary spreading code periods (K=20).

4.5 Known Pilot Overlay Code Phase

Various circumstances exist when the code phase of the deterministic overlay code on the pilot component may be known by the receiver. In this section, various L1C detectors which exploit knowledge of the pilot overlay code phase are presented, and their performance is compared. First, when only the pilot component is used for acquisition, differentially-coherent integration is compared to coherent and noncoherent integration. Next, coherent integration of the data and pilot components, using relative pilot/data bit estimation is proposed.

If the pilot overlay code phase is known, then coherent integration can be performed on the pilot component:

$$Z_{\text{chp}}^{\text{kp}} = \left| \sum_{k=1}^{K} d_{P,k} \left(I_{P,k} + jQ_{P,k} \right) \right|^2, \tag{4.22}$$

where the *kp* in the superscript stands for known pilot overlay code phase, and *chp* in the subscript stands for coherent integration of the pilot component only. The total coherent integration time is limited by the phase error caused by the reference frequency error and unmodeled receiver velocity.

4.5.1 Differentially-Coherent Integration of the Pilot Component

Differentially-coherent integration has previously been proposed [40, 41, 42] to maintain the differential phase information between successive correlator outputs so that the detector is:

$$Z_{\text{diff}}^{\text{kp}} = Re\Big\{ \sum_{k=2}^{K} d_{P,k} d_{P,k-1} \left(I_{P,k} + jQ_{P,k} \right) \left(I_{P,k-1} + jQ_{P,k-1} \right)^* \Big\}, \tag{4.23}$$

where $*$ stands for the complex conjugate operation; *kp* in the superscript stands for known pilot overlay code phase; and *diff* in the subscript stands for differentially-coherent integration. The detector in (4.23) assumes that there is no Doppler uncertainty between successive correlator outputs.

If there is Doppler uncertainty between successive correlator outputs, then the detector

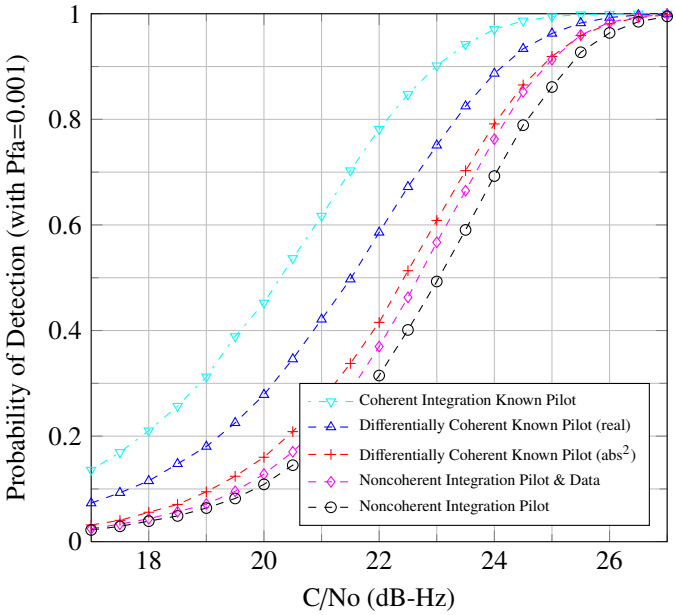

Figure 4.12: Simulation results that show the detection probability of the coherent combining detector using the pilot only, the differentially-coherent detector using the real part, the differentially-coherent detector using the magnitude squared and the noncoherent combining detectors for pilot plus data and pilot-only over eight (K=8) primary spreading code periods at a fixed false alarm rate of 0.001.

can be modified to capture information in the imaginary component of the product term:

$$Z_{\text{diffd}}^{\text{kp}} = \left| \sum_{k=2}^{K} d_{P,k} d_{P,k-1} \left(I_{P,k} + jQ_{P,k}\right) \left(I_{P,k-1} + jQ_{P,k-1}\right)^* \right|^2. \tag{4.24}$$

Figs. 4.12 and 4.13 show the performance of these differentially-coherent combining detectors is better than the noncoherent combining detectors when using extended total integration times. When the pilot overlay code phase is known, and coherent integration is not viable, due to local reference frequency error or user dynamics, differentially-coherent integration of the pilot component provides a performance advantage over noncoherent integration.

4.5.2 Coherent Integration using Relative Pilot/Data Sign Estimation

If the pilot overlay code phase is known, and the incoming signal is correlated with the local composite codes of pilot plus data and pilot minus data as in semi-coherent integration, then an estimate of the navigation bit can be found by estimating the relative sign between the

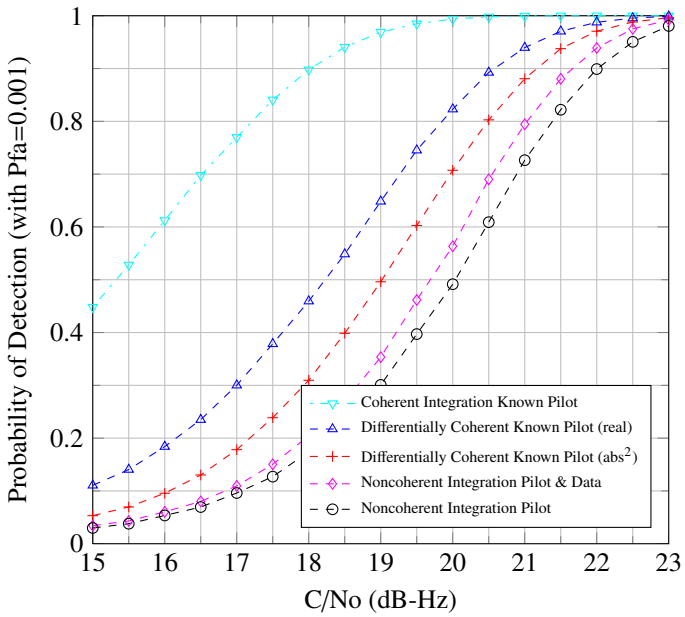

Figure 4.13: Simulation results that show the detection probability of the coherent combining detector using the pilot only, the differentially-coherent detector using the real part, the differentially-coherent detector using the magnitude squared and the noncoherent combining detectors for pilot plus data and pilot-only over twenty-five (K=25) primary spreading code periods at a fixed false alarm rate of 0.001.

pilot overlay code bit and the navigation data bit ($d_P d_D$):

$$\text{if } \max\left\{|z_k^+|^2, |z_k^-|^2\right\} = |z_k^+|^2 \text{ then } d_P d_D = +1,$$
$$\text{if } \max\left\{|z_k^+|^2, |z_k^-|^2\right\} = |z_k^-|^2 \text{ then } d_P d_D = -1.$$

Using either the pilot plus data or the pilot minus data correlator outputs with the highest power, as well as the known pilot overlay code phase, allows for coherent integration:

$$Z_{\text{chrel}}^{\text{kp}} = \left| \sum_{k=1}^{K} d_{P,k} z_k^{\pm} \right|^2, \tag{4.25}$$

where *kp* in the superscript stands for known pilot overlay code phase, and *chrel* in the subscript stands for coherent integration by estimating the relative sign between the pilot/data bits.

The previous detector is compared to the clairvoyant detector, which has knowledge of the deterministic pilot overlay code phase and the navigation data bits, and therefore, can

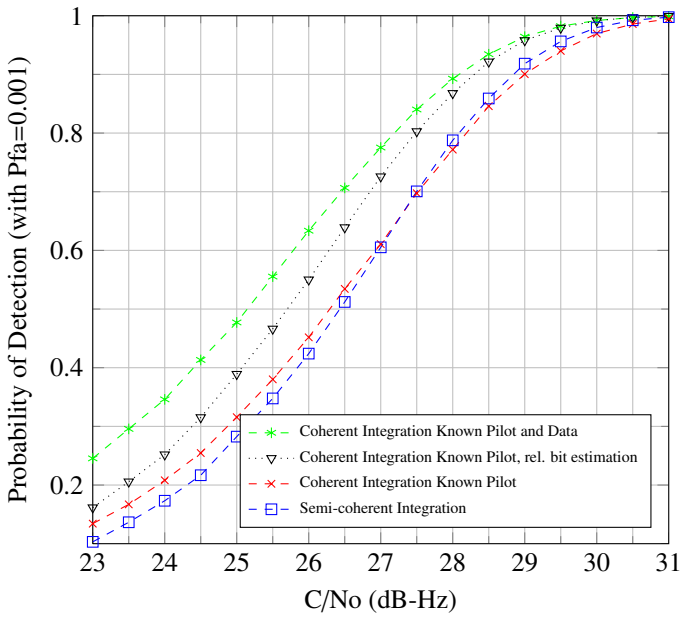

Figure 4.14: Simulation results that show the detection probability of coherent integration using relative pilot/data bit estimation and known pilot overlay code phase, semi-coherent integration, and standard coherent integration over two (K=2) primary spreading code periods at a fixed false alarm rate of 0.001.

perform coherent integration:

$$Z_{\text{ch}}^{\text{kpkd}} = \left| \sum_{k=1}^{K} d_{P,k} \sqrt{\alpha} \left(I_{P,k} + jQ_{P,k} \right) + d_{D,k} \sqrt{\beta} \left(I_{D,k} + jQ_{D,k} \right) \right|^2. \tag{4.26}$$

The total coherent integration time of these detectors is limited by the phase error caused by the reference frequency error and unmodeled receiver velocity.

Figs. 4.14, 4.15, and 4.16 show the performance of coherent integration using relative pilot/data bit estimation compared to semi-coherent integration and standard coherent integration. These results verify that when the pilot overlay code phase is known, coherent integration using relative pilot/data bit estimation provides better performance than coherent integration on the pilot alone, until the C/N_o degrades to approximately 23 dB-Hz. This technique also provides an estimation of the data bit since the pilot overlay code bit is known, and the relative sign between the pilot overlay code bit and navigation data bit has been estimated.

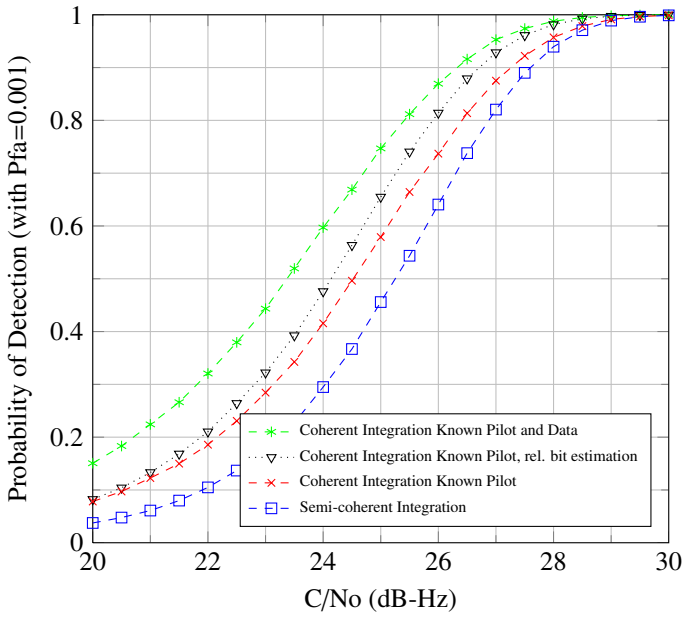

Figure 4.15: Simulation results that show the detection probability of coherent integration using relative pilot/data bit estimation and known pilot overlay code phase, semi-coherent integration and standard coherent integration over three (K=3) primary spreading code periods at a fixed false alarm rate of 0.001.

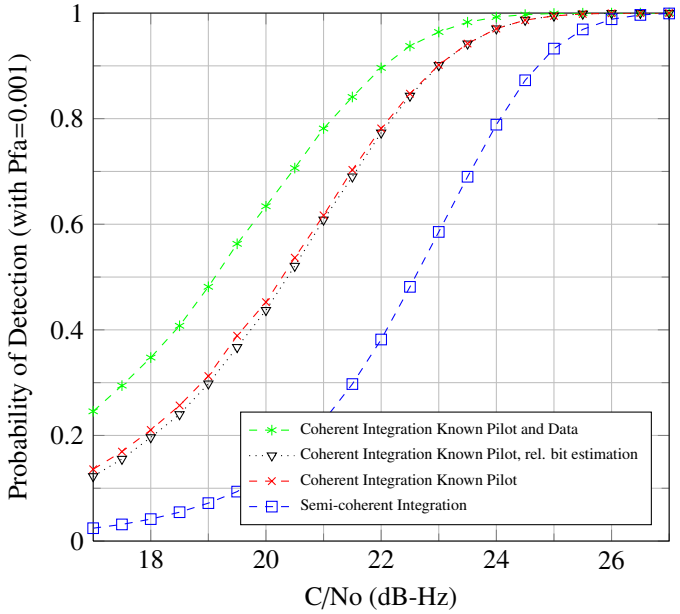

Figure 4.16: Simulation results that show the detection probability of coherent integration using relative pilot/data bit estimation and known pilot overlay code phase, semi-coherent integration and standard coherent integration over eight (K=8) primary spreading code periods at a fixed false alarm rate of 0.001.

4.6 Chapter Summary

Modernized GNSS signals allow a variety of GNSS receiver implementations. In acquisition of GPS L1C, receivers can use either the pilot component or the pilot and the data components. Several detectors with various integration schemes were presented herein and compared to traditional noncoherent integration and coherent integration. This chapter focused on two scenarios: when the pilot overlay code phase is known and when it is unknown.

Performance based on probability of detection at a fixed false alarm rate for various GPS L1C detectors was presented and compared. Differentially coherent integration when the pilot overlay code phase is known was shown to provide performance improvement over noncoherent integration when there is the need for extended integration times that prevent coherent integration. A new technique that uses the known pilot overlay code phase and relative pilot/data bit estimation provided better performance than coherent integration of the data component alone at higher SNR. Limits on the performance improvement for this technique, as well as semi-coherent integration, were presented.

CHAPTER 5

JOINT ACQUISITION OF GPS C/A AND L1C SIGNALS

5.1 Introduction

The upper L-Band will be the only frequency band with two different GPS civil signals available to users at the same carrier frequency with the legacy C/A code signal and the new L1C signal. The null-to-null bandwidth of the C/A code signal is 2.046 MHz. The TMBOC modulation of the L1C signal creates bandwidth of 4.092 MHz between the outer nulls of the largest spectral lobes in the split-spectrum signal. Without the need to have two separate radio-frequency chains in the front-end of a GPS receiver, using the GPS C/A and L1C signals will improve acquisition sensitivity with limited additional complexity. These two signals are transmitted in phase quadrature with the C/A signal lagging L1C by 90 degrees since the L1C signal is transmitted with the same phase as the the L1 P(Y) code military signal.

This chapter will explore various techniques for joint acquisition of GPS L1C and C/A signals. First, the nominal received power of these two signals is discussed along with the power split parameters required for optimal combining of the signals. Next, a model for the composite C/A code and L1C signal is presented. An optimal detector for joint acquisition is then derived and simulation results provided. Finally, sub-optimal, but more efficient, techniques are proposed and evaluated.

5.2 Received Power and Power Split Parameters

For optimal detection of composite signals with unequal power levels, the receiver needs to scale each signal by its relative power level, as demonstrated in this dissertation. Table 5.1 shows the nominal received power levels for C/A and L1C according to the specification documents [10, 14].

Since the L1C nominal received signal is 1.5 dBW higher than the C/A code, L1C has a

Table 5.1: Nominal Received Power Levels

Signal	Received Power
C/A Code	-158.5 dBW
L1C Pilot	-158.25 dBW
L1C Data	-163 dBW
L1C Composite	-157 dBW

received strength that is $10^{\frac{1.5}{10}} = 1.4125$ times higher than C/A on a linear scale:

$$\begin{aligned} 1.4125\gamma + \gamma &= 1, \\ \gamma &= 0.4145, \end{aligned} \tag{5.1}$$

so that C/A has a fraction γ of the total power and L1C has a fraction $1-\gamma$ of the total power in the composite signal. While keeping the convention in this dissertation of α and β representing the power split for the L1C pilot and data components, γ is added to represent the power split for the C/A component:

$$\begin{aligned} \text{Composite Power} &= \alpha(\text{L1C Pilot Power}) + \beta(\text{L1C Data Power}) + \gamma(\text{C/A Signal Power}) \\ &= (1-0.4145)\left[\tfrac{3}{4}(\text{L1C Pilot Power}) + \tfrac{1}{4}(\text{L1C Data Power})\right] \\ &\quad +0.4145(\text{C/A Signal Power}) \\ &= 0.4391(\text{L1C Pilot Power}) + 0.1464(\text{L1C Data Power}) \\ &\quad +0.4145(\text{C/A Signal Power}), \end{aligned} \tag{5.2}$$

so that the power split parameters are:

$$\alpha = 0.4391,\ \beta = 0.1464 \text{ and } \gamma = 0.4145. \tag{5.3}$$

These power split parameters are used in both the optimal and sub-optimal detectors for joint acquisition of C/A and L1C. Before proposing the various detectors, a signal model is developed.

5.3 Signal Model for Composite GPS L1C and C/A Signal

The signal from one satellite defined in (2.36) is now adjusted to not only contain the two components of of L1C, but also the C/A code. After signal conditioning in the front end of the GNSS receiver, the signal from one satellite is:

$$\begin{aligned} s(t) = & \sqrt{2\alpha C} d_P(t-\tau) c_P(t-\tau) g_P(t-\tau) \cos(2\pi(f_{IF}+f_d)t+\theta) \\ & + \sqrt{2\beta C} d_D(t-\tau) c_D(t-\tau) g_D(t-\tau) \cos(2\pi(f_{IF}+f_d)t+\theta) \\ & + \sqrt{2\gamma C} d_{C/A}(t-\tau) c_{C/A}(t-\tau) \sin(2\pi(f_{IF}+f_d)t+\theta) + n(t), \end{aligned} \tag{5.4}$$

where:

- the signal power is now denoted as C (Watts), which includes any antenna gain and receiver implementation losses;
- α, β, and γ are the power split parameters defined in (5.3);
- $d_D(t)$, $d_P(t)$, and $d_{C/A}(t)$ are the series of L1C data, L1C overlay code, and C/A data bits;
- c_D, c_P, and $c_{C/A}$ are the periodic repetition of each spreading code series;
- $g_D(t)$ and $g_P(t)$ are the periodic repetition of the spreading symbols, also called the subcarrier, for the L1C data and pilot components (the C/A code spreading symbol is the rectangular pulse which is fully described by the spreding code);
- τ and f_d are the unknown delay and Doppler frequency;
- the signal is now at an intermediate frequency f_{IF} (Hertz); and,
- θ is the unknown phase term.

After multiplication by two reference signals that are in phase quadrature and subsequent low-pass filtering, the inphase and quadrature receiver channels are:

$$\begin{aligned}\text{I} - \text{Channel} = \; & \sqrt{2\alpha C} d_P(t-\tau) c_P(t-\tau) g_P(t-\tau) \cos(2\pi \Delta f_d t + \Delta\theta) \\ & + \sqrt{2\beta C} d_D(t-\tau) c_D(t-\tau) g_D(t-\tau) \cos(2\pi \Delta f_d t + \Delta\theta) \\ & + \sqrt{2\gamma C} d_{C/A}(t-\tau) c_{C/A}(t-\tau) \sin(2\pi \Delta f_d t + \Delta\theta) + n_I(t), \end{aligned} \tag{5.5}$$

and

$$\begin{aligned}\text{Q} - \text{Channel} = \; & \sqrt{2\alpha C} d_P(t-\tau) c_P(t-\tau) g_P(t-\tau) \sin(2\pi \Delta f_d t + \Delta\theta) \\ & + \sqrt{2\beta C} d_D(t-\tau) c_D(t-\tau) g_D(t-\tau) \sin(2\pi \Delta f_d t + \Delta\theta) \\ & - \sqrt{2\gamma C} d_{C/A}(t-\tau) c_{C/A}(t-\tau) \cos(2\pi \Delta f_d t + \Delta\theta) + n_Q(t), \end{aligned} \tag{5.6}$$

where $\Delta f_d = f_d - \hat{f}_d$ is the error in Doppler estimate, and $\Delta\theta = \theta - \hat{\theta}$ is the carrier phase offset between the local replica and the received signal[1].

The inphase and quadrature channels are coherently-integrated after each is multiplied by the local code, and for L1C, the spreading symbol replicas. Each coherent integration gives a scalar output every integer multiple, k, of the coherent integration time, T_{coh}:

$$\begin{aligned}
I_{P,k} &= \frac{\sqrt{\alpha C}\, d_{P,k}}{T_{coh}} \int_{kT_{coh}}^{kT_{coh}+T_{coh}} c_P(t-\tau) c_P(t-\hat{\tau}) g_P(t-\tau) g_P(t-\hat{\tau}) \cos(2\pi \Delta f_d t + \Delta\theta)\, \mathrm{d}t + \eta_{P,I,k}, \\
Q_{P,k} &= \frac{\sqrt{\alpha C}\, d_{P,k}}{T_{coh}} \int_{kT_{coh}}^{kT_{coh}+T_{coh}} c_P(t-\tau) c_P(t-\hat{\tau}) g_P(t-\tau) g_P(t-\hat{\tau}) \sin(2\pi \Delta f_d t + \Delta\theta)\, \mathrm{d}t + \eta_{P,Q,k}, \\
I_{D,k} &= \frac{\sqrt{\beta C}\, d_{D,k}}{T_{coh}} \int_{kT_{coh}}^{kT_{coh}+T_{coh}} c_D(t-\tau) c_D(t-\hat{\tau}) g_D(t-\tau) g_D(t-\hat{\tau}) \cos(2\pi \Delta f_d t + \Delta\theta)\, \mathrm{d}t + \eta_{D,I,k}, \\
Q_{D,k} &= \frac{\sqrt{\beta C}\, d_{D,k}}{T_{coh}} \int_{kT_{coh}}^{kT_{coh}+T_{coh}} c_D(t-\tau) c_D(t-\hat{\tau}) g_D(t-\tau) g_D(t-\hat{\tau}) \sin(2\pi \Delta f_d t + \Delta\theta)\, \mathrm{d}t + \eta_{D,Q,k}, \\
I_{C/A,k} &= \frac{\sqrt{\gamma C}\, d_{C/A,k}}{T_{cosh}} \int_{kT_{coh}}^{kT_{coh}+T_{coh}} c_{C/A}(t-\tau) c_{C/A}(t-\hat{\tau}) \sin(2\pi \Delta f_d t + \Delta\theta)\, \mathrm{d}t + \eta_{C/A,I,k}, \\
Q_{C/A,k} &= \frac{-\sqrt{\gamma C}\, d_{C/A,k}}{T_{coh}} \int_{kT_{coh}}^{kT_{coh}+T_{coh}} c_{C/A}(t-\tau) c_{C/A}(t-\hat{\tau}) \cos(2\pi \Delta f_d t + \Delta\theta)\, \mathrm{d}t + \eta_{C/A,Q,k},
\end{aligned} \tag{5.7}$$

[1]Note that the C/A component in the I-Channel contains the sine term since the C/A code signal lags L1C by 90 degrees, likewise, the C/A component in the Q-Channel contains a negative cosine term.

where $\hat{\tau}$ is the estimated delay; and η's are the uncorrelated noise terms, each with the same variance [5]:

$$\sigma^2 = N_0/2T_{coh}. \tag{5.8}$$

Two assumptions are applied herein: that the coherent integration time is the length of the L1C spreading code period (10 ms), which is the same as the L1C overlay and data code bit duration; and that bit transitions are avoided. When the signal from the satellite is present, and correct delay ($\hat{\tau} = \tau$) and Doppler estimates are used, the output of the correlators are now:

$$\begin{aligned}
I_{P,k} &= \sqrt{\alpha C}\, d_{P,k} \cos(\Delta\theta) + \eta_{P,I,k}, \\
Q_{P,k} &= \sqrt{\alpha C}\, d_{P,k} \sin(\Delta\theta) + \eta_{P,Q,k}, \\
I_{D,k} &= \sqrt{\beta C}\, d_{D,k} \cos(\Delta\theta) + \eta_{D,I,k}, \\
Q_{D,k} &= \sqrt{\beta C}\, d_{D,k} \sin(\Delta\theta) + \eta_{D,Q,k}, \\
I_{C/A,k} &= \sqrt{\gamma C}\, d_{C/A,k} \sin(\Delta\theta) + \eta_{C/A,I,k}, \\
Q_{C/A,k} &= -\sqrt{\gamma C}\, d_{C/A,k} \cos(\Delta\theta) + \eta_{C/A,Q,k}.
\end{aligned} \tag{5.9}$$

Due to the autocorrelation properties of the spreading code, the correlator outputs are modeled as noise only when incorrect delay estimates ($\hat{\tau} \neq \tau$) are used. In this joint acquisition scenario however, there are actually incorrect L1C spreading code delay estimates that correspond with correct C/A code phase estimates and will lead to energy in the C/A code correlator outputs, $I_{C/A,k}$ and $Q_{C/A,k}$. The C/A spreading codes repeat every 1ms, while the L1C codes repeat every 10 ms. Noise only for incorrect code phase estimates is still assumed, but these secondary peaks in the correlation due to the repetition of the C/A code within one L1C spreading code period are discussed further in section 5.7. With a model to represent the composite C/A and L1C signal, an optimal detector for acquisition is now investigated.

5.4 Optimal Detector for Acquisition With GPS C/A and L1C

The optimal detector for joint acquisition of L1 C/A and L1C is derived in Appendix D. This detector provides an upper bound on the performance that can be achieved by combining these two L1 civil signals for GPS acquisition. The likelihood ratio for this optimal detector from (D.12) is:

$$\Lambda(\mathbf{r}) = \sum_{\mathbf{d}_P,\mathbf{d}_D,\mathbf{d}_{C/A}\in\{B\}} p(\mathbf{d}_P,\mathbf{d}_D,\mathbf{d}_{C/A}) I_0\left(\frac{\sqrt{C}}{\sigma^2}\sqrt{x^2+y^2}\right), \tag{5.10}$$

where the vectors $\mathbf{d}$ contain the data during each 10 ms integration for each component, $\{B\}$ is the set of all possible bit combinations, I_0 is the modified Bessel function of zeroth order, and x and y are defined as:

$$\begin{aligned} x &= \sum_{k=1}^{K}\Big(\sqrt{\alpha}I_{P,k}d_{P,k} + \sqrt{\beta}I_{D,k}d_{D,k} - \sqrt{\gamma}Q_{C/A,k}d_{C/A,k}\Big), \\ y &= \sum_{k=1}^{K}\Big(\sqrt{\alpha}Q_{P,k}d_{P,k} + \sqrt{\beta}Q_{D,k}d_{D,k} + \sqrt{\gamma}I_{C/A,k}d_{C/A,k}\Big). \end{aligned} \tag{5.11}$$

Unlike the optimal detector for L1C only, presented in Chapter 3, the set of all possible bit combinations $\{B\}$ is reduced in this joint case by some impossible combinations of L1C pilot overlay code bits, L1C navigation data bits, and C/A navigation data bits. The bit period for L1C is 10 ms, whereas the bit period for C/A is 20 ms. Since $\mathbf{d}_{C/A}$ represents the navigation bit on C/A every 10 ms, all combinations in which three consecutive C/A data bits are different are not possible and therefore, not included in $\{B\}$.

The detection probabilities of the optimal detector for joint acquisition referenced to the C/No of the L1C signal are shown in Figs. 5.1 and 5.2, while using one and three spreading code periods. As expected, the increased signal power used in the joint detector increases acquisition sensitivity by about 2 dB. The first use of L1C will most likely be in C/A code receivers while the L1C signals is deployed one or two satellites at a time; therefore, the detection probability for this optimal detector and all other detectors presented in this chapter are also shown in Appendix E with the C/No referenced to C/A code signal power.

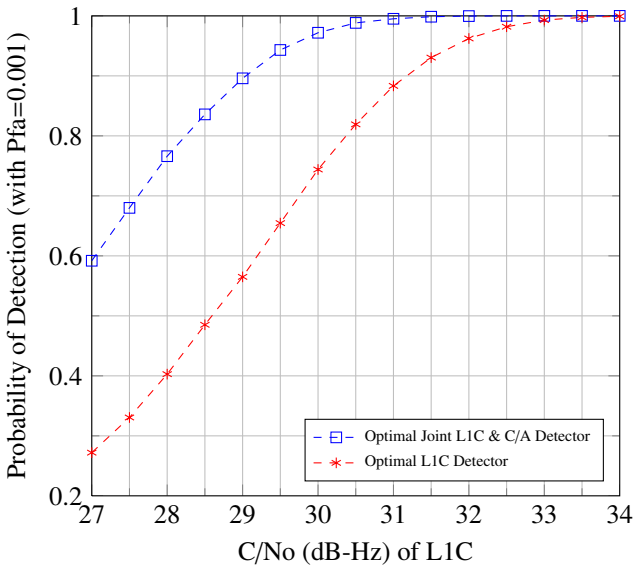

Figure 5.1: Detection probability of optimal joint L1C and C/A detector compared to optimal L1C detector for acquisition over one L1C spreading code period referenced to L1C signal power.

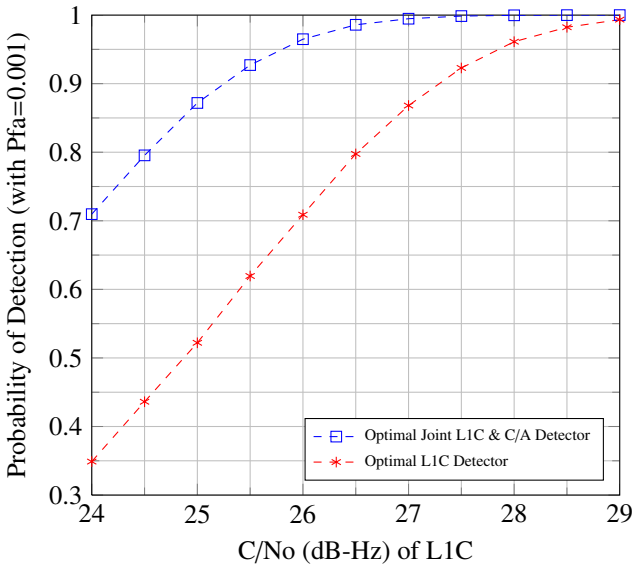

Figure 5.2: Detection probability of optimal joint L1C and C/A detector compared to optimal L1C detector for acquisition over three L1C spreading code periods referenced to L1C signal power.

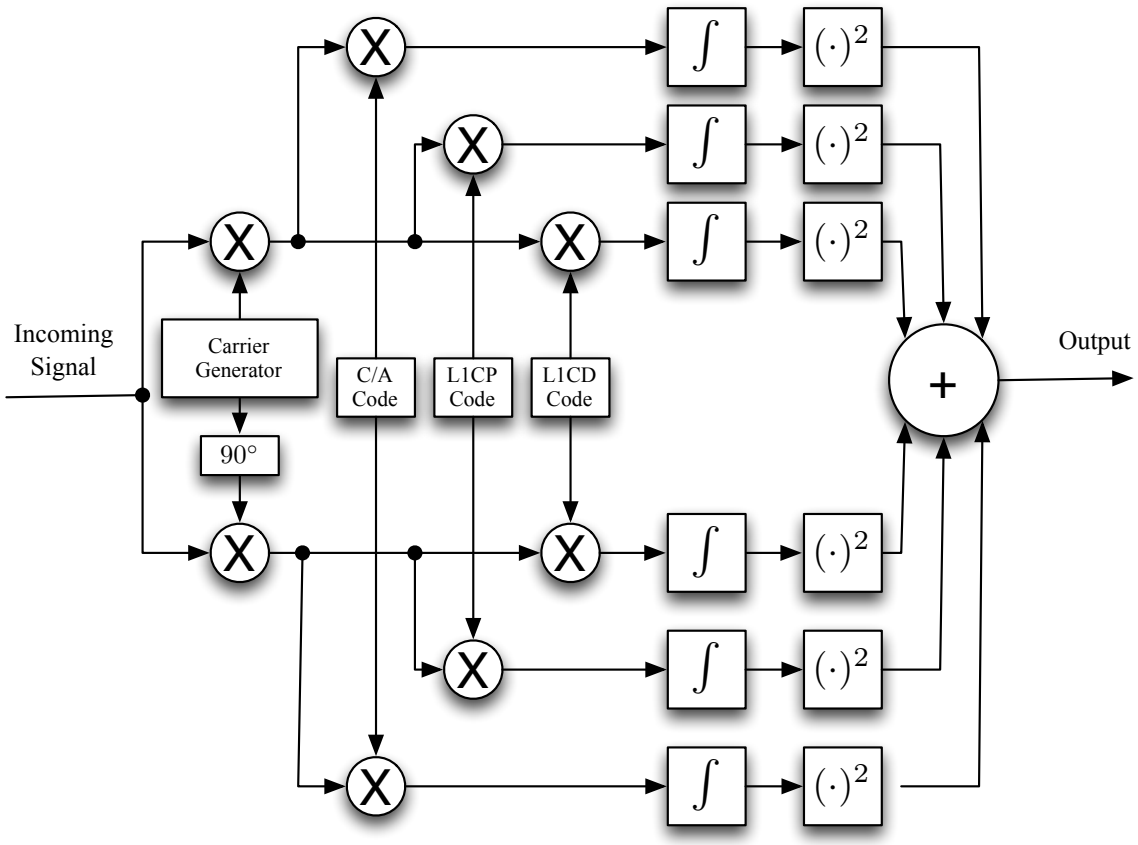

Figure 5.3: Block diagram of noncoherent combining detector for joint acquisition of GPS L1C and C/A.

5.5 Sub-Optimal Detectors for Joint C/A and L1C Acquisition

With the optimal joint detector as a benchmark for the best possible performance of joint acquisition of the legacy C/A code and L1C signals, this section proposes various sub-optimal, but more computationally efficient, detectors.

5.5.1 Noncoherent Combining Detector

Noncoherent combining is the separate acquisition of each component, including C/A code, and the subsequent combination of the correlator powers. The incoming signal can be correlated separately with a local replica of the L1C pilot, the L1C data, and the C/A spreading codes as shown in Fig. 5.3. Noncoherent channel combining is the squaring,

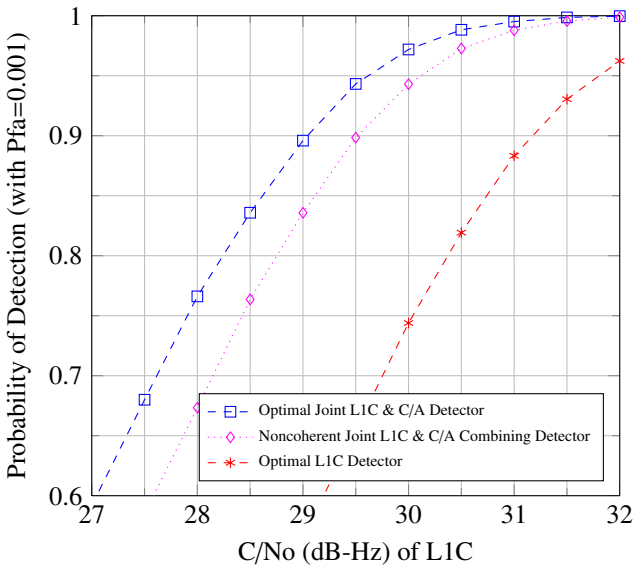

Figure 5.4: Detection probability of noncoherent combining joint L1C and C/A detector for acquisition over one L1C spreading code period referenced to L1C signal power.

scaling and summing of correlator outputs to obtain the decision variable:

$$Z_{\text{ncw}}^{\text{joint}} = \sum_{k=1}^{K} \left(\alpha I_{P,k}^2 + \alpha Q_{P,k}^2 + \beta I_{D,k}^2 + \beta Q_{D,k}^2 + \gamma I_{C/A,k}^2 + \gamma Q_{C/A,k}^2 \right), \tag{5.12}$$

where α, β, and γ, are the power split parameters from (5.3).

Since the underlying Gaussian random variables have three different variances based on the power split factors, the decision statistic, $Z_{\text{ncw}}^{\text{joint}}$, is a sum of three chi-square random variables, each with $2K$ degrees of freedom. When the signal is not present, or when incorrect delay and Doppler estimates are used, the random variables have a central chi-square distribution. When the delay and Doppler estimates are correct, the random variables have a non-central chi-square distribution. Performance of this noncoherent combining detector is shown in Figs. 5.4 and 5.5. The figures illustrate that the noncoherent detector performance is within 0.5 dB of the optimal joint detector over one spreading code period but as the total integration time increases, the performance gap between the optimal and noncoherent combining detectors also increases. Other combining techniques to improve performance for joint acquisition are now considered.

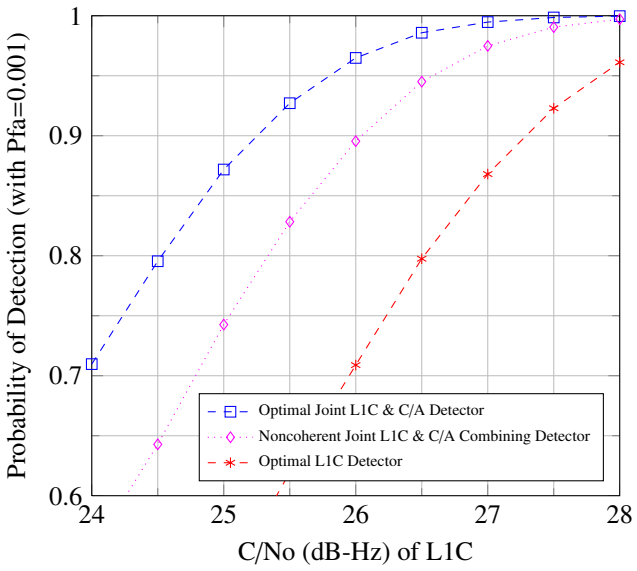

Figure 5.5: Detection probability of noncoherent combining joint L1C and C/A detector for acquisition over three L1C spreading code periods referenced to L1C signal power.

5.5.2 Coherent Combining

If the relative sign between the overlay/data bits on L1C pilot, L1C data, and C/A were known, the three components could be coherently combined. The receiver can estimate this relative sign by testing four combinations using the combination with the maximum power as the decision statistic:

$$Z_{\text{chw}}^{\text{joint}} = \max\left\{|z_1|^2, |z_2|^2, |z_3|^2, |z_4|^2\right\}, \tag{5.13}$$

where:

$$z_1 = \sqrt{\alpha}I_P + \text{j}\sqrt{\alpha}Q_P + \sqrt{\beta}I_D + \text{j}\sqrt{\beta}Q_D - \sqrt{\gamma}Q_{C/A} + \text{j}\sqrt{\gamma}I_{C/A}, \tag{5.14a}$$

$$z_2 = \sqrt{\alpha}I_P + \text{j}\sqrt{\alpha}Q_P + \sqrt{\beta}I_D + \text{j}\sqrt{\beta}Q_D + \sqrt{\gamma}Q_{C/A} - \text{j}\sqrt{\gamma}I_{C/A}, \tag{5.14b}$$

$$z_3 = \sqrt{\alpha}I_P + \text{j}\sqrt{\alpha}Q_P - \sqrt{\beta}I_D - \text{j}\sqrt{\beta}Q_D + \sqrt{\gamma}Q_{C/A} - \text{j}\sqrt{\gamma}I_{C/A}, \tag{5.14c}$$

$$z_4 = \sqrt{\alpha}I_P + \text{j}\sqrt{\alpha}Q_P - \sqrt{\beta}I_D - \text{j}\sqrt{\beta}Q_D - \sqrt{\gamma}Q_{C/A} + \text{j}\sqrt{\gamma}I_{C/A}, \tag{5.14d}$$

and

$$|z_1|^2 = \left(\sqrt{\alpha}I_P + \sqrt{\beta}I_D - \sqrt{\gamma}Q_{C/A}\right)^2 + \left(\sqrt{\alpha}Q_P + \sqrt{\beta}Q_D + \sqrt{\gamma}I_{C/A}\right)^2, \tag{5.15a}$$

$$|z_2|^2 = \left(\sqrt{\alpha}I_P + \sqrt{\beta}I_D + \sqrt{\gamma}Q_{C/A}\right)^2 + \left(\sqrt{\alpha}Q_P + \sqrt{\beta}Q_D - \sqrt{\gamma}I_{C/A}\right)^2, \tag{5.15b}$$

$$|z_3|^2 = \left(\sqrt{\alpha}I_P - \sqrt{\beta}I_D + \sqrt{\gamma}Q_{C/A}\right)^2 + \left(\sqrt{\alpha}Q_P - \sqrt{\beta}Q_D - \sqrt{\gamma}I_{C/A}\right)^2, \tag{5.15c}$$

$$|z_4|^2 = \left(\sqrt{\alpha}I_P - \sqrt{\beta}I_D - \sqrt{\gamma}Q_{C/A}\right)^2 + \left(\sqrt{\alpha}Q_P - \sqrt{\beta}Q_D + \sqrt{\gamma}I_{C/A}\right)^2, \tag{5.15d}$$

with:

$$\alpha = 0.4391,\ \beta = 0.1464 \text{ and } \gamma = 0.4145.$$

The powers of the various combinations, $|z_x|^2$, are chi-square random variables with two degrees of freedom. With the weights applied for the unequal power compensation, the underlying Gaussian random variables have a variance of σ^2. Without the unequal power compensation, the variance of the underlying Gaussian random variables in the chi-square random variable would be $3\sigma^2$. When the desired signal is not present or with incorrect code delay and Doppler estimates, the $|z_x|^2$ terms are central chi-square random variables.

When the signal is present with correct estimates of delay and Doppler, there are four possibilities for the noncentrality parameter, depending on the relative sign between the

overlay/data bits on the three components. For $|z_1|^2$, the noncentrality parameter is:

$$\begin{aligned}
a_1^2 &= \left(\alpha\sqrt{C}d_P\cos(\Delta\theta) + \beta\sqrt{C}d_D\cos(\Delta\theta) + \gamma\sqrt{C}d_{C/A}\cos(\Delta\theta)\right)^2 \\
&\quad + \left(\alpha\sqrt{C}d_P\sin(\Delta\theta) + \beta\sqrt{C}d_D\sin(\Delta\theta) + \gamma\sqrt{C}d_{C/A}\sin(\Delta\theta)\right)^2 \\
&= \left(\alpha^2+\beta^2+\gamma^2+2\alpha\beta d_P d_D + 2\alpha\gamma d_P d_{C/A} + 2\beta\gamma d_D d_{C/A}\right)C\cos^2(\Delta\theta) \\
&\quad + \left(\alpha^2+\beta^2+\gamma^2+2\alpha\beta d_P d_D + 2\alpha\gamma d_P d_{C/A} + 2\beta\gamma d_D d_{C/A}\right)C\sin^2(\Delta\theta) \\
&= \left(\alpha^2+\beta^2+\gamma^2+2\alpha\beta d_P d_D + 2\alpha\gamma d_P d_{C/A} + 2\beta\gamma d_D d_{C/A}\right)C \\
&= \begin{cases}
(\alpha+\beta+\gamma)^2 C = C, \text{ correct rel. signs } (d_P d_{C/A} = d_P d_{C/A} = +1) \\
\left(\alpha^2+\beta^2+\gamma^2+2\alpha\beta-2\alpha\beta-2\beta\gamma\right)C = 0.0292C, \ (d_P d_{C/A} = d_P d_{C/A} = -1) \\
\left(\alpha^2+\beta^2+\gamma^2-2\alpha\beta-2\alpha\beta+2\beta\gamma\right)C = 0.0148C, \ (d_P d_{C/A} = -1, d_P d_{C/A} = +1) \\
\left(\alpha^2+\beta^2+\gamma^2-2\alpha\beta+2\alpha\beta-2\beta\gamma\right)C = 0.5001C, \ (d_P d_{C/A} = +1, d_P d_{C/A} = -1).
\end{cases}
\end{aligned} \tag{5.16}$$

Likewise, the noncentrality parameters for the other three combinations are:

$$a_2^2 = \begin{cases}
0.0292C, \text{ incorrect rel. signs } (d_P d_{C/A} = d_P d_{C/A} = +1) \\
C, \text{ correct rel. signs } (d_P d_{C/A} = d_P d_{C/A} = -1) \\
0.5001C, \text{ incorrect rel. signs } (d_P d_{C/A} = -1, d_P d_{C/A} = +1) \\
0.0148C, \text{ incorrect rel. signs } (d_P d_{C/A} = +1, d_P d_{C/A} = -1),
\end{cases} \tag{5.17}$$

and

$$a_3^2 = \begin{cases}
0.0148C, \text{ incorrect rel. signs } (d_P d_{C/A} = d_P d_{C/A} = +1) \\
0.5001C, \text{ incorrect rel. signs } (d_P d_{C/A} = d_P d_{C/A} = -1) \\
C, \text{ correct rel. signs } (d_P d_{C/A} = -1, d_P d_{C/A} = +1) \\
0.0292C, \text{ incorrect rel. signs } (d_P d_{C/A} = +1, d_P d_{C/A} = -1),
\end{cases} \tag{5.18}$$

and

$$a_4^2 = \begin{cases} 0.5001C, \text{ incorrect rel. signs } (d_P d_{C/A} = d_P d_{C/A} = +1) \\ 0.0148C, \text{ incorrect rel. signs } (d_P d_{C/A} = d_P d_{C/A} = -1) \\ 0.0292C, \text{ incorrect rel. signs } (d_P d_{C/A} = -1, d_P d_{C/A} = +1) \\ C, \text{ correct rel. signs } (d_P d_{C/A} = +1, d_P d_{C/A} = -1). \end{cases} \tag{5.19}$$

Using the fact that

$$\begin{aligned} P(Z > \lambda) &= P\left(\max\left\{|z_1|^2, |z_2|^2, |z_3|^2, |z_4|^2\right\} > \lambda\right) \\ &= 1 - P\left(\max\left\{|z_1|^2, |z_2|^2, |z_3|^2, |z_4|^2\right\} < \lambda\right) \\ &= 1 - P\left(|z_1|^2 < \lambda, |z_2|^2 < \lambda, |z_3|^2 < \lambda, |z_4|^2 < \lambda\right) \\ &= 1 - P\left(|z_1|^2 < \lambda\right) P\left(|z_2|^2 < \lambda\right) P\left(|z_3|^2 < \lambda\right) P\left(|z_4|^2 < \lambda\right), \end{aligned} \tag{5.20}$$

the noncentrality parameters lead to the following false alarm and detection probabilities for joint acquisition using coherent combining:

$$\begin{aligned} P_{fa}^{joint,chw}(\lambda) &= 1 - P\left(|z_1|^2 < \lambda \mid H_0\right) P\left(|z_2|^2 < \lambda \mid H_0\right) P\left(|z_3|^2 < \lambda \mid H_0\right) P\left(|z_4|^2 < \lambda \mid H_0\right) \\ &= 1 - \left[1 - \exp\left(\frac{-\lambda}{2\sigma^2}\right)\right]^4, \end{aligned} \tag{5.21}$$

and

$$\begin{aligned} P_d^{joint,chw}(\lambda) &= 1 - P\left(|z_1|^2 < \lambda \mid H_1\right) P\left(|z_2|^2 < \lambda \mid H_1\right) P\left(|z_3|^2 < \lambda \mid H_1\right) P\left(|z_4|^2 < \lambda \mid H_1\right) \\ &= 1 - \left[1 - Q_1\left(\frac{\sqrt{C}}{\sigma}, \frac{\sqrt{\lambda}}{\sigma}\right)\right]\left[1 - Q_1\left(\frac{\sqrt{0.0292C}}{\sigma}, \frac{\sqrt{\lambda}}{\sigma}\right)\right] \\ &\quad \cdot \left[1 - Q_1\left(\frac{\sqrt{0.0148C}}{\sigma}, \frac{\sqrt{\lambda}}{\sigma}\right)\right]\left[1 - Q_1\left(\frac{\sqrt{0.5001C}}{\sigma}, \frac{\sqrt{\lambda}}{\sigma}\right)\right], \end{aligned} \tag{5.22}$$

where Q_1 is the Marcum's Q function. Fig. 5.6 shows that this coherent combining technique for joint acquisition of all GPS L1 civil signals has the same performance as the optimal detector. This technique can be extended over multiple L1C spreading code periods by using semi-coherent integration.

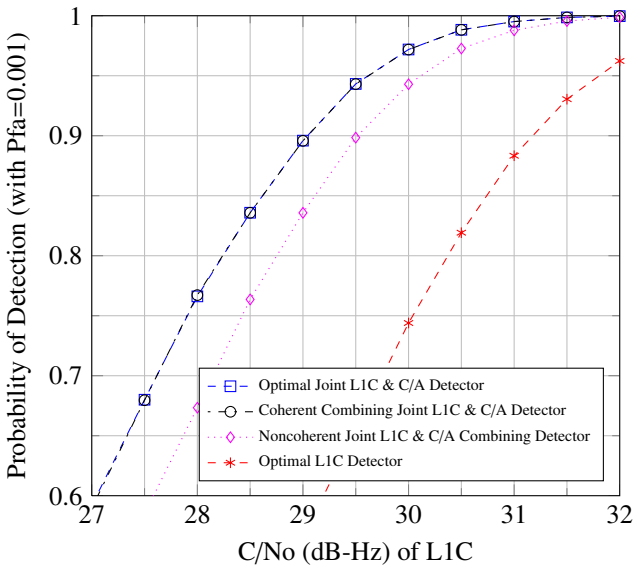

Figure 5.6: Detection probability of coherent combining joint L1C and C/A detector for acquisition over one L1C spreading code period referenced to L1C signal power.

5.5.3 Semi-Coherent Integration

The coherent combinations of GPS L1C pilot, L1C data, and C/A code every 10 ms coherent integration period can be noncoherently combined using an integer number K sequential coherent combinations in a technique known as semi-coherent integration:

$$Z_{\text{semi}}^{\text{joint}} = \sum_{k=1}^{K} \max\left\{|z_{1,k}|^2, |z_{2,k}|^2, |z_{3,k}|^2, |z_{4,k}|^2\right\}, \tag{5.23}$$

where:

$$z_{1,k} = \sqrt{\alpha} I_{P,k} + \mathrm{j}\sqrt{\alpha} Q_{P,k} + \sqrt{\beta} I_{D,k} + \mathrm{j}\sqrt{\beta} Q_{D,k} - \sqrt{\gamma} Q_{C/A,k} + \mathrm{j}\sqrt{\gamma} I_{C/A,k}, \tag{5.24a}$$

$$z_{2,k} = \sqrt{\alpha} I_{P,k} + \mathrm{j}\sqrt{\alpha} Q_{P,k} + \sqrt{\beta} I_{D,k} + \mathrm{j}\sqrt{\beta} Q_{D,k} + \sqrt{\gamma} Q_{C/A,k} - \mathrm{j}\sqrt{\gamma} I_{C/A,k}, \tag{5.24b}$$

$$z_{3,k} = \sqrt{\alpha} I_{P,k} + \mathrm{j}\sqrt{\alpha} Q_{P,k} - \sqrt{\beta} I_{D,k} - \mathrm{j}\sqrt{\beta} Q_{D,k} + \sqrt{\gamma} Q_{C/A,k} - \mathrm{j}\sqrt{\gamma} I_{C/A,k}, \tag{5.24c}$$

$$z_{4,k} = \sqrt{\alpha} I_{P,k} + \mathrm{j}\sqrt{\alpha} Q_{P,k} - \sqrt{\beta} I_{D,k} - \mathrm{j}\sqrt{\beta} Q_{D,k} - \sqrt{\gamma} Q_{C/A,k} + \mathrm{j}\sqrt{\gamma} I_{C/A,k}, \tag{5.24d}$$

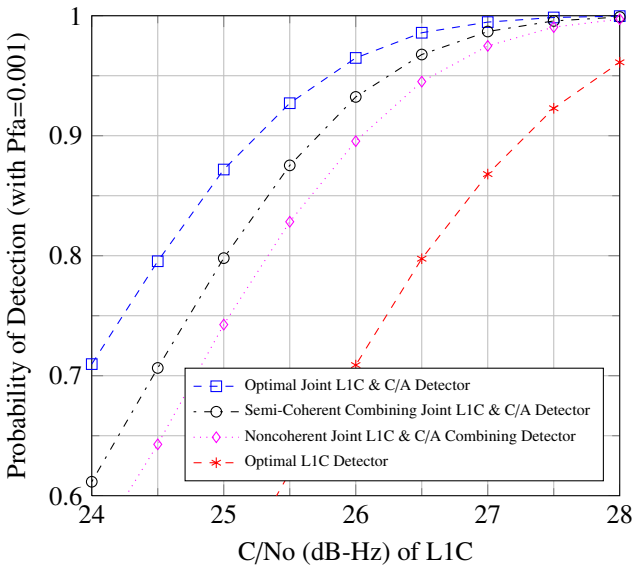

Figure 5.7: Detection probability of semi-coherent joint L1C and C/A detector for acquisition over three L1C spreading code periods referenced to L1C signal power.

and

$$|z_{1,k}|^2 = \left(\sqrt{\alpha}I_{P,k} + \sqrt{\beta}I_{D,k} - \sqrt{\gamma}Q_{C/A,k}\right)^2 + \left(\sqrt{\alpha}Q_{P,k} + \sqrt{\beta}Q_{D,k} + \sqrt{\gamma}I_{C/A,k}\right)^2, \quad (5.25a)$$

$$|z_{2,k}|^2 = \left(\sqrt{\alpha}I_{P,k} + \sqrt{\beta}I_{D,k} + \sqrt{\gamma}Q_{C/A,k}\right)^2 + \left(\sqrt{\alpha}Q_{P,k} + \sqrt{\beta}Q_{D,k} - \sqrt{\gamma}I_{C/A,k}\right)^2, \quad (5.25b)$$

$$|z_{3,k}|^2 = \left(\sqrt{\alpha}I_{P,k} - \sqrt{\beta}I_{D,k} + \sqrt{\gamma}Q_{C/A,k}\right)^2 + \left(\sqrt{\alpha}Q_{P,k} - \sqrt{\beta}Q_{D,k} - \sqrt{\gamma}I_{C/A,k}\right)^2, \quad (5.25c)$$

$$|z_{4,k}|^2 = \left(\sqrt{\alpha}I_{P,k} - \sqrt{\beta}I_{D,k} - \sqrt{\gamma}Q_{C/A,k}\right)^2 + \left(\sqrt{\alpha}Q_{P,k} - \sqrt{\beta}Q_{D,k} + \sqrt{\gamma}I_{C/A,k}\right)^2, \quad (5.25d)$$

with the following weights for GPS L1C and C/A joint acquisition:

$$\alpha = 0.4391, \ \beta = 0.1464, \ \text{and} \ \gamma = 0.4145.$$

Simulation results are used to show how this semi-coherent integration technique outperforms the noncoherent detector in Fig. 5.7 for acquisition over three L1C spreading code periods (30 ms). Since the coherent combinations depend on relative sign estimates between the overlay/data bits, the performance advantage of semi-coherent integration over noncoherent combining is expected to disappear eventually as C/No decreases. Fig. 5.8 shows this point with an extended integration time of twenty-five spreading code periods.

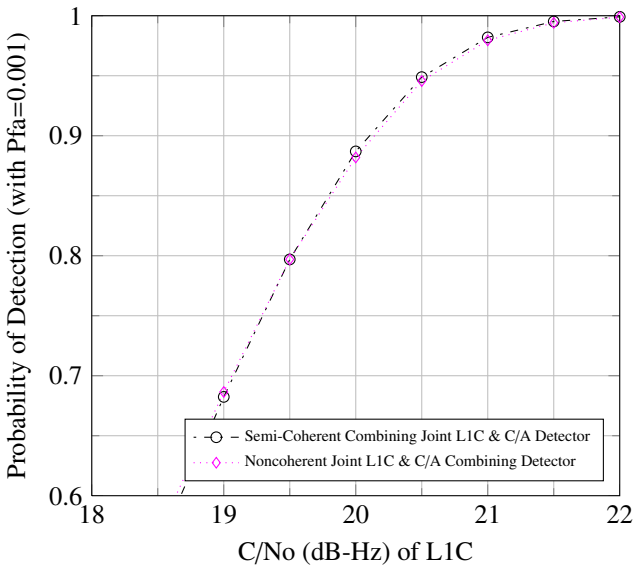

Figure 5.8: Detection probability of semi-coherent joint L1C and C/A detector for acquisition with an extended integration time over twenty-five spreading code periods referenced to L1C signal power.

5.6 Joint L1C Pilot and C/A Acquisition

Joint acquisition of the GPS L1C and C/A code signals is an attractive solution to improving acquisition sensitivity. The cost, however, is increased receiver complexity and additional correlator requirements. In the composite L1C and C/A code signal, the L1C data component contributes less than 15 percent of the total signal power. One possible tradeoff is to ignore the L1C data component and perform joint L1C pilot and C/A code acquisition. In this section, detectors that use only the pilot component of L1C along with the C/A code signal for acquisition are proposed and their performance is analyzed.

5.6.1 Optimal

Since the L1C pilot nominal received signal is 0.25 dBW higher than the C/A code, L1C pilot has a received strength that is $10^{\frac{0.25}{10}} = 1.0593$ times higher than C/A on a linear scale:

$$\begin{aligned} 1.0593\gamma' + \gamma' &= 1, \\ \gamma' &= 0.4856, \end{aligned} \tag{5.26}$$

so that the power split parameters are:

$$\alpha' = 0.5144, \text{ and } \gamma' = 0.4856. \tag{5.27}$$

The likelihood ratio in the optimal detector for joint acquisition of L1C pilot and L1 C/A comes directly from making adjustments to the optimal joint detector in (5.11) which results in:

$$\Lambda(\mathbf{r}) = \sum_{\mathbf{d}_P, \mathbf{d}_{C/A} \in \{B\}} p(\mathbf{d}_P, \mathbf{d}_{C/A}) I_0 \left(\frac{\sqrt{C'}}{\sigma^2} \sqrt{x^2 + y^2} \right), \tag{5.28}$$

where C' represents the total received signal power from the two components, the vectors $\mathbf{d}$ contain the overlay/data bits during each 10 ms integration for each component, $\{B\}$ is the set of all possible bit combinations, I_0 is the modified Bessel function of zeroth order, and x and y are defined as:

$$\begin{aligned} x &= \sum_{k=1}^{K} \left(\sqrt{\alpha'} I_{P,k} d_{P,k} - \sqrt{\gamma'} Q_{C/A,k} d_{C/A,k} \right), \\ y &= \sum_{k=1}^{K} \left(\sqrt{\alpha'} Q_{P,k} d_{P,k} + \sqrt{\gamma'} I_{C/A,k} d_{C/A,k} \right). \end{aligned} \tag{5.29}$$

As noted previously for the joint L1C and C/A optimal detector, the set of all possible bit combinations $\{B\}$ is reduced in this joint case by removal of some impossible combinations of L1C pilot overlay code bits and C/A navigation data bits. The bit period for L1C is 10 ms; whereas, the bit period for C/A is 20 ms. Since $\mathbf{d}_{C/A}$ represents the navigation bit on C/A every 10 ms, all combinations in which three consecutive C/A data bits are different are not possible and therefore, not included in $\{B\}$.

The detection probabilities of this optimal detector for joint L1C pilot and L1 C/A acquisition referenced to the C/No of the L1C signal are shown in Figs. 5.9 and 5.10, while using one and three spreading code periods. The C/No is still referenced to the L1C signals so that the performance of the joint L1C pilot and C/A code detectors can easily be compared to previous acquisition schemes. It is interesting to note that the optimal joint detector using the L1C pilot and L1 C/A signals outperforms the noncoherent combining detector of both L1C data and pilot components with the L1 C/A signal.

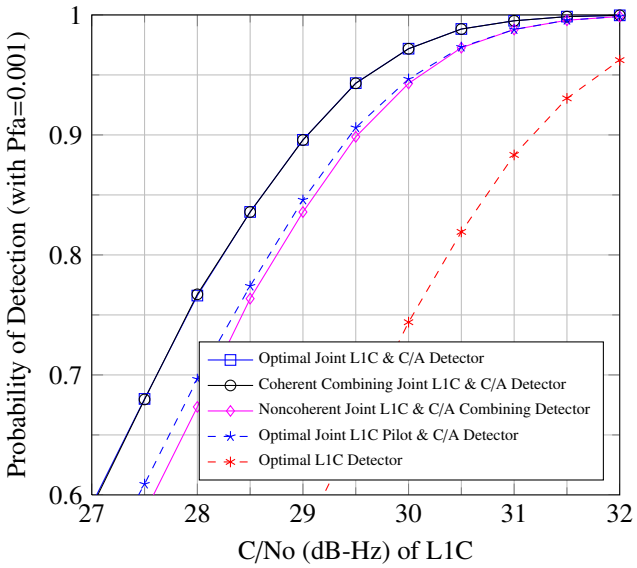

Figure 5.9: Detection probability of optimal joint L1C pilot and C/A detector for acquisition over one L1C spreading code period referenced to L1C signal power.

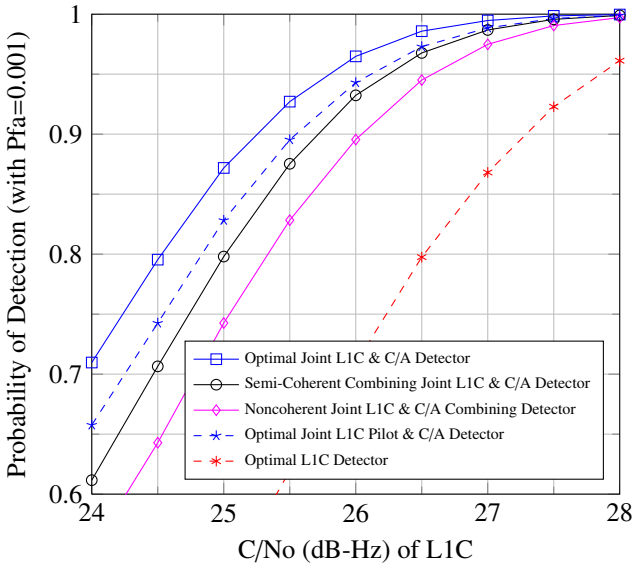

Figure 5.10: Detection probability of optimal joint L1C pilot and C/A detector for acquisition over three L1C spreading code periods referenced to L1C signal power.

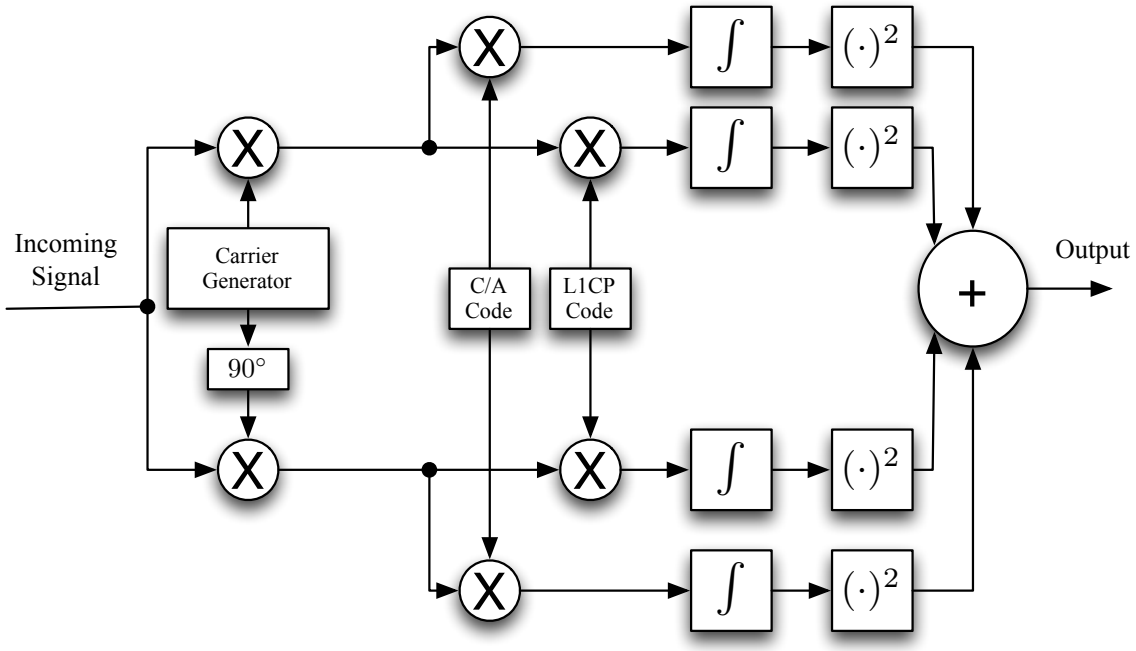

Figure 5.11: Block diagram of noncoherent combining detector for joint acquisition of GPS L1C Pilot and L1 C/A.

5.6.2 Noncoherent Combining

Noncoherent combining is a separate acquisition of the L1C pilot component and the C/A code and the subsequent combination of their correlator powers. The incoming signal can be correlated separately with a local replica of the L1C pilot and the C/A spreading codes as shown in Fig. 5.11. Noncoherent channel combining is the squaring, scaling, and summing of correlator outputs to obtain the decision variable:

$$Z_{\text{ncw}}^{\text{jointpc}} = \sum_{k=1}^{K} \left(\alpha' I_{P,k}^2 + \alpha' Q_{P,k}^2 + \gamma' I_{C/A,k}^2 + \gamma' Q_{C/A,k}^2 \right), \tag{5.30}$$

where α', and γ', are the power split parameters from (5.27).

Since the underlying Gaussian random variables have two different variances based on the power split factors, the decision statistic, $Z_{\text{ncw}}^{\text{jointpc}}$, is a sum of two chi-square random variables, each with $2K$ degrees of freedom. When the signal is not present, or when incorrect delay and Doppler estimates are used, the random variables have a central chi-square distribution. When the delay and Doppler estimates are correct, the random variables

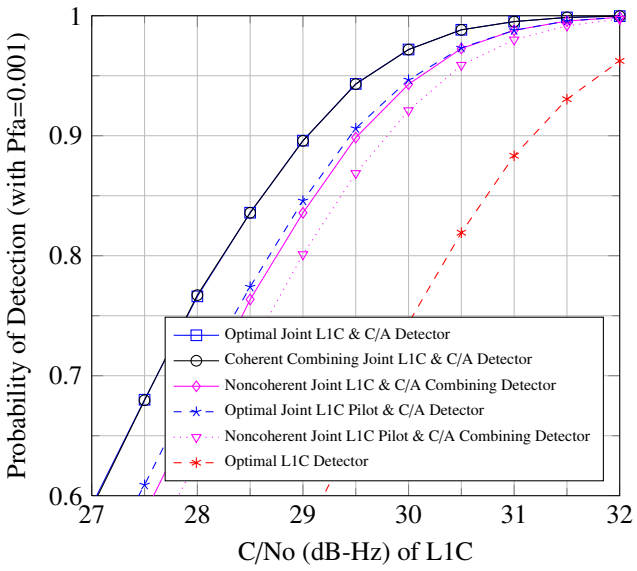

Figure 5.12: Detection probability of noncoherent combining joint L1C pilot and C/A detector for acquisition over one L1C spreading code period referenced to L1C signal power.

have a non-central chi-square distribution. Performance of this noncoherent combining detector is shown in Figs. 5.12 and 5.13. These figures illustrate that as the total integration time increases, the performance gap between the optimal and noncoherent combining detectors also increases. Other combining techniques to improve performance for joint acquisition of the L1C pilot and C/A code are now considered.

5.6.3 Coherent Combining

The coherent channel combining technique presented for the the two L1C components is adjusted so that the L1C data component is replaced by the C/A code:

$$Z_{\text{chw}}^{\text{jointpc}} = \max\left\{|z^+|^2, |z^-|^2\right\}, \tag{5.31}$$

where:

$$z^+ = \sqrt{\alpha'} I_P + \text{j}\sqrt{\alpha'} Q_P - \sqrt{\gamma'} Q_{C/A} + \text{j}\sqrt{\gamma'} I_{C/A}, \tag{5.32a}$$

$$z^- = \sqrt{\alpha'} I_P + \text{j}\sqrt{\alpha'} Q_P + \sqrt{\gamma'} Q_{C/A} - \text{j}\sqrt{\gamma'} I_{C/A}, \tag{5.32b}$$

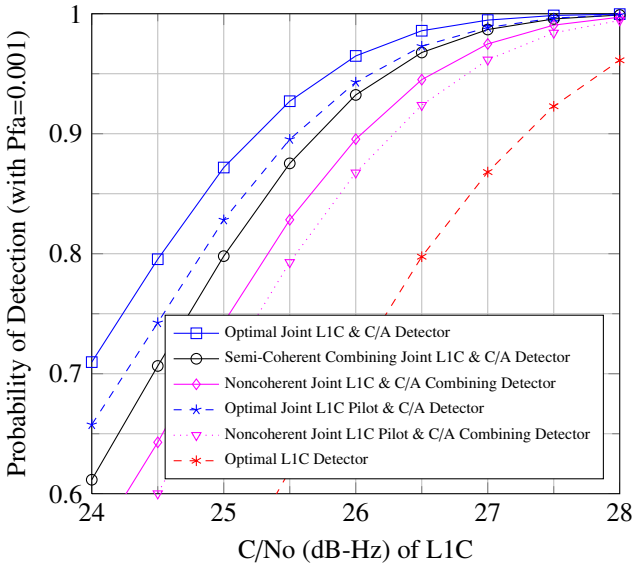

Figure 5.13: Detection probability of noncoherent combining joint L1C pilot and C/A detector for acquisition over three L1C spreading code periods referenced to L1C signal power.

and

$$|z^+|^2 = \left(\sqrt{\alpha'}I_P - \sqrt{\gamma'}Q_{C/A}\right)^2 + \left(\sqrt{\alpha'}Q_P + \sqrt{\gamma'}I_{C/A}\right)^2, \tag{5.33a}$$

$$|z^-|^2 = \left(\sqrt{\alpha'}I_P + \sqrt{\gamma'}Q_{C/A}\right)^2 + \left(\sqrt{\alpha'}Q_P - \sqrt{\gamma'}I_{C/A}\right)^2, \tag{5.33b}$$

with:

$$\alpha' = 0.5144 \quad \text{and} \quad \gamma' = 0.4856.$$

The $|z^+|^2$ and $|z^-|^2$ terms are chi-square random variables with two degrees of freedom. With the scale factors, the underlying Gaussian random variables have a variance of σ^2, instead of $2\sigma^2$. When the signal is present with correct estimates of delay and Doppler, the noncentrality parameter for $|z^+|^2$ is:

$$\begin{aligned} a_+^2 &= \left(\alpha' \sqrt{C'} d_P \cos(\Delta\theta) + \gamma' \sqrt{C'} d_{C/A} \cos(\Delta\theta)\right)^2 + \left(\alpha' \sqrt{C'} d_P \sin(\Delta\theta) + \gamma' \sqrt{C'} d_{C/A} \sin(\Delta\theta)\right)^2 \\ &= \left(\alpha'^2 + \gamma'^2 + 2\alpha'\gamma' d_P d_{C/A}\right) C \cos^2(\Delta\theta) + \left(\alpha'^2 + \gamma'^2 + 2\alpha'\gamma' d_P d_{C/A}\right) C \sin^2(\Delta\theta) \\ &= \left(\alpha'^2 + \gamma'^2 + 2\alpha'\gamma' d_P d_{C/A}\right) C \\ &= \begin{cases} C, \text{ correct rel. sign } (d_P d_{C/A} = +1) \\ (0.0008)C, \text{ incorrect rel. sign } (d_P d_{C/A} = -1). \end{cases} \end{aligned} \tag{5.34}$$

The noncentrality parameter for $|z^-|^2$ is:

$$\begin{aligned} a_-^2 &= \left(\alpha'^2 + \gamma'^2 - 2\alpha'\gamma' d_P d_{C/A}\right) C \\ &= \begin{cases} C, \text{ correct rel. sign } (d_P d_{C/A} = -1) \\ (0.0008)C, \text{ incorrect rel. sign } (d_P d_{C/A} = +1). \end{cases} \end{aligned} \tag{5.35}$$

These noncentrality parameters lead to the following false alarm and detection probabilities:

$$\begin{aligned} P_{fa}^{chw}(\lambda) &= 1 - P\left(|z^+|^2 < \lambda \mid H_0\right) P\left(|z^-|^2 < \lambda \mid H_0\right) \\ &= 1 - \left[1 - \exp\left(\frac{-\lambda}{2\sigma^2}\right)\right]^2, \end{aligned} \tag{5.36}$$

and

$$\begin{aligned} P_d^{chw}(\lambda) &= 1 - P\left(|z^+|^2 < \lambda \mid H_1\right) P\left(|z^-|^2 < \lambda \mid H_1\right) \\ &= 1 - \left[1 - Q_1\left(\frac{\sqrt{C}}{\sigma}, \frac{\sqrt{\lambda}}{\sigma}\right)\right]\left[1 - Q_1\left(\frac{\sqrt{(0.0008)C}}{\sigma}, \frac{\sqrt{\lambda}}{\sigma}\right)\right], \end{aligned} \tag{5.37}$$

where Q_1 is the Marcum's Q function. Fig. 5.14 shows that this coherent combining technique for joint acquisition of the L1C pilot and L1 C/A has better performance than noncoherently combining all the GPS L1 civil signals. This technique can be extended over multiple L1C spreading code periods by using semi-coherent integration.

5.6.4 Semi-Coherent Integration

The coherent channel combining technique presented for the the two L1C components is adjusted so that the L1C data component is replaced by the C/A code:

$$Z_{\text{chw}}^{\text{jointpc}} = \sum_{k=1}^{K} \max\left\{|z_k^+|^2, |z_k^-|^2\right\}, \tag{5.38}$$

where:

$$z_k^+ = \sqrt{\alpha'} I_{P,k} + \mathrm{j}\sqrt{\alpha'} Q_{P,k} - \sqrt{\gamma'} Q_{C/A,k} + \mathrm{j}\sqrt{\gamma'} I_{C/A,k}, \tag{5.39a}$$

$$z_k^- = \sqrt{\alpha'} I_{P,k} + \mathrm{j}\sqrt{\alpha'} Q_{P,k} + \sqrt{\gamma'} Q_{C/A,k} - \mathrm{j}\sqrt{\gamma'} I_{C/A,k}, \tag{5.39b}$$

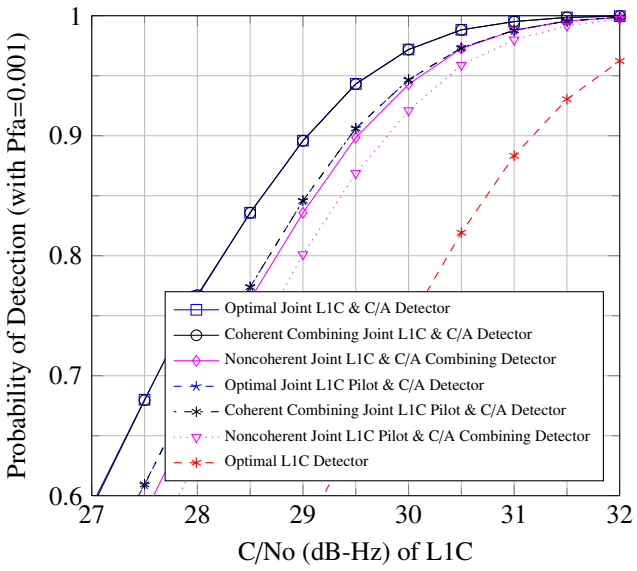

Figure 5.14: Detection probability of coherent combining joint L1C pilot and C/A detector for acquisition over one L1C spreading code period referenced to L1C signal power.

and

$$|z_k^+|^2 = \left(\sqrt{\alpha'}I_{P,k} - \sqrt{\gamma'}Q_{C/A,k}\right)^2 + \left(\sqrt{\alpha'}Q_{P,k} + \sqrt{\gamma'}I_{C/A,k}\right)^2, \tag{5.40a}$$

$$|z_k^-|^2 = \left(\sqrt{\alpha'}I_{P,k} + \sqrt{\gamma'}Q_{C/A,k}\right)^2 + \left(\sqrt{\alpha'}Q_{P,k} - \sqrt{\gamma'}I_{C/A,k}\right)^2, \tag{5.40b}$$

with:

$$\alpha' = 0.5144 \quad \text{and} \quad \gamma' = 0.4856.$$

Simulation results are used in Fig. 5.15 to show how this semi-coherent integration technique outperforms the the noncoherent detectors (using all L1C signals or just L1C pilot plus L1 C/A) for acquisition over three L1C spreading code periods (30 ms). Since the coherent combinations depend on relative sign estimates between the overlay/data bits, the performance advantage of semi-coherent integration over noncoherent combining is expected to disappear eventually as the C/No decreases. Fig. 5.16 shows this point with an extended integration time of twenty-five spreading code periods.

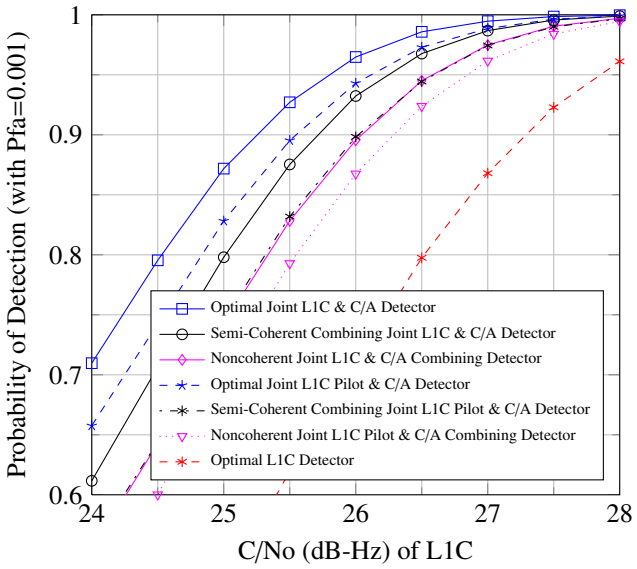

Figure 5.15: Detection probability of semi-coherent combining joint L1C pilot and C/A detector for acquisition over three L1C spreading code periods referenced to L1C signal power.

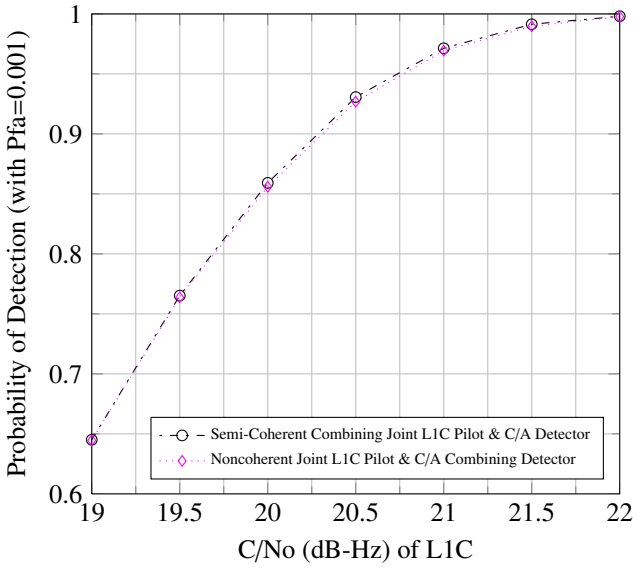

Figure 5.16: Detection probability of semi-coherent combining joint L1C pilot and C/A detector for acquisition over extended integration time of twenty-five spreading code period referenced to L1C signal power.

5.7 Correct C/A Code Phase and Incorrect L1C Code Phase

The previous work in this chapter is based on the assumption that when incorrect estimates for code delay and Doppler are used, the outputs of the correlators contain the noise terms only. The scenario when this assumption is invalid is discussed in this section. The coherent integration time in the acquisition schemes presented here is the length of the L1C spreading code, or 10 ms. Since the L1 C/A code period is only 1ms, it repeats ten times during one L1C spreading code period. This leads to the situation that nine different code delay estimates will be incorrect for L1C but correct for L1 C/A. If correlator spacing of one chip is used, then nine out of 10,230 possible code phase estimates will have noise only on the L1C correlator outputs while having signal energy in the C/A code correlator outputs:

$$\begin{aligned} I_{P,k} &= \eta_{P,I,k}, \\ Q_{P,k} &= \eta_{P,Q,k}, \\ I_{D,k} &= \eta_{D,I,k}, \\ Q_{D,k} &= \eta_{D,Q,k}, \\ I_{C/A,k} &= \sqrt{\gamma C}\, d_{C/A,k} \sin(\Delta\theta) + \eta_{C/A,I,k}, \\ Q_{C/A,k} &= -\sqrt{\gamma C}\, d_{C/A,k} \cos(\Delta\theta) + \eta_{C/A,Q,k}. \end{aligned} \tag{5.41}$$

A strategy to deal with this possibility may be implemented in the GPS receiver. For example, if the decision statistic of a particular detector crosses the detection threshold, power in the L1C correlator outputs can be checked. If it determined that the correct C/A code phase but incorrect L1C code phase has been found, acquisition can proceed with just the C/A code signal.

To determine the probability that an incorrect L1C code delay estimate but correct C/A code delay estimate would cross the detection threshold, simulations with this scenario were performed for various joint detection schemes presented in this chapter. Figs. 5.17-5.22 show the detection probability of the detectors along with the detection probability for a correct C/A code phase but incorrect L1C code phase for each detector. (represented by the

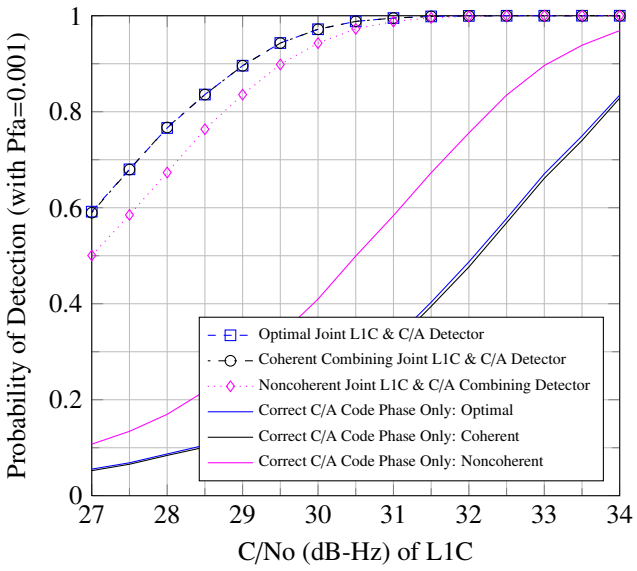

Figure 5.17: Detection probability of joint L1C and C/A detectors with incorrect L1C code phase estimate but correct C/A code phase estimate for acquisition over one L1C spreading code period referenced to L1C signal power.

solid lines) The latter can almost be considered a C/A code detector, however, the detector does contain extra noise terms from the L1C correlators. These figures show that in the infrequent cases that the detector has the correct C/A code phase but incorrect L1C code phase, the detector will declare signal present about 20 percent of the time in the SNR range that joint detectors are beneficial. As the SNR increases, the problem becomes worse, and the receiver will need to implement an algorithm to check if it is acquiring the C/A signal at the correct code phase but the L1C signal at an incorrect code phase.

5.8 Chapter Summary

The trend for future GNSS receivers is multi-signal and multi-constellation capability. Receiver manufacturers are seeking to design devices that use multiple signals from a system while also using multiple satellite navigation systems to get a position, navigation, and timing solution. This chapter aids this trend by focusing on joint detection schemes for acquisition of the composite L1C and L1 C/A in order to improve acquisition sensitivity.

The optimal detector for joint GPS L1C and L1 C/A was derived and its performance

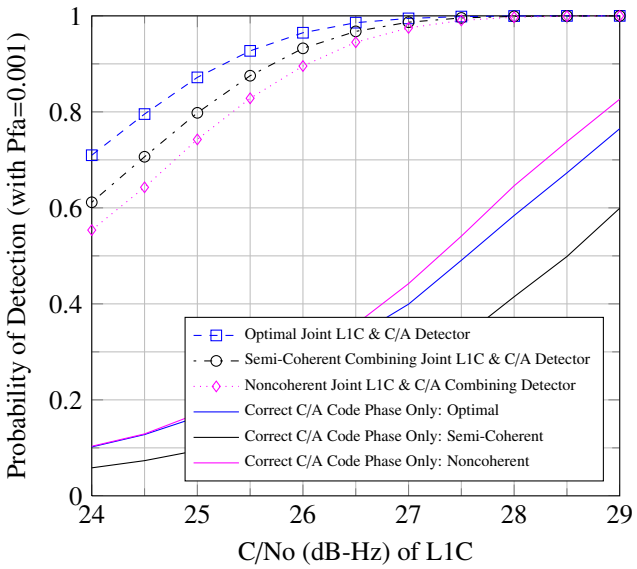

Figure 5.18: Detection probability of joint L1C and C/A detectors with incorrect L1C code phase estimate but correct C/A code phase estimate for acquisition over three L1C spreading code periods referenced to L1C signal power.

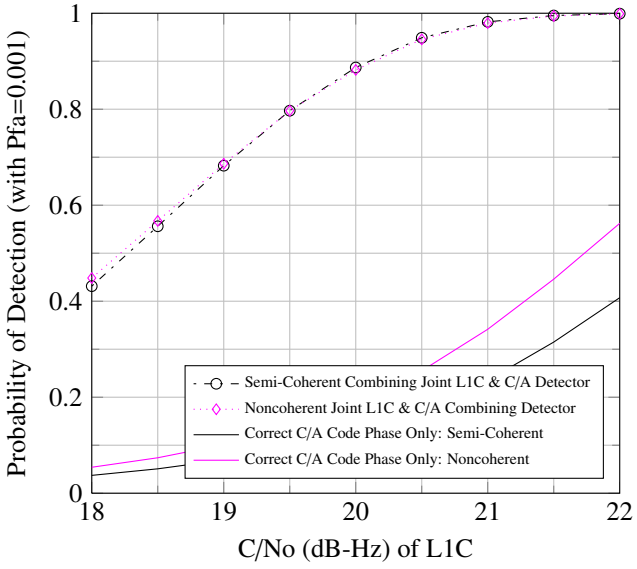

Figure 5.19: Detection probability of joint L1C and C/A detectors with incorrect L1C code phase estimate but correct C/A code phase estimate for acquisition over extended integration time of twenty-five L1C spreading code periods referenced to L1C signal power.

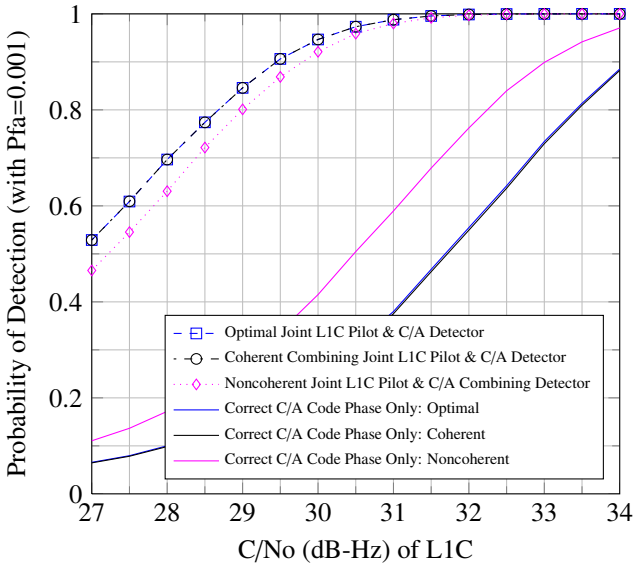

Figure 5.20: Detection probability of joint L1C pilot and C/A detectors with incorrect L1C code phase estimate but correct C/A code phase estimate for acquisition over one L1C spreading code period referenced to L1C signal power.

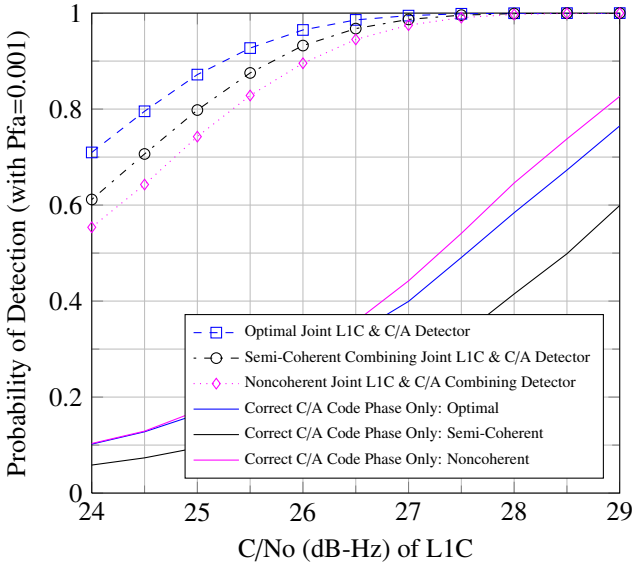

Figure 5.21: Detection probability of joint L1C pilot and C/A detectors with incorrect L1C code phase estimate but correct C/A code phase estimate for acquisition over three L1C spreading code periods referenced to L1C signal power.

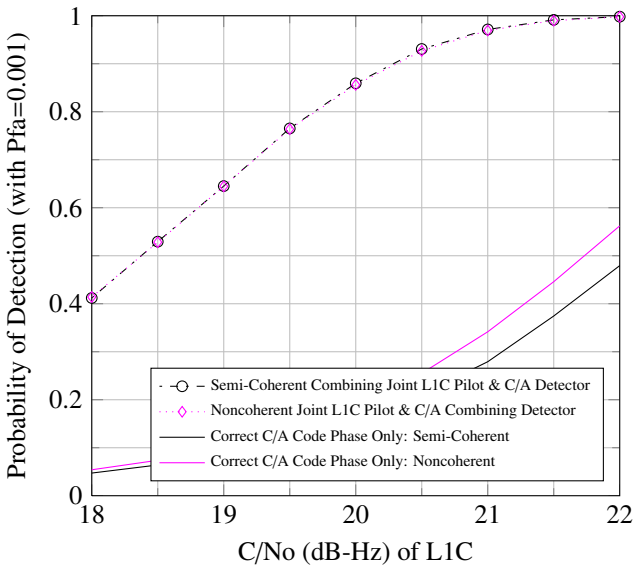

Figure 5.22: Detection probability of joint L1C pilot and C/A detectors with incorrect L1C code phase estimate but correct C/A code phase estimate for acquisition over extended integration time of twenty-five L1C spreading code periods referenced to L1C signal power.

used as a benchmark for other joint acquisition schemes. Coherent combining over one L1C spreading code period by trying all four possible coherent combinations was shown to have optimal performance. Analytical expressions for the detection and false alarm probabilities were derived. Semi-coherent integration used these coherent combinations over multiple spreading code periods. Similar techniques for acquisition were also considered for only using the L1C pilot component along with the C/A code signal. This latter technique may be most attractive to GNSS receiver designers due to the low power contribution from the L1C data component.

CHAPTER 6

CONCLUSIONS AND FUTURE WORK

Modern GPS signals and new satellite navigation systems have created the opportunity for employing new processing techniques for acquisition and tracking in GNSS receivers. As the most recently designed GPS signal, L1C has some novel features that can be exploited to improved receiver performance. The first satellites transmitting the L1C signal are expected to be in orbit by 2015. GNSS receiver designers are starting to incorporate modern GNSS signals, including L1C, into their equipment.

As described in Chapter 1, the objective of this dissertation is to provide a comprehensive evaluation of L1C acquisition and to propose techniques to improve acquisition sensitivity. The unique features of this signal, such as the unequal power in the data and pilot components, are exploited when applicable to achieve better performance. The optimal detectors are derived to provide a benchmark.

6.1 Optimal Detectors

The deployment of new satellite navigation systems such as Galileo and Beidou along with the modernization of GPS and GLONASS, has led to increased research efforts in the field of GNSS, including more sophisticated acquisition techniques. The derivation of the optimal detector for GPS L1C acquisition in this dissertation provides the GNSS community a a benchmark for the best acquisition performance possible in terms of single trial detection and false alarm probabilities.

While this optimal detector may be used in a GNSS receiver, the implementation depends on knowledge of the carrier-to-noise density ratio and the computationally complex modified Bessel function. The noncoherent combining detector was shown to be an approximation to the GPS L1C optimal detector based on a Bessel function approximation. As the coherent integration time is extended, the performance gap between the optimal and noncoherent

detectors was shown to increase. Since the GNSS receiver may have *a priori* knowledge of the pilot overlay code phase and possibly the navigation data, optimal detectors were also derived for these two scenarios.

6.2 Sub-Optimal Detectors

A novel feature of the L1C signal is the unequal power split between the data and pilot components. It was shown that for improved acquisition performance, signal combining techniques need to use unequal power compensation which is a scaling of each signal by their relative power levels. The performance of noncoherent combining with unequal power compensation was shown along with the derivation of analytical detection and false alarm probabilities. Using one spreading code period for acquisition, the noncoherent combining technique reaches within 0.75 dB of the optimal detector acquisition sensitivity, however, this gap increases as the total integration time increases. Techniques to improve on the performance of noncoherent combining for L1C acquisition were proposed and their performance compared to that of the optimal detectors.

Since the relative sign between the pilot and data components is unknown by the receiver, coherent combining of the two components can be achieved by using each combination and selecting the one with the highest power. Analytical expressions for the detection and false alarm probabilities for GPS L1C acquisition using coherent combining were derived. This coherent combining technique was shown to have the same performance as the optimal detector for acquisition using one spreading code period, or 10 ms.

For challenging signal environments where extended integration times are needed for successful acquisition, the coherent combinations from each coherent integration can be noncoherently combined in a technique known as semi-coherent integration. This technique was shown to also outperform noncoherent combining down to a C/No of about 22 dB-Hz. After this point the estimation of the relative sign between components is no longer reliable.

Two acquisition techniques, when the phase of the deterministic L1C pilot overlay

code is known *a priori* by the receiver, were proposed. The first, differentially-coherent integration of the pilot component only was shown to provide up to 2 dB better detection performance over the noncoherent combining of both components. The second technique used the knowledge of the pilot overlay code phase to estimate the navigation data bits allowing for extended coherent integration over multiple code periods.

6.3 Joint Acquisition of L1C and L1 C/A

The GPS L1C and L1 C/A codes share the same carrier frequency, making the joint acquisition of both signals an attractive solution for increased acquisition sensitivity. The optimal detector for joint acquisition was derived, and performance in terms of detection and false alarm probabilities found using Monte Carlo computer simulations. Results showed the expected 2.5 dB increase in acquisition performance at a 0.9 detection probability due to higher received signal power.

The sub-optimal detectors proposed for L1C acquisition were adapted for joint acquisition of three components: L1C pilot, L1C data, and C/A code. The noncoherent combining detector with unequal power compensation had about 0.75 dB in decreased acquisition sensitivity as compared to the optimal joint detector using one spreading code period. This performance gap increases as the number of spreading code periods for acquisition increases in lower SNR environments.

In the composite L1C and L1 C/A signal, the L1C data component contributes to less than 15 percent of the total signal power. A potential tradeoff between receiver complexity and performance is to perform joint acquisition of the L1C pilot component and L1 C/A while ignoring the L1C data component. Various detectors using this technique were proposed. The optimal and coherent combing detectors ignoring the L1C data component were shown to have better detection performance than the noncoherent combining detector using all three components.

6.4 Recommendations for Future Work

In addition to acquisition sensitivity, another important factor is the time it takes to acquire the GNSS signal. For all of the techniques proposed here, the mean acquisition time could be investigated to assist in the engineering tradeoffs between performance and complexity.

The L1C spreading code, with a period of 10 ms, is ten times longer than the legacy L1C C/A code. GNSS chipset designers for cell phones prefer the shorter code to decrease acquisition time. Strategies that use C/A code for initial acquisition and aiding to acquire the L1C signal to facilitate a shift over to L1C for improved tracking performance may be of interest. This returns to the origin of the C/A code, a Coarse Acquisition code originally designed to acquire the military P(Y) signal.

Once GNSS receivers acquire the signal from a satellite, most will shift into tracking the signal as the spreading code delay and Doppler change over time. Joint tracking of multiple GNSS signals is an area of active research and directly applies here to L1C. Whether it is joint tracking of the pilot and data components, or also adding the L1 C/A code signal, performance improvements in joint tracking and position solutions can be investigated.

While it seems as if GPS is already ubiquitous, with improved acquisition techniques along with other tracking enhancements, integration with other sensors, and external out of band assistance, the possible applications for GNSS will expand beyond current imagination.

The sextant, however, may not go away entirely. Coast Guard ships are required to compare GPS positions to an unrelated positioning source at various prescribed intervals depending on distance from land. For open ocean navigation, a celestial observation meets this requirement, and therefore, ships are required to maintain proficiency in the art of celestial navigation. Future Coast Guard cadets onboard the tall-ship *Eagle* should have the opportunity to steady their legs on the rolling and pitching deck, while attempting to swing the arc with a sextant, even as the GPS watch on their wrist is ready to precisely calculate the distance they run for exercise around the deck.

APPENDIX A

ADDITIONAL INFORMATION ON THE POWER SPECTRA OF GPS L1C

The amplitude spectrum of L1C can be found by taking the Fourier Transform of one period of the baseband L1C signal and ignoring the data modulation and overlay code. One period of the data component was described earlier in (2.14):

$$h_D(t) = \sum_{n=0}^{N-1} c_{D,n} g_{BOC(1,1)}(t - nT_c). \tag{A.1}$$

Each spreading code chip, $c_{D,n}$ modulates a BOC(1,1) spreading symbol. Equation (A.1) can be written as a convolution by using impulse functions:

$$h_D(t) = g_{BOC(1,1)}(t) * \sum_{n=0}^{N-1} c_{D,n}\delta(t - nT_c), \tag{A.2}$$

where $*$ indicates convolution and $\delta(t)$ is the unit impulse function. Using the Fourier Transform results in $H_D(f)$:

$$\begin{aligned}
\mathcal{F}\Big\{h_D(t)\Big\} &= \mathcal{F}\left\{g_{BOC(1,1)}(t) * \sum_{n=0}^{N-1} c_{D,n}\delta(t - nT_c)\right\} \\
&= \mathcal{F}\left\{g_{BOC(1,1)}(t)\right\}\mathcal{F}\left\{\sum_{n=0}^{N-1} c_{D,n}\delta(t - nT_c)\right\} \\
&= G(f)\int_{\infty}^{\infty}\sum_{n=0}^{N-1} c_{D,n}\delta(t - nT_c)\mathrm{e}^{-\mathrm{j}2\pi ft}\ \mathrm{d}t \\
&= G(f)\sum_{n=0}^{N-1} c_{D,n}\mathrm{e}^{-\mathrm{j}2\pi fnT_c} \\
&= \sqrt{N}G(f)C(f).
\end{aligned} \tag{A.3}$$

Thus, the Fourier Transform of the data component is the product of the spreading symbol Transform, $G(f)$, and the code Transform, $C(f)$, the latter of which only depends on the spreading code.

APPENDIX B

AMBIGUITY FUNCTION AND CORRELATOR OUTPUTS

To simplify notation for the correlator outputs and to highlight the ambiguity function, complex notation is now used to follow the receiver inphase and quadrature processing. The complex reference signal is:

$$\exp\left(-\mathrm{j}\left(2\pi\left(f_{IF}+\hat{f}_d\right)t+\hat{\theta}\right)\right). \tag{B.1}$$

After multiplying the received GPS L1C signal by the reference signal and low-pass filtering, the inphase and quadrature channels are:

$$\begin{aligned} I+Q = &\sqrt{\tfrac{3}{2}C}d_P(t-\tau)c_P(t-\tau)g_P(t-\tau)\exp\left(\mathrm{j}\left(2\pi\Delta f_d t+\Delta\theta\right)\right) \\ &+\sqrt{\tfrac{1}{2}C}d_D(t-\tau)c_D(t-\tau)g_D(t-\tau)\exp\left(\mathrm{j}\left(2\pi\Delta f_d t+\Delta\theta\right)\right)+\tilde{n}(t), \end{aligned} \tag{B.2}$$

where $\tilde{}$ is used to denote a complex quantity. The output of the complex correlator is:

$$\begin{aligned} \tilde{S} &= I_P+\mathrm{j}Q_P+I_D+\mathrm{j}Q_D \\ &= \sqrt{\tfrac{3}{2}C}\,d_P\exp\left(j\Delta\theta\right)\tilde{R}_P\left(\Delta\tau,\Delta f_d\right)+\sqrt{\tfrac{1}{2}C}\,d_D\exp\left(j\Delta\theta\right)\tilde{R}_D\left(\Delta\tau,\Delta f_d\right)+\tilde{\eta}, \end{aligned} \tag{B.3}$$

where:

$$\tilde{R}_P\left(\Delta\tau,\Delta f_d\right)=\frac{1}{T_c}\int_o^{T_c}c_P(t-\tau)c_P(t-\hat{\tau})g_P(t-\tau)g_P(t-\hat{\tau})\exp\left(\mathrm{j}2\pi\Delta f_d t\right)\,\mathrm{d}t, \tag{B.4}$$

$$\tilde{R}_D\left(\Delta\tau,\Delta f_d\right)=\frac{1}{T_c}\int_o^{T_c}c_D(t-\tau)c_D(t-\hat{\tau})g_D(t-\tau)g_D(t-\hat{\tau})\exp\left(\mathrm{j}2\pi\Delta f_d t\right)\,\mathrm{d}t. \tag{B.5}$$

$\tilde{R}$ is the ambiguity function and depends on both the Doppler error and the code phase error. The magnitude of $\tilde{S}$ can be found to eliminate the two nuisance parameters, the data/overlay code bit and the carrier offset, $\Delta\theta$.

Making the assumption that the spreading codes are random allows for a compact expression for the ambiguity function:

$$E\{\tilde{R}\}=\bar{R}\left(\Delta\tau\right)\exp\left(\mathrm{j}\pi\Delta f_d T_c\right)\mathrm{sinc}\left(\pi\Delta f_d T_c\right), \tag{B.6}$$

where $\bar{R}(\Delta\tau)$ is the average auto-correlation function derived using random codes. Now the expected value of the complex correlator output is:

$$\begin{aligned} E\left\{\tilde{S}\right\} &= \sqrt{\tfrac{3}{2}C}\, d_P \exp(\mathrm{j}\Delta\theta)\, E\{R_P\} + \sqrt{\tfrac{1}{2}C}\, d_D \exp(\mathrm{j}\Delta\theta)\, E\{R_D\} + \tilde{\eta} \\ &= \sqrt{\tfrac{3}{2}C}\, d_P \exp(\mathrm{j}\Delta\theta)\, \bar{R}_P(\Delta\tau) \exp(\mathrm{j}\pi\Delta f_d T_c) \operatorname{sinc}(\pi\Delta f_d T_c) \\ &\quad + \sqrt{\tfrac{1}{2}C}\, d_D \exp(\mathrm{j}\Delta\theta)\, \bar{R}_D(\Delta\tau) \exp(\mathrm{j}\pi\Delta f_d T_c) \operatorname{sinc}(\pi\Delta f_d T_c) + \tilde{\eta}. \end{aligned} \tag{B.7}$$

Substituting $\Delta\theta' = \Delta\theta + \pi\Delta f_d T_c$, the output of the complex correlator is:

$$\begin{aligned} E\left\{\tilde{S}\right\} &= \sqrt{\tfrac{3}{2}C}\, d_P \exp(\mathrm{j}\Delta\theta')\, \bar{R}_P(\Delta\tau) \operatorname{sinc}(\pi\Delta f_d T_c) \\ &\quad + \sqrt{\tfrac{1}{2}C}\, d_D \exp(\mathrm{j}\Delta\theta')\, \bar{R}_D(\Delta\tau) \operatorname{sinc}(\pi\Delta f_d T_c) + \tilde{\eta}. \end{aligned} \tag{B.8}$$

Separating complex correlator outputs into the separate inphase and quadrature channels for both the pilot and data components gives the simplified notation for the expected value of the correlator outputs under the assumption of random codes:

$$\bar{I}_P(\Delta\tau, \Delta f_d, \Delta\theta) = \sqrt{\tfrac{3}{2}C}\, d_P \cos(\Delta\theta')\, \bar{R}_P(\Delta\tau) \operatorname{sinc}(\pi\Delta f_d T_c) + \eta_{P,I}, \tag{B.9}$$

$$\bar{Q}_P(\Delta\tau, \Delta f_d, \Delta\theta) = \sqrt{\tfrac{3}{2}C}\, d_P \sin(\Delta\theta')\, \bar{R}_P(\Delta\tau) \operatorname{sinc}(\pi\Delta f_d T_c) + \eta_{P,Q}, \tag{B.10}$$

$$\bar{I}_D(\Delta\tau, \Delta f_D, \Delta\theta) = \sqrt{\tfrac{1}{2}C}\, d_D \cos(\Delta\theta')\, \bar{R}_D(\Delta\tau) \operatorname{sinc}(\pi\Delta f_d T_c) + \eta_{D,I}, \tag{B.11}$$

$$\bar{Q}_D(\Delta\tau, \Delta f_D, \Delta\theta) = \sqrt{\tfrac{1}{2}C}\, d_D \sin(\Delta\theta')\, \bar{R}_D(\Delta\tau) \operatorname{sinc}(\pi\Delta f_d T_c) + \eta_{D,Q}. \tag{B.12}$$

APPENDIX C

DERIVATION OF OPTIMAL DETECTORS FOR L1C ACQUISITION

The optimal detectors for GPS L1C acquistion presented in Chapter 3 are derived here by finding the ratio of joint probabilities of the observation $\mathbf{r}$ under the hypotheses that the signal is present and that is not present:

$$\Lambda(\mathbf{r}) \triangleq \frac{p(\mathbf{r} \mid H_1)}{p(\mathbf{r} \mid H_0)}, \tag{C.1}$$

where the observation $\mathbf{r}$ is defined as:

$$H_1 : \ \mathbf{r} = \begin{bmatrix} \mathbf{I}_P \\ \mathbf{Q}_P \\ \mathbf{I}_D \\ \mathbf{Q}_D \end{bmatrix} + \mathbf{n} = \begin{bmatrix} \sqrt{\alpha C}\mathbf{d}_P \cos(\Delta\theta) \\ \sqrt{\alpha C}\mathbf{d}_P \sin(\Delta\theta) \\ \sqrt{\beta C}\mathbf{d}_D \cos(\Delta\theta) \\ \sqrt{\beta C}\mathbf{d}_D \sin(\Delta\theta) \end{bmatrix} + \mathbf{n}$$

$$H_0 : \ \mathbf{r} = \mathbf{n}. \tag{C.2}$$

This observation is over integer K spreading code periods. Under H_1, the observation is the $4K \times 1$ vector of correlator outputs from the $K \times 10$ ms observation. The $4K \times 1$ noise vector, $\mathbf{n}$, is white and Gaussian with covariance $\sigma^2\mathbf{I}$, where $\mathbf{I}$ is the identity matrix, and $\sigma^2 = N_0/(2T_{coh})$ [5], with T_{coh} being the coherent integration time. The received signal power is C, with the parameters α and β describing the power split between the two components, so that $\alpha + \beta = 1$. For the GPS L1C signal, $\alpha = 3/4$ and $\beta = 1/4$. The carrier phase residual, or phase offset between the local replica and the received signal, is $\Delta\theta$. Each component may have data, d_P or d_D, which represents any navigation data, overlay code, or a combination of these two items that may be present. These data vectors, $\mathbf{d}_P$ or $\mathbf{d}_D$, are each $K \times 1$ vectors which represent the data bit during each code period.

C.1 Unknown Pilot Overlay Code Phase and Data Bits

The joint probability density function of $\mathbf{r}$ is expressed as a product of the marginal probability density functions, since all of the noise terms are mutually-uncorrelated, and therefore, statistically-independent zero-mean Gaussian random variables. The joint probability density function under hypothesis H_0 (no satellite signal present) is:

$$p(\mathbf{r} \mid H_0) = \left(\frac{1}{(2\pi)^2\sigma^4}\right)^K \exp\left(\frac{-|\mathbf{r}|^2}{2\sigma^2}\right). \tag{C.3}$$

The joint probability density function under hypothesis H_1 (satellite signal is present) is:

$$\begin{aligned} p(\mathbf{r} \mid H_1) &= \left[\frac{1}{(2\pi)^2\,\sigma^4}\right]^K \exp\left[\frac{1}{2\sigma^2}\left|\mathbf{r} - \mathrm{e}^{j\Delta\theta}\begin{bmatrix}\sqrt{\alpha C}\mathbf{d_p}\\ \sqrt{\beta C}\mathbf{d_D}\end{bmatrix}\right|^2\right] \\ &= \left[\frac{1}{(2\pi)^2\,\sigma^4}\right]^K \exp\left(\frac{-p^2}{2\sigma^2}\right), \end{aligned} \tag{C.4}$$

where:

$$\begin{aligned} p^2 = |\mathbf{r}|^2 + KC - 2\sqrt{C}\cos(\Delta\theta)\sum_{k=1}^{K}\left(\sqrt{\alpha}I_{P,k}d_{P,k} + \sqrt{\beta}I_{D,k}d_{D,k}\right) \\ - 2\sqrt{C}\sin(\Delta\theta)\sum_{k=1}^{K}\left(\sqrt{\alpha}Q_{P,k}d_{P,k} + \sqrt{\beta}Q_{D,k}d_{D,k}\right). \end{aligned} \tag{C.5}$$

By substituting (C.5) into (C.4) for p^2, the joint probability density function is now:

$$\begin{aligned} p(\mathbf{r} \mid H_1) = \left[\frac{1}{(2\pi)^2\,\sigma^4}\right]^K \exp\left(\frac{-|\mathbf{r}|^2}{2\sigma^2}\right)\exp\left(\frac{-KC}{2\sigma^2}\right) \\ \cdot\exp\left(\frac{\sqrt{C}}{\sigma^2}\cos(\Delta\theta)\sum_{k=1}^{K}\left(\sqrt{\alpha}I_{P,k}d_{P,k} + \sqrt{\beta}I_{D,k}d_{D,k}\right)\right) \\ \cdot\exp\left(\frac{\sqrt{C}}{\sigma^2}\sin(\Delta\theta)\sum_{k=1}^{K}\left(\sqrt{\alpha}Q_{P,k}d_{P,k} + \sqrt{\beta}Q_{D,k}d_{D,k}\right)\right). \end{aligned} \tag{C.6}$$

Since the carrier phase residual ($\Delta\theta$), overlay code bit (d_P), and data bit (d_D), are unknown, each is considered a random variable with a known *a priori* density. The conditional probability density functions in the likelihood ratio can be found by averaging

$p(\mathbf{r} \mid H_0, \theta, d_P, d_D)$ and $p(\mathbf{r} \mid H_1, \theta, d_P, d_D)$ over the probability density function of the random carrier phase residual and the probability mass function of the random bits:

$$p(\mathbf{r} \mid H_1) = \sum_{\mathbf{d_P}, \mathbf{d_D} \in \{B\}} p(\mathbf{d_P}, \mathbf{d_D}) \int_0^{2\pi} p(\mathbf{r} \mid H_1, \Delta\theta, d_P, d_D)\, p(\Delta\theta \mid H_1)\, \mathrm{d}\Delta\theta,$$
$$p(\mathbf{r} \mid H_0) = \sum_{\mathbf{d_P}, \mathbf{d_D} \in \{B\}} p(\mathbf{d_P}, \mathbf{d_D}) \int_0^{2\pi} p(\mathbf{r} \mid H_0, \Delta\theta, d_P, d_D)\, p(\Delta\theta \mid H_0)\, \mathrm{d}\Delta\theta, \tag{C.7}$$

where B represents all 2^{2K} combinations of the data and pilot bits over the observation interval.

The likelihood ratio is now:

$$\begin{aligned}
\Lambda(\mathbf{r}) &= \frac{p(\mathbf{r} \mid H_1)}{p(\mathbf{r} \mid H_0)} \\
&= \sum_{\mathbf{d_P}, \mathbf{d_D} \in \{B\}} p(\mathbf{d_P}, \mathbf{d_D}) \frac{1}{2\pi} \int_0^{2\pi} \left[\left[\frac{1}{(2\pi)^2\, \sigma^4} \right]^K \exp\left(\frac{-|\mathbf{r}|^2}{2\sigma^2} \right) \exp\left(\frac{-KC}{2\sigma^2} \right) \right. \\
&\quad \cdot \exp\left(\frac{\sqrt{C}}{\sigma^2} \cos(\Delta\theta) \sum_{k=1}^{K} \left(\sqrt{\alpha} I_{P,k} d_{P,k} + \sqrt{\beta} I_{D,k} d_{D,k} \right) \right) \\
&\quad \left. \cdot \exp\left(\frac{\sqrt{C}}{\sigma^2} \sin(\Delta\theta) \sum_{k=1}^{K} \left(\sqrt{\alpha} Q_{P,k} d_{P,k} + \sqrt{\beta} Q_{D,k} d_{D,k} \right) \right) \left((2\pi)^2 \sigma^4 \right)^K \exp\left(\frac{+|\mathbf{r}|^2}{2\sigma^2} \right) \right] \mathrm{d}\Delta\theta \\
&= \exp\left(\frac{-KC}{2\sigma^2} \right) \sum_{\mathbf{d_P}, \mathbf{d_D} \in \{B\}} p(\mathbf{d_P}, \mathbf{d_D}) \frac{1}{2\pi} \int_0^{2\pi} \exp\left(\frac{\sqrt{C}}{\sigma^2} \cos(\Delta\theta)\, (x) \right) \exp\left(\frac{\sqrt{C}}{\sigma^2} \sin(\Delta\theta)\, (y) \right) \mathrm{d}\Delta\theta,
\end{aligned} \tag{C.8}$$

where:

$$\begin{aligned}
x &= \sum_{k=1}^{K} \left(\sqrt{\alpha} I_{P,k} d_{P,k} + \sqrt{\beta} I_{D,k} d_{D,k} \right), \\
y &= \sum_{k=1}^{K} \left(\sqrt{\alpha} Q_{P,k} d_{P,k} + \sqrt{\beta} Q_{D,k} d_{D,k} \right).
\end{aligned} \tag{C.9}$$

The first exponential function in (C.8) is neither a function of the observation, of the carrier phase offset, nor of the overlay/data bits; thus, this function is incorporated with the threshold so that the likelihood ratio for the optimal GPS L1C detector becomes:

$$\begin{aligned}
\Lambda'(\mathbf{r}) &= \sum_{\mathbf{d_P}, \mathbf{d_D} \in \{B\}} p(\mathbf{d_P}, \mathbf{d_D}) \frac{1}{2\pi} \int_0^{2\pi} \left[\exp\left(\frac{\sqrt{C}}{\sigma^2} \cos(\Delta\theta)\, (x) \right) \exp\left(\frac{\sqrt{C}}{\sigma^2} \sin(\Delta\theta)\, (y) \right) \right] \mathrm{d}\Delta\theta \\
&= \sum_{\mathbf{d_P}, \mathbf{d_D} \in \{B\}} p(\mathbf{d_P}, \mathbf{d_D}) I_0 \left(\frac{\sqrt{C}}{\sigma^2} \sqrt{x^2 + y^2} \right),
\end{aligned} \tag{C.10}$$

where I_0 is the modified Bessel function of zeroth order, and x and y are defined in (C.9). This result is similar to the optimal detector for acquisition of the GPS L5 signal derived in [33]; however, the optimal GPS L1C detector presented here includes scale factors based on the power split between the data and pilot components. In addition, there is a different ordering of terms since the L1C components are in-phase as opposed to in-phase quadrature for the L5 signal.

Under the assumption that all combinations of pilot and data bits are possible and equally probable, and therefore incorporating these probabilities into the threshold, the likelihood ratio is now:

$$\Lambda'(\mathbf{r}) = \sum_{\mathbf{d_P},\mathbf{d_D}\in\{B\}} I_0\left(\frac{\sqrt{C}}{\sigma^2}\sqrt{x^2+y^2}\right). \tag{C.11}$$

Comparing this new likelihood ratio to a threshold gives the optimal detector:

$$\sum_{\mathbf{d_P},\mathbf{d_D}\in\{B\}} I_0\left(\frac{\sqrt{C}}{\sigma^2}\sqrt{x^2+y^2}\right) \underset{H_0}{\overset{H_1}{\gtrless}} \lambda'. \tag{C.12}$$

C.2 Known Pilot Overlay Code Phase and Unknown Data Bits

The likelihood ratio is again derived, starting with the same joint probability densities of the observation vector under the two hypotheses as defined in equations (C.3) and (C.6).

Since the carrier phase residual ($\Delta\theta$) and data bit (d_D) are unknown, each is considered a random variable with a known *a priori* density; however, this time, the pilot overlay code bits are known. The conditional probability density functions in the likelihood ratio can be found by averaging $p(\mathbf{r} \mid H_0, \theta, d_D)$ and $p(\mathbf{r} \mid H_1, \theta, d_D)$ over the probability density function of the random carrier phase residual and the probability mass function of the random data bits:

$$\begin{aligned} p(\mathbf{r} \mid H_1) &= \sum_{\mathbf{d_D}\in\{B\}} p(\mathbf{d_D}) \int_0^{2\pi} p(\mathbf{r} \mid H_1, \Delta\theta, d_D)\, p(\Delta\theta \mid H_1)\, \mathrm{d}\Delta\theta, \\ p(\mathbf{r} \mid H_0) &= \sum_{\mathbf{d_D}\in\{B\}} p(\mathbf{d_D}) \int_0^{2\pi} p(\mathbf{r} \mid H_0, \Delta\theta, d_D)\, p(\Delta\theta \mid H_0)\, \mathrm{d}\Delta\theta, \end{aligned} \tag{C.13}$$

where B now represents the 2^K possible combinations of the data bits over the observation interval which has been reduced from 2^{2K} possible combinations when the pilot bits were unknown.

The likelihood ratio is now:

$$\begin{aligned}\Lambda(\mathbf{r}) &= \frac{p\left(\mathbf{r} \mid H_1\right)}{p\left(\mathbf{r} \mid H_0\right)} \\ &= \sum_{\mathbf{d_D}\in\{B\}} p(\mathbf{d_D}) \frac{1}{2\pi} \int_0^{2\pi} \left[\left[\frac{1}{(2\pi)^2 \sigma^4} \right]^K \exp\left(\frac{-|\mathbf{r}|^2}{2\sigma^2} \right) \exp\left(\frac{-KC}{2\sigma^2} \right) \right. \\ &\quad \cdot \exp\left(\frac{\sqrt{C}}{\sigma^2} \cos(\Delta\theta) \sum_{k=1}^{K} \left(\sqrt{\alpha} I_{P,k} d_{P,k} + \sqrt{\beta} I_{D,k} d_{D,k} \right) \right) \\ &\quad \left. \cdot \exp\left(\frac{\sqrt{C}}{\sigma^2} \sin(\Delta\theta) \sum_{k=1}^{K} \left(\sqrt{\alpha} Q_{P,k} d_{P,k} + \sqrt{\beta} Q_{D,k} d_{D,k} \right) \right) \left((2\pi)^2 \sigma^4 \right)^K \exp\left(\frac{+|\mathbf{r}|^2}{2\sigma^2} \right) \right] \mathrm{d}\Delta\theta \\ &= \exp\left(\frac{-KC}{2\sigma^2} \right) \sum_{\mathbf{d_D}\in\{B\}} p(\mathbf{d_D}) \frac{1}{2\pi} \int_0^{2\pi} \exp\left(\frac{\sqrt{C}}{\sigma^2} \cos(\Delta\theta)\,(x) \right) \exp\left(\frac{\sqrt{C}}{\sigma^2} \sin(\Delta\theta)\,(y) \right) \mathrm{d}\Delta\theta, \end{aligned} \tag{C.14}$$

where:

$$\begin{aligned} x &= \sum_{k=1}^{K} \left(\sqrt{\alpha} I_{P,k} d_{P,k} + \sqrt{\beta} I_{D,k} d_{D,k} \right), \\ y &= \sum_{k=1}^{K} \left(\sqrt{\alpha} Q_{P,k} d_{P,k} + \sqrt{\beta} Q_{D,k} d_{D,k} \right). \end{aligned} \tag{C.15}$$

Once again, the first exponential function in (C.14) is not a function of the observable, the carrier phase offset, or data bits; thus, this function is incorporated with the threshold so that the likelihood ratio for the optimal GPS L1C detector in this particular scenario becomes:

$$\begin{aligned} \Lambda'(\mathbf{r}) &= \sum_{\mathbf{d_D}\in\{B\}} p(\mathbf{d_D}) \frac{1}{2\pi} \int_0^{2\pi} \left[\exp\left(\frac{\sqrt{C}}{\sigma^2} \cos(\Delta\theta)\,(x) \right) \exp\left(\frac{\sqrt{C}}{\sigma^2} \sin(\Delta\theta)\,(y) \right) \right] \mathrm{d}\Delta\theta \\ &= \sum_{\mathbf{d_D}\in\{B\}} p(\mathbf{d_D}) I_0\left(\frac{\sqrt{C}}{\sigma^2} \sqrt{x^2 + y^2} \right), \end{aligned} \tag{C.16}$$

or, since the data bits are assumed to be equally likely:

$$\Lambda'(\mathbf{r}) = \sum_{\mathbf{d_D}\in\{B\}} I_0\left(\frac{\sqrt{C}}{\sigma^2} \sqrt{x^2 + y^2} \right), \tag{C.17}$$

where I_0 is the modified Bessel function of zeroth order, and x and y are defined in (C.15), with each $d_{P,k}$ known.

C.3 Known Pilot Overlay Code Phase and Known Data Bits

In the scenario in which the receiver has knowlege of both the pilot overlay code phase and navigation data bits, the carrier phase residual ($\Delta\theta$) is still unknown and considered a random variable with a uniform probability density. The conditional probability density functions in the likelihood ratio are now:

$$\begin{aligned} p\left(\mathbf{r} \mid H_1\right) &= \int_0^{2\pi} p\left(\mathbf{r} \mid H_1, \Delta\theta\right) p\left(\Delta\theta \mid H_1\right) \, \mathrm{d}\Delta\theta, \\ p\left(\mathbf{r} \mid H_0\right) &= \int_0^{2\pi} p\left(\mathbf{r} \mid H_0, \Delta\theta\right) p\left(\Delta\theta \mid H_0\right) \, \mathrm{d}\Delta\theta. \end{aligned} \tag{C.18}$$

The optimal detector is now:

$$\begin{aligned} \Lambda(\mathbf{r}) &= \frac{1}{2\pi} \int_0^{2\pi} \left[\exp\left(\frac{\sqrt{C}}{\sigma^2} \cos(\Delta\theta) \, (x) \right) \exp\left(\frac{\sqrt{C}}{\sigma^2} \sin(\Delta\theta) \, (y) \right) \right] \mathrm{d}\Delta\theta \\ &= I_0\left(\frac{\sqrt{C}}{\sigma^2} \sqrt{x^2 + y^2} \right), \end{aligned} \tag{C.19}$$

where I_0 is the modified Bessel function of zeroth order, and x and y are:

$$\begin{aligned} x &= \sum_{k=1}^{K} \left(\sqrt{\alpha} I_{P,k} d_{P,k} + \sqrt{\beta} I_{D,k} d_{D,k} \right), \\ y &= \sum_{k=1}^{K} \left(\sqrt{\alpha} Q_{P,k} d_{P,k} + \sqrt{\beta} Q_{D,k} d_{D,k} \right), \end{aligned} \tag{C.20}$$

where each $d_{P,k}$ and $d_{D,k}$ are known. The modified Bessel function is monotone and is removed by adjusting the threshold. A simplified, yet equivalent, optimal detector when the data bits and the pilot overlay code phase are known is:

$$\Lambda'(\mathbf{r}) = \left[\sum_{k=1}^{K} \left(\sqrt{\alpha} I_{P,k} d_{P,k} + \sqrt{\beta} I_{D,k} d_{D,k} \right) \right]^2 + \left[\sum_{k=1}^{K} \left(\sqrt{\alpha} Q_{P,k} d_{P,k} + \sqrt{\beta} Q_{D,k} d_{D,k} \right) \right]^2. \tag{C.21}$$

APPENDIX D

DERIVATION OF OPTIMAL DETECTOR FOR JOINT L1C AND C/A ACQUISITION

In this appendix, classical detection theory is used, following the same procedure as in Appendix C, to derive the optimal detector for joint L1C and C/A acquisition. Processing is performed over an arbitrary integer number of primary spreading code periods of the GPS L1C signal. The signal specification requires that the spreading code chips for the two signals be synchronized [14]; therefore, each period of the L1C code is assumed to contain 10 complete periods of the C/A code. Despite having a shorter spreading code period, C/A code has a data bit duration that is twice as long as L1C: $T_{d,C/A} = 20$ ms. Possible data transitions on the C/A signal occur at the same time as every other possible data transition on each L1C component.

The outputs of the correlators are used here as the observation since they are sufficient statistics for detecting the signal in an additive white Gaussian noise channel [46, 27]. Due to autocorrelation properties of the codes, it is assumed that the correlator outputs contain noise only if an incorrect delay estimate is used. If the correlation outputs are observed every 10 ms a total of K times, then observation at the output of the complex correlators are the following two hypotheses:

$$H_1 : \ \mathbf{r} = \begin{bmatrix} \sqrt{\alpha C}\mathbf{d}_P \mathrm{e}^{\mathrm{j}\Delta\theta} \\ \sqrt{\beta C}\mathbf{d}_D \mathrm{e}^{\mathrm{j}\Delta\theta} \\ \sqrt{\gamma C}\mathbf{d}_{C/A}\left(-\mathrm{j}\mathrm{e}^{\mathrm{j}\Delta\theta}\right) \end{bmatrix} + \mathbf{n}$$

$$H_0 : \ \mathbf{r} = \mathbf{n}, \tag{D.1}$$

where the data, $\mathbf{d}_P$, $\mathbf{d}_D$ and $\mathbf{d}_{C/A}$, are each $K \times 1$ vectors which contain the data bit during 10 ms correlation. Under H_1, the observation is the $3K \times 1$ vector of correlator outputs from the $K \times 10$ ms observation. The $3K \times 1$ noise vector, $\mathbf{n}$, is white and Gaussian with covariance

$\sigma^2\mathbf{I}$, where $\mathbf{I}$ is the identity matrix and $\sigma^2 = N_0/(2T_c)$ [5]. The received signal power is C, with the parameters α, β, and γ describing the power split among the three components (L1C Pilot, L1C Data, C/A Code), so that $\alpha + \beta + \gamma = 1$. For the joint GPS L1C and C/A acquisition, $\alpha = 20/48, \beta = 7/48$ and $\gamma = 20/48$ as noted in (5.3). The carrier phase residual is $\Delta\theta$. Each component contains data which represent any navigation bits, overlay code, or a combination of these two items which may be present.

Since the *a priori* probabilities of a signal's presence are unknown, the Neyman-Pearson criterion is used to maximize the probability of detection (P_d) under a particular probability of false alarm constraint (P_f). The optimum test consists of using the observation $\mathbf{r}$ to find the likelihood ratio $\Lambda(\mathbf{r})$ and comparing this result to a threshold to make a decision [46]. The likelihood ratio consists of conditional joint probabilities:

$$\Lambda(\mathbf{r}) \triangleq \frac{p(\mathbf{r} \mid H_1)}{p(\mathbf{r} \mid H_0)}. \tag{D.2}$$

The likelihood ratio test is:

$$\Lambda(\mathbf{r}) \underset{H_0}{\overset{H_1}{\gtrless}} TH, \tag{D.3}$$

where the threshold, TH, is determined as follows for a fixed P_f:

$$P_f = \int_{TH}^{\infty} p(\Lambda \mid H_0)\, \mathrm{d}\Lambda. \tag{D.4}$$

The joint probability density function of $\mathbf{r}$ is expressed as a product of the marginal probability density functions since all of the noise terms are mutually-uncorrelated, and therefore, statistically-independent zero-mean Gaussian random variables. The joint probability density function under hypothesis H_0 (no satellite signal present) is:

$$p(\mathbf{r} \mid H_0) = \left(\frac{1}{(2\pi)^3\sigma^6}\right)^K \exp\left(\frac{-|\mathbf{r}|^2}{2\sigma^2}\right). \tag{D.5}$$

The joint probability density function under hypothesis H_1 (satellite signal is present) is:

$$p(\mathbf{r} \mid H_1) = \left[\frac{1}{(2\pi)^3\,\sigma^6}\right]^K \exp\left[\frac{-1}{2\sigma^2}\left|\mathbf{r} - \begin{bmatrix} \sqrt{\alpha C}\,\mathbf{d}_P e^{j\Delta\theta} \\ \sqrt{\beta C}\,\mathbf{d}_D e^{j\Delta\theta} \\ \sqrt{\gamma C}\,\mathbf{d}_{C/A}\left(-je^{j\Delta\theta}\right) \end{bmatrix}\right|^2\right]$$
$$= \left[\frac{1}{(2\pi)^3\,\sigma^6}\right]^K \exp\left(\frac{-p^2}{2\sigma^2}\right), \tag{D.6}$$

where:

$$p^2 = |\mathbf{r}|^2 + KC - 2\sqrt{C}\cos(\Delta\theta)\sum_{k=1}^{K}\left(\sqrt{\alpha}I_{P,k}d_{P,k} + \sqrt{\beta}I_{D,k}d_{D,k} - \sqrt{\gamma}Q_{C/A,k}d_{C/A,k}\right)$$
$$- 2\sqrt{C}\sin(\Delta\theta)\sum_{k=1}^{K}\left(\sqrt{\alpha}Q_{P,k}d_{P,k} + \sqrt{\beta}Q_{D,k}d_{D,k} + \sqrt{\gamma}I_{C/A,k}d_{C/A,k}\right). \tag{D.7}$$

By substituting (C.5) into (C.4) for p^2, the joint probability density function is now:

$$p(\mathbf{r} \mid H_1) = \left[\frac{1}{(2\pi)^3\,\sigma^6}\right]^K \exp\left(\frac{-|\mathbf{r}|^2}{2\sigma^2}\right)\exp\left(\frac{-KC}{2\sigma^2}\right)$$
$$\cdot \exp\left(\frac{\sqrt{C}}{\sigma^2}\cos(\Delta\theta)\sum_{k=1}^{K}\left(\sqrt{\alpha}I_{P,k}d_{P,k} + \sqrt{\beta}I_{D,k}d_{D,k} - \sqrt{\gamma}Q_{C/A,k}d_{C/A,k}\right)\right)$$
$$\cdot \exp\left(\frac{\sqrt{C}}{\sigma^2}\sin(\Delta\theta)\sum_{k=1}^{K}\left(\sqrt{\alpha}Q_{P,k}d_{P,k} + \sqrt{\beta}Q_{D,k}d_{D,k} + \sqrt{\gamma}I_{C/A,k}d_{C/A,k}\right)\right). \tag{D.8}$$

Since the carrier phase residual ($\Delta\theta$), the overlay code bit (d_P), and the data bits (d_D, $d_{C/A}$), are unknown, each is considered a random variable with a known *a priori* density. The conditional probability density functions in the likelihood ratio can be found by averaging $p(\mathbf{r} \mid H_0, \theta, d_P, d_D, d_C)$ and $p(\mathbf{r} \mid H_1, \theta, d_P, d_D, d_C)$ over the probability density function of the random carrier phase residual and the probability mass function of the random bits:

$$p(\mathbf{r} \mid H_1) = \sum_{\mathbf{d}_P,\mathbf{d}_D,\mathbf{d}_{C/A}\in\{B\}} p(\mathbf{d}_P, \mathbf{d}_D, \mathbf{d}_{C/A}) \int_0^{2\pi} p(\mathbf{r} \mid H_1, \Delta\theta, d_P, d_D, d_{C/A})\, p(\Delta\theta \mid H_1)\, \mathrm{d}\Delta\theta,$$
$$p(\mathbf{r} \mid H_0) = \sum_{\mathbf{d}_P,\mathbf{d}_D,\mathbf{d}_{C/A}\in\{B\}} p(\mathbf{d}_P, \mathbf{d}_D, \mathbf{d}_{C/A}) \int_0^{2\pi} p(\mathbf{r} \mid H_0, \Delta\theta, d_P, d_D, d_{C/A})\, p(\Delta\theta \mid H_0)\, \mathrm{d}\Delta\theta, \tag{D.9}$$

where B represents all possible combinations of the L1C data, the L1C pilot, and the C/A navigation symbols over the observation interval.

The likelihood ratio is now:

$$\begin{aligned}
\Lambda(\mathbf{r}) &= \frac{p\left(\mathbf{r} \mid H_1\right)}{p\left(\mathbf{r} \mid H_0\right)} \\
&= \sum_{\mathbf{d}_P,\mathbf{d}_D,\mathbf{d}_{C/A}\in\{B\}} p(\mathbf{d}_P,\mathbf{d}_D,\mathbf{d}_{C/A})\frac{1}{2\pi}\int_0^{2\pi}\left[\left[\frac{1}{(2\pi)^6\,\sigma^6}\right]^K \exp\left(\frac{-|\mathbf{r}|^2}{2\sigma^2}\right)\exp\left(\frac{-KC}{2\sigma^2}\right)\right. \\
&\quad \cdot \exp\left(\frac{\sqrt{C}}{\sigma^2}\cos(\Delta\theta)\sum_{k=1}^{K}\left(\sqrt{\alpha}I_{P,k}d_{P,k}+\sqrt{\beta}I_{D,k}d_{D,k}-\sqrt{\gamma}Q_{C/A,k}d_{C/A,k}\right)\right) \\
&\quad \left.\cdot \exp\left(\frac{\sqrt{C}}{\sigma^2}\sin(\Delta\theta)\sum_{k=1}^{K}\left(\sqrt{\alpha}Q_{P,k}d_{P,k}+\sqrt{\beta}Q_{D,k}d_{D,k}+\sqrt{\gamma}I_{C/A,k}d_{C/A,k}\right)\right)\left((2\pi)^3\sigma^6\right)^K \exp\left(\frac{+|\mathbf{r}|^2}{2\sigma^2}\right)\right]\mathrm{d}\Delta\theta \\
&= \exp\left(\frac{-KC}{2\sigma^2}\right)\sum_{\mathbf{d}_P,\mathbf{d}_D,\mathbf{d}_{C/A}\in\{B\}} p(\mathbf{d}_P,\mathbf{d}_D,\mathbf{d}_{C/A}) \\
&\quad \cdot\frac{1}{2\pi}\int_0^{2\pi}\exp\left(\frac{\sqrt{C}}{\sigma^2}\cos(\Delta\theta)\,(x)\right)\exp\left(\frac{\sqrt{C}}{\sigma^2}\sin(\Delta\theta)\,(y)\right)\mathrm{d}\Delta\theta, \qquad \text{(D.10)}
\end{aligned}$$

where:

$$\begin{aligned}
x &= \sum_{k=1}^{K}\left(\sqrt{\alpha}I_{P,k}d_{P,k} + \sqrt{\beta}I_{D,k}d_{D,k}-\sqrt{\gamma}Q_{C/A,k}d_{C/A,k}\right), \\
y &= \sum_{k=1}^{K}\left(\sqrt{\alpha}Q_{P,k}d_{P,k} + \sqrt{\beta}Q_{D,k}d_{D,k}+\sqrt{\gamma}I_{C/A,k}d_{C/A,k}\right). \qquad \text{(D.11)}
\end{aligned}$$

The first exponential function in (D.10) is not a function of the observable, the carrier phase offset, or overlay/data bits; thus, the offset is incorporated into the threshold so that the likelihood ratio for the optimal GPS C/A and L1C joint detector becomes:

$$\begin{aligned}
\Lambda(\mathbf{r}) &= \sum_{\mathbf{d}_P,\mathbf{d}_D,\mathbf{d}_{C/A}\in\{B\}} p(\mathbf{d}_P,\mathbf{d}_D,\mathbf{d}_{C/A})\frac{1}{2\pi}\int_0^{2\pi}\left[\exp\left(\frac{\sqrt{C}}{\sigma^2}\cos(\Delta\theta)\,(x)\right)\exp\left(\frac{\sqrt{C}}{\sigma^2}\sin(\Delta\theta)\,(y)\right)\right]\mathrm{d}\Delta\theta \\
&= \sum_{\mathbf{d}_P,\mathbf{d}_D,\mathbf{d}_{C/A}\in\{B\}} p(\mathbf{d}_P,\mathbf{d}_D,\mathbf{d}_{C/A})I_0\left(\frac{\sqrt{C}}{\sigma^2}\sqrt{x^2+y^2}\right), \qquad \text{(D.12)}
\end{aligned}$$

where I_0 is the modified Bessel function of zeroth order and where x and y are defined in (D.11).

APPENDIX E

JOINT ACQUISITION DETECTION PROBABILITIES REFERENCED TO C/N_O OF L1 C/A CODE SIGNAL

This appendix contains figures to show the detection probabilities for the joint acquisition schemes presented in Chapter 5. The only difference in these results to those already presented and described in Chapter 5 is a carrier-to-noise density (C/No) that is referenced to the L1 C/A code signal instead of the L1C signal. These results may be more useful to GNSS receiver designers comparing the performance of these new joint detectors to that of legacy GPS C/A code only receivers.

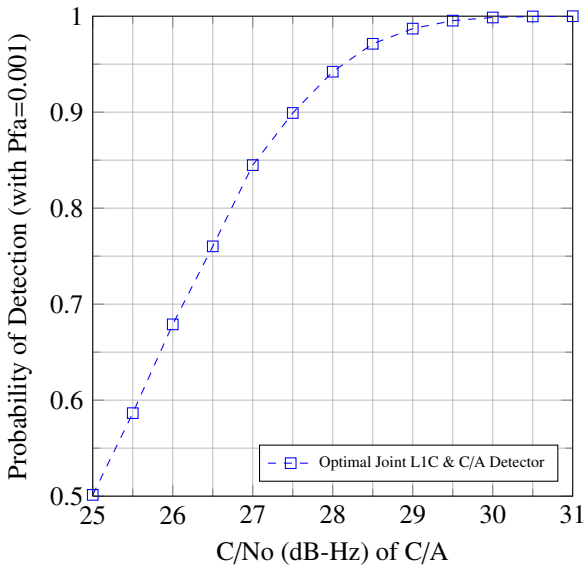

Figure E.1: Detection probability of optimal joint L1C and C/A detector compared to optimal L1C detector for acquisition over one L1C spreading code period referenced to L1 C/A signal power.

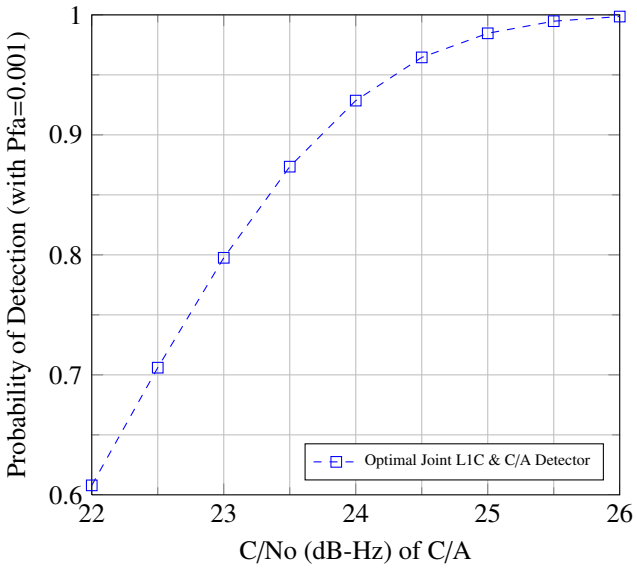

Figure E.2: Detection probability of optimal joint L1C and C/A detector compared to optimal L1C detector for acquisition over three L1C spreading code periods referenced to L1 C/A signal power.

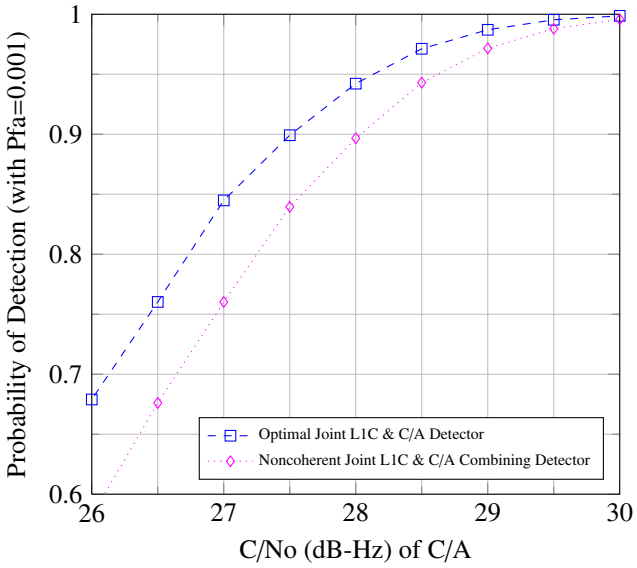

Figure E.3: Detection probability of noncoherent combining joint L1C and C/A detector for acquisition over one L1C spreading code period referenced to L1 C/A signal power.

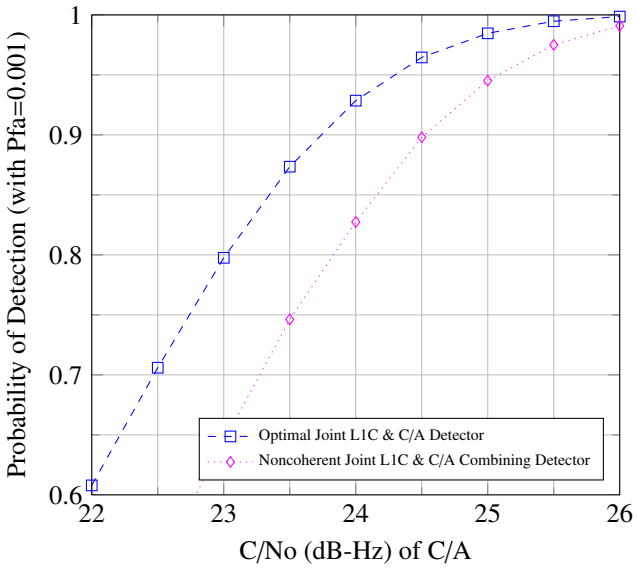

Figure E.4: Detection probability of noncoherent combining joint L1C and C/A detector for acquisition over three L1C spreading code periods referenced to L1 C/A signal power.

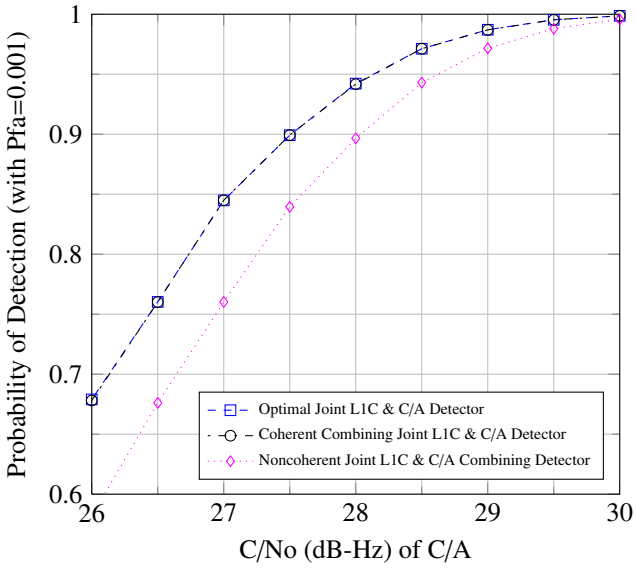

Figure E.5: Detection probability of coherent combining joint L1C and C/A detector for acquisition over one L1C spreading code period referenced to L1 C/A signal power.

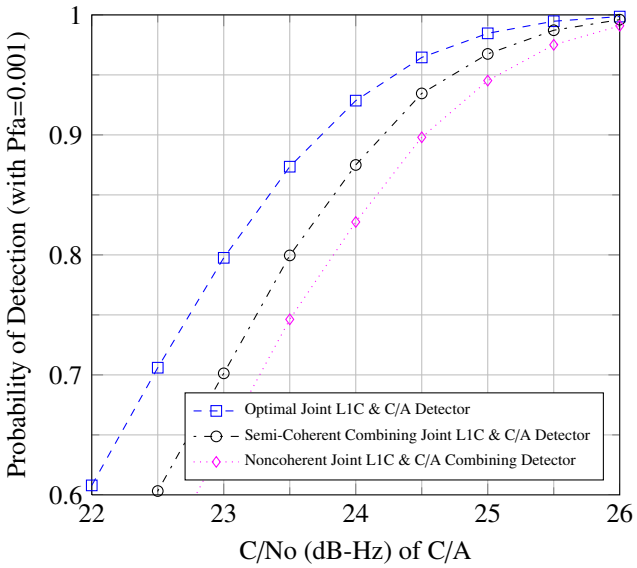

Figure E.6: Detection probability of semi-coherent joint L1C and C/A detector for acquisition over three L1C spreading code periods referenced to L1 C/A signal power.

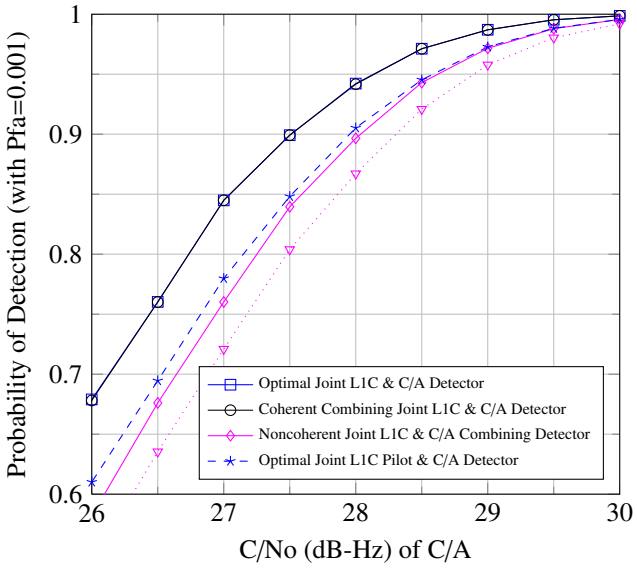

Figure E.7: Detection probability of optimal joint L1C pilot and C/A detector for acquisition over one L1C spreading code period referenced to L1 C/A signal power.

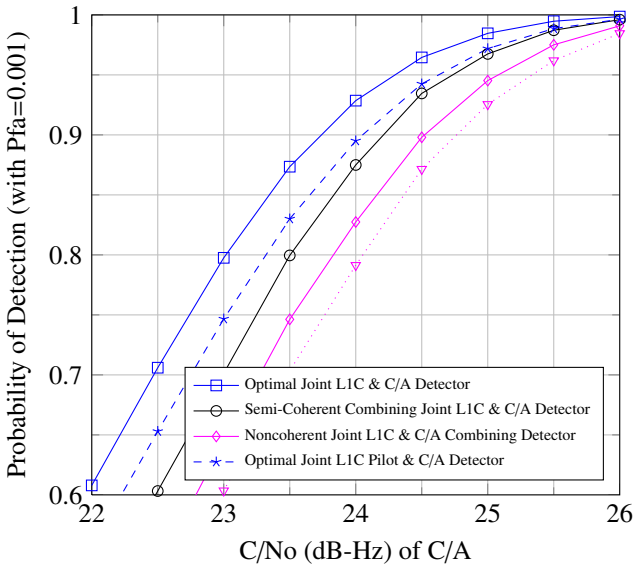

Figure E.8: Detection probability of optimal joint L1C pilot and C/A detector for acquisition over three L1C spreading code periods referenced to L1 C/A signal power.

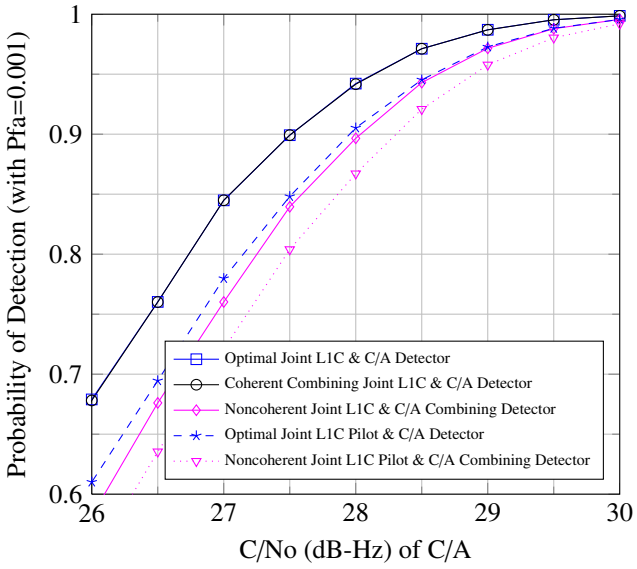

Figure E.9: Detection probability of noncoherent combining joint L1C pilot and C/A detector for acquisition over one L1C spreading code period referenced to L1 C/A signal power.

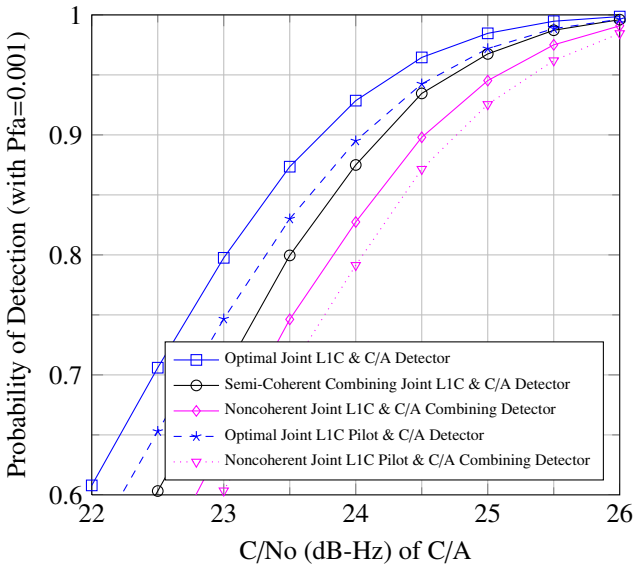

Figure E.10: Detection probability of noncoherent combining joint L1C pilot and C/A detector for acquisition over three L1C spreading code periods referenced to L1 C/A signal power.

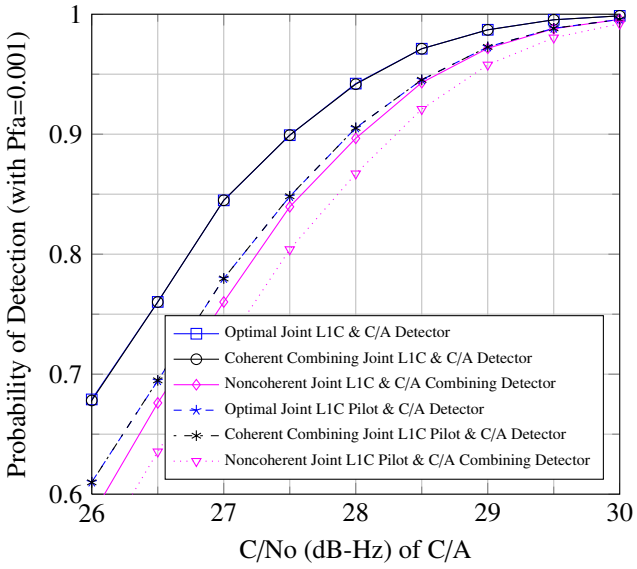

Figure E.11: Detection probability of coherent combining joint L1C pilot and C/A detector for acquisition over one L1C spreading code period referenced to L1 C/A signal power.

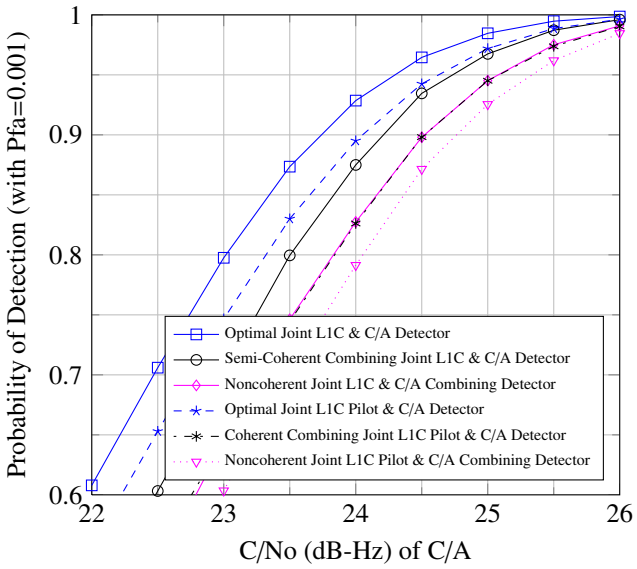

Figure E.12: Detection probability of semi-coherent combining joint L1C pilot and C/A detector for acquisition over three L1C spreading code periods referenced to L1 C/A signal power.

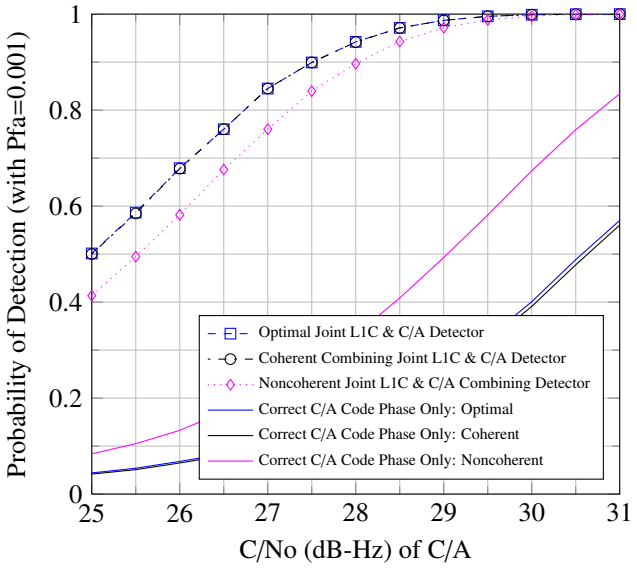

Figure E.13: Detection probability of joint L1C and C/A detectors with incorrect L1C code phase estimate but correct C/A code phase estimate for acquisition over one L1C spreading code period referenced to L1 C/A signal power.

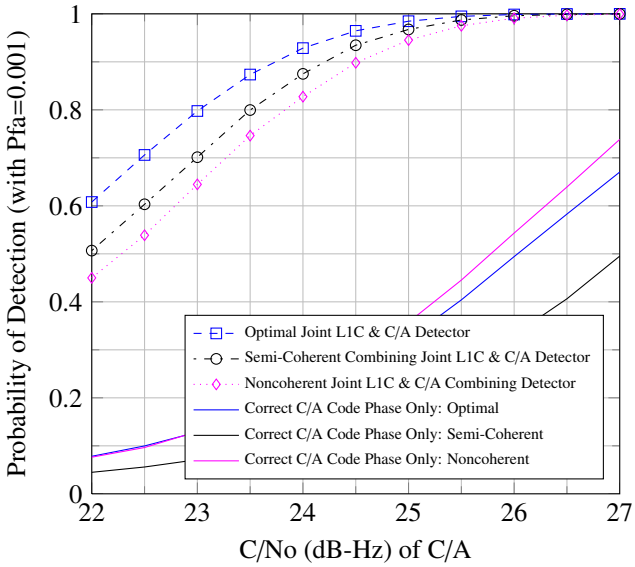

Figure E.14: Detection probability of joint L1C and C/A detectors with incorrect L1C code phase estimate but correct C/A code phase estimate for acquisition over three L1C spreading code periods referenced to L1 C/A signal power.

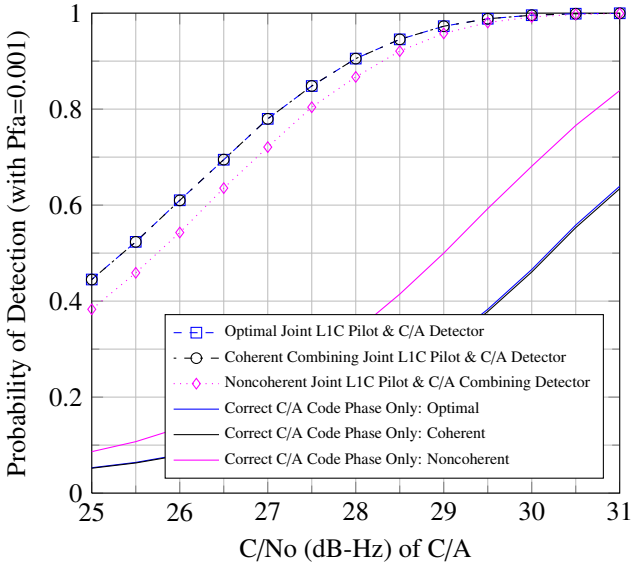

Figure E.15: Detection probability of joint L1C pilot and C/A detectors with incorrect L1C code phase estimate but correct C/A code phase estimate for acquisition over one L1C spreading code period referenced to L1 C/A signal power.

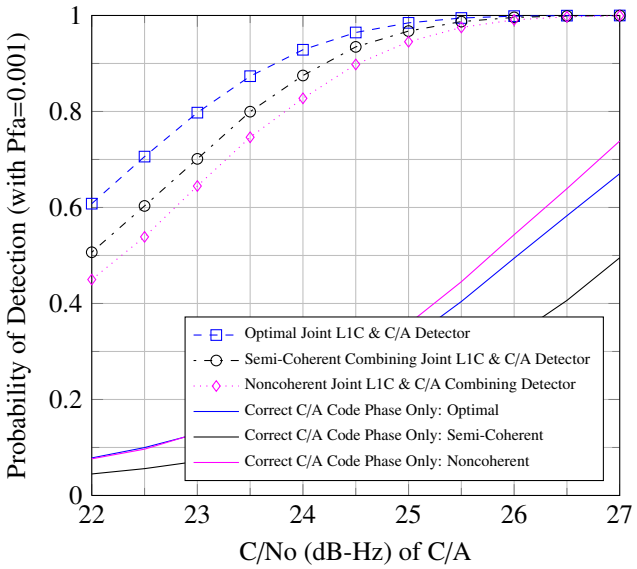

Figure E.16: Detection probability of joint L1C pilot and C/A detectors with incorrect L1C code phase estimate but correct C/A code phase estimate for acquisition over three L1C spreading code periods referenced to L1 C/A signal power.

APPENDIX F

JOINT ACQUISITION DETECTION PROBABILITIES REFERENCED TO C/N_O OF COMPOSITE SIGNAL

This appendix contains figures to show the detection probabilities for the joint acquisition schemes presented in Chapter 5. The only difference in these results to those already presented and described in Chapter 5 is a carrier-to-noise density (C/No) that is referenced to the composite L1C and C/A code signal instead of the L1C signal.

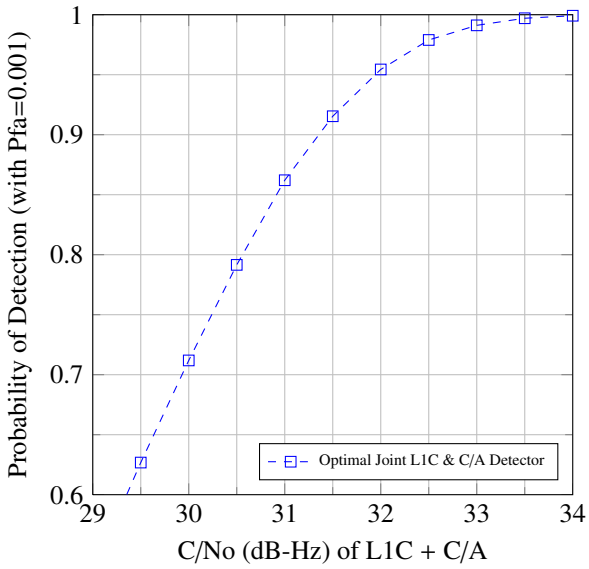

Figure F.1: Detection probability of optimal joint L1C and C/A detector compared to optimal L1C detector for acquisition over one L1C spreading code period referenced to the L1C and C/A composite signal power.

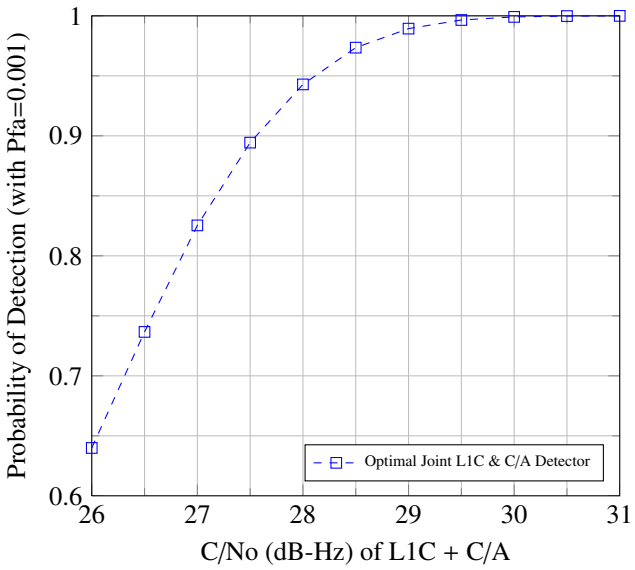

Figure F.2: Detection probability of optimal joint L1C and C/A detector compared to optimal L1C detector for acquisition over three L1C spreading code periods referenced to the L1C and C/A composite signal power.

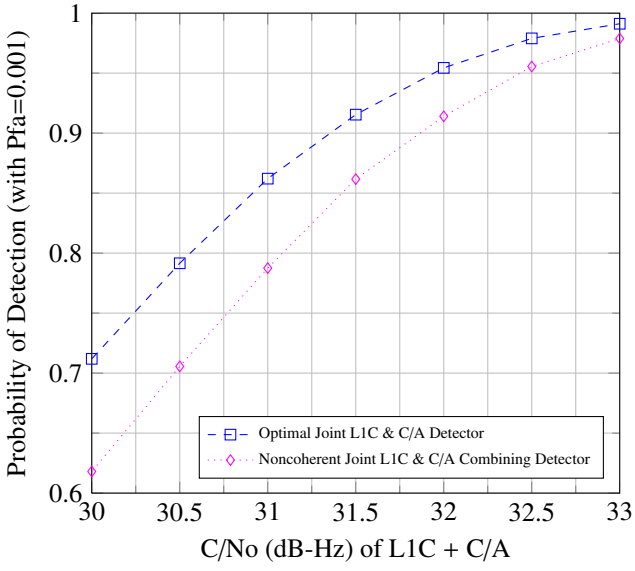

Figure F.3: Detection probability of noncoherent combining joint L1C and C/A detector for acquisition over one L1C spreading code period referenced to the L1C and C/A composite signal power.

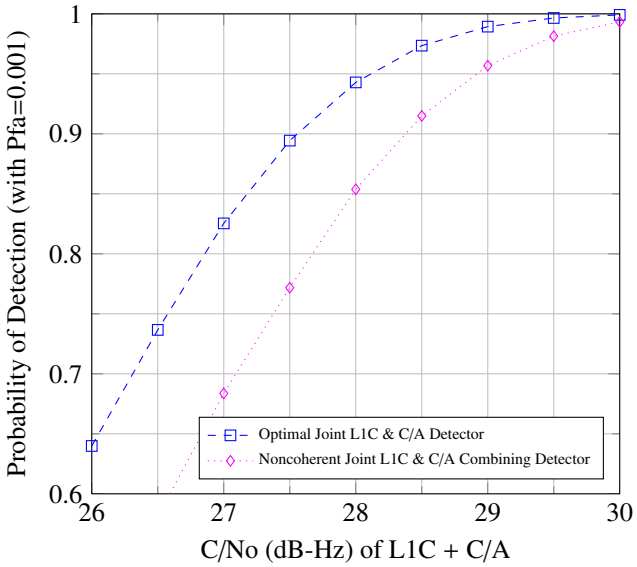

Figure F.4: Detection probability of noncoherent combining joint L1C and C/A detector for acquisition over three L1C spreading code periods referenced to the L1C and C/A composite signal power.

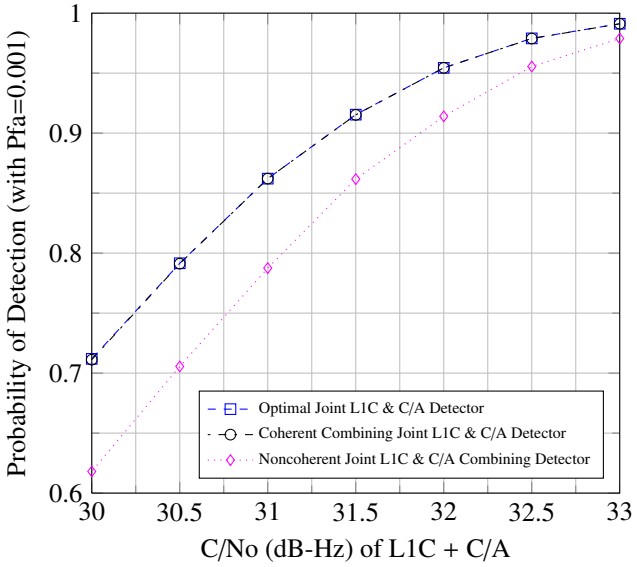

Figure F.5: Detection probability of coherent combining joint L1C and C/A detector for acquisition over one L1C spreading code period referenced to the L1C and C/A composite signal power.

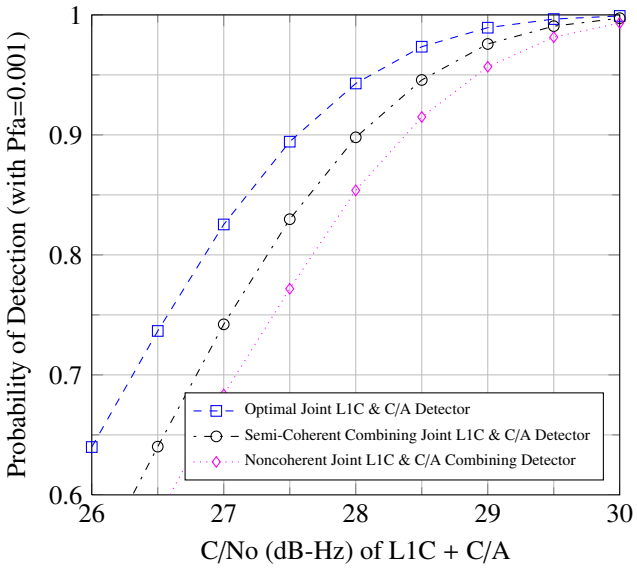

Figure F.6: Detection probability of semi-coherent joint L1C and C/A detector for acquisition over three L1C spreading code periods referenced to the L1C and C/A composite signal power.

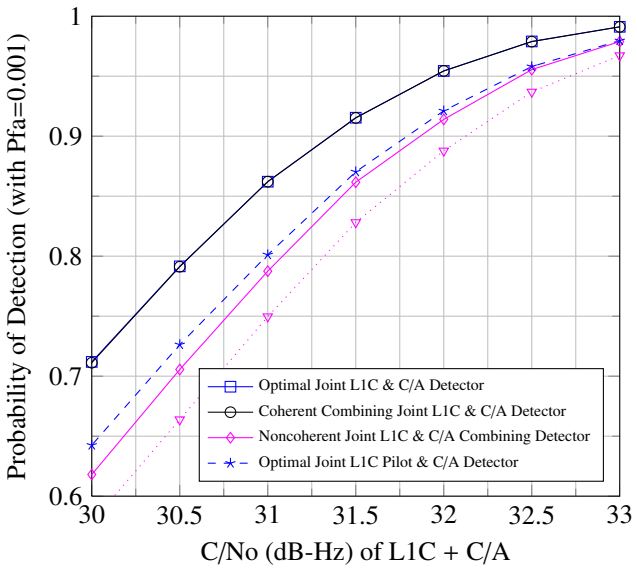

Figure F.7: Detection probability of optimal joint L1C pilot and C/A detector for acquisition over one L1C spreading code period referenced to the L1C and C/A composite signal power.

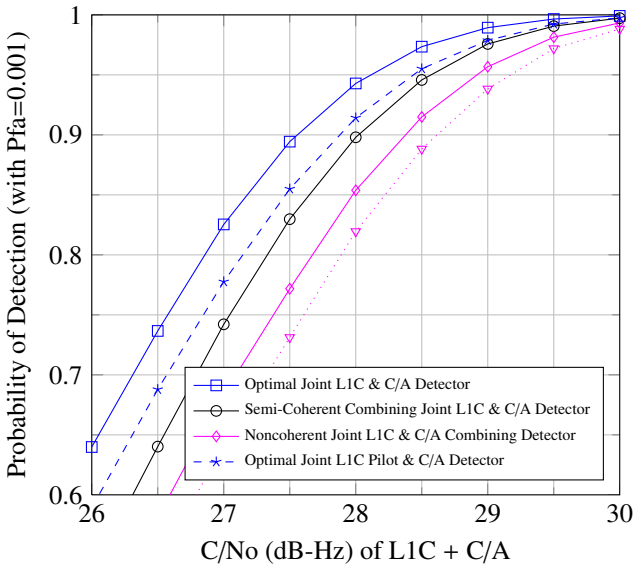

Figure F.8: Detection probability of optimal joint L1C pilot and C/A detector for acquisition over three L1C spreading code periods referenced to the L1C and C/A composite signal power.

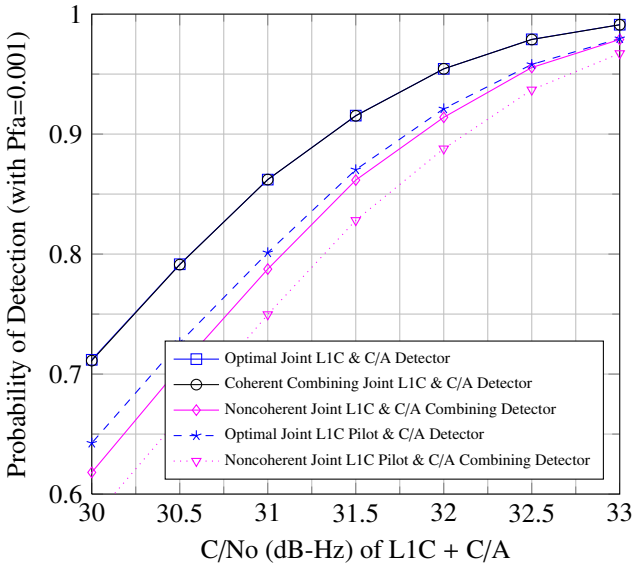

Figure F.9: Detection probability of noncoherent combining joint L1C pilot and C/A detector for acquisition over one L1C spreading code period referenced to the L1C and C/A composite signal power.

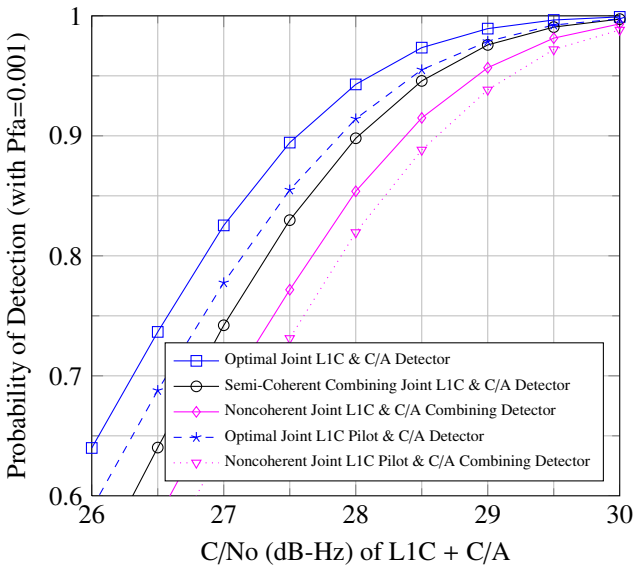

Figure F.10: Detection probability of noncoherent combining joint L1C pilot and C/A detector for acquisition over three L1C spreading code periods referenced to the L1C and C/A composite signal power.

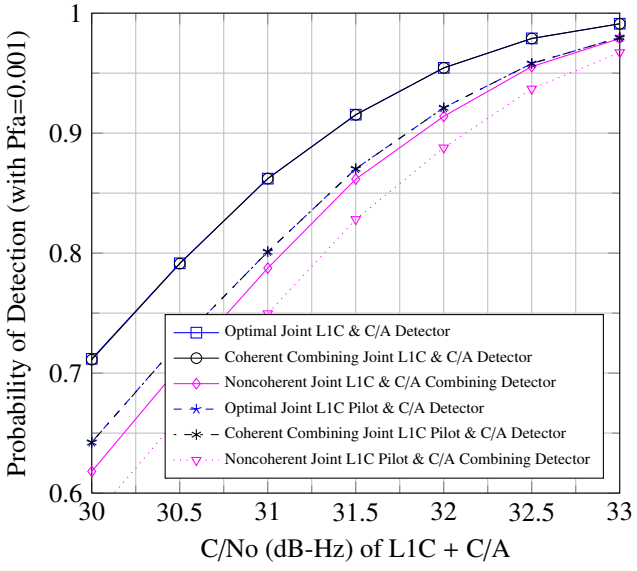

Figure F.11: Detection probability of coherent combining joint L1C pilot and C/A detector for acquisition over one L1C spreading code period referenced to the L1C and C/A composite signal power.

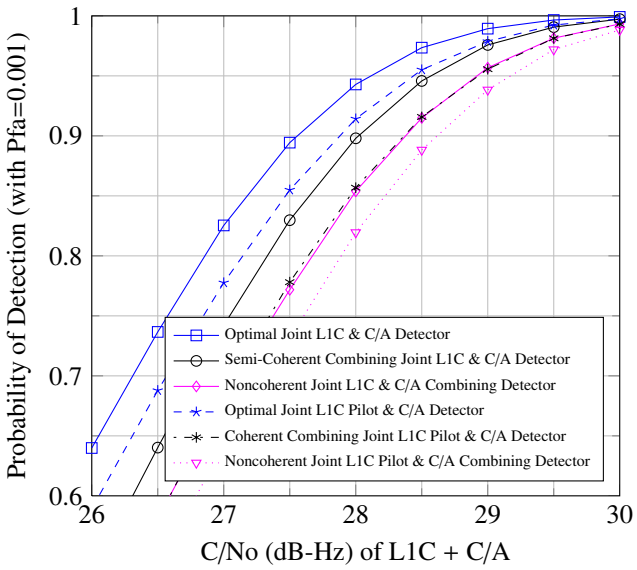

Figure F.12: Detection probability of semi-coherent combining joint L1C pilot and C/A detector for acquisition over three L1C spreading code periods referenced to the L1C and C/A composite signal power.

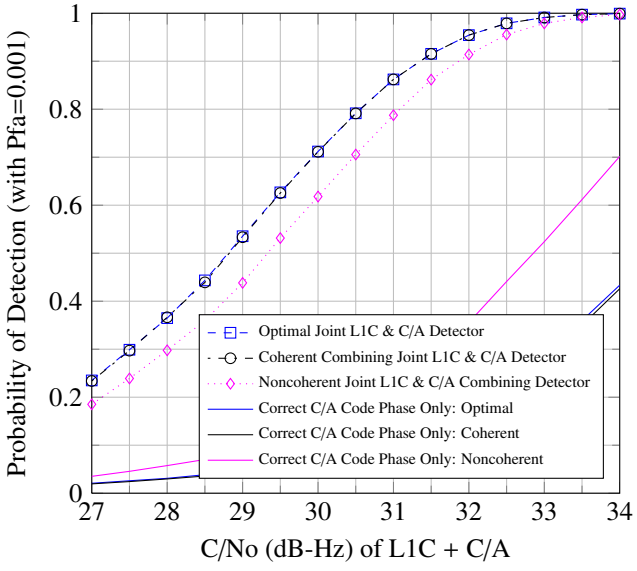

Figure F.13: Detection probability of joint L1C and C/A detectors with incorrect L1C code phase estimate but correct C/A code phase estimate for acquisition over one L1C spreading code period referenced to the L1C and C/A composite signal power.

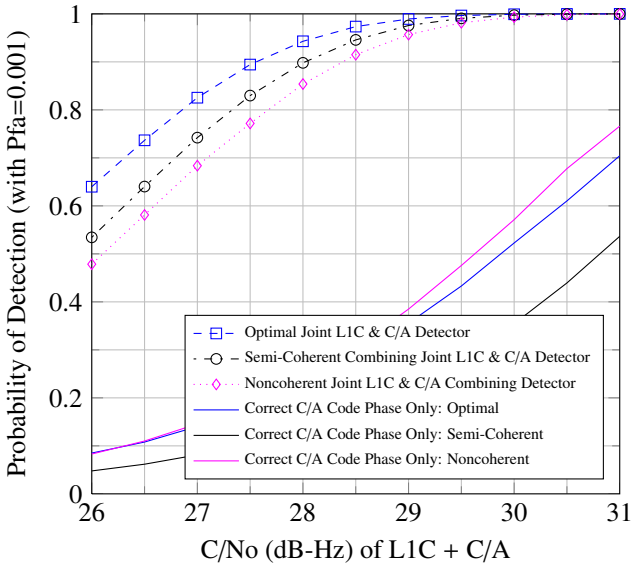

Figure F.14: Detection probability of joint L1C and C/A detectors with incorrect L1C code phase estimate but correct C/A code phase estimate for acquisition over three L1C spreading code periods referenced to the L1C and C/A composite signal power.

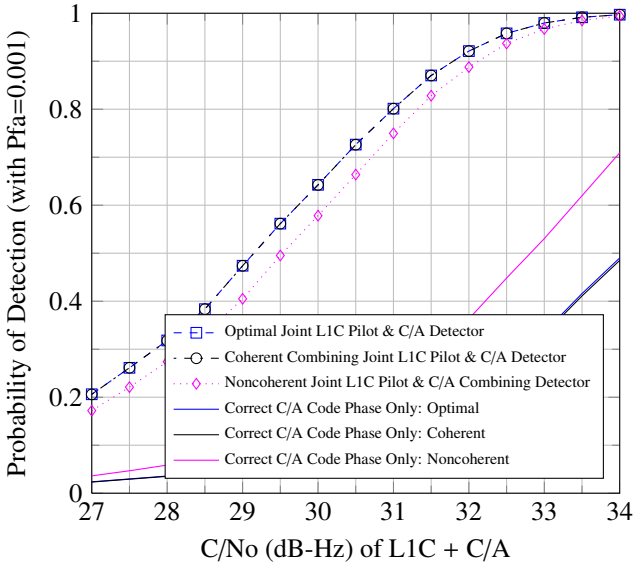

Figure F.15: Detection probability of joint L1C pilot and C/A detectors with incorrect L1C code phase estimate but correct C/A code phase estimate for acquisition over one L1C spreading code period referenced to the L1C and C/A composite signal power.

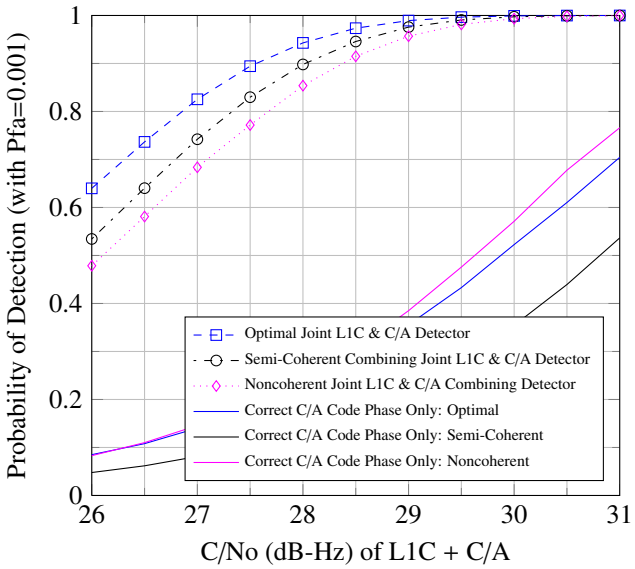

Figure F.16: Detection probability of joint L1C pilot and C/A detectors with incorrect L1C code phase estimate but correct C/A code phase estimate for acquisition over three L1C spreading code periods referenced to the L1C and C/A composite signal power.

REFERENCES

[1] N. Bowditch, *American Practical Navigator*, vol. I. Defense Mapping Agency Hydrographic/Topographic Center, 1984.

[2] R. R. Hobbs, *Marine Navigation: Piloting Celestial and Electronic Navigation*. Naval Institute Press, Annapolis, Maryland, 3rd ed., 1990.

[3] F. van Diggelen, *A-GPS: Assisted GPS, GNSS, and SBAS*. Artech House, 2009.

[4] B. W. Parkinson and J. J. Spilker, eds., *Global Positioning System: Theory and Applications*. Washington, D.C.: American Institute of Aeronautics and Astronautics, Inc., 1996.

[5] P. Misra and P. Enge, *Global Positioning System: Signals, Measurements and Performance*. Lincoln, MA: Ganga-Jamuna Press, revised second edition ed., 2011.

[6] E. D. Kaplan and C. J. Hegarty, eds., *Understanding GPS Principles and Applications*. Artech House, 2006.

[7] B. W. Parkinson, T. Stansell, R. Beard, and K. Gromov, "A history of satellite navigation," *NAVIGATION: Journal of The Institute of Navigation*, vol. 42, no. 1, 1995.

[8] Aeronautics and N. R. C. Space Engineering Board, *The Global Positioning System: A Shared National Asset*. National Academy Press, 1995.

[9] W. Cheung, T. Stansell, and R. D. Fontana, "The modernized l2 civil signal," *GPS World*, September 2001.

[10] SAIC, *Navstar GPS Space Segment / Navigation User Interfaces, IS-GPS-200E*. Science Applications International Corporation, El Segundo, CA, June 8, 2010.

[11] "Navstar gps l5 signal specification," tech. rep., RTCA SC-159, December 2000.

[12] SAIC, "Navstar gps space segment / user segment l5 interfaces, is-gps-705a," tech. rep., Science Applications International Corporation, El Segundo, CA, June 8, 2010.

[13] J. Betz, M. Blanco, C. Cahn, P. Dafesh, C. Hegarty, K. Hudnut, V. Kasemsri, R. Keegan, K. Kovach, L. Lenahan, H. Ma, J. Rushanan, J. Rushanan, D. Sklar, T. Stansell, C. Wang, and S. Yi, "Description of the l1c signal," *Proceedings of the 19th International Technical Meeting of the Satellite Division of The Institute of Navigation (ION GNSS 2006)*, pp. 2080 – 2091, September 2006.

[14] SAIC, "Navstar gps space segment / user segment l1c interface, is-gps-800a," tech. rep., Science Applications International Corporation, June 8, 2010.

[15] H. Martin, "Gps status and modernization." Ninth Meeting of the National Space-Based Positioning, Navigation, and Timing Advisory Board, November 2011.

[16] S. Butman and U. Timor, "Interplex–an efficient multichannel psk/pm telemetry system," *IEEE Transactions on Communications*, vol. 20, June 1972.

[17] J. J. S. Jr. and R. S. Orr, "Code multiplexing via majority logic for gps modernization," *Proceedings of the 11th International Technical Meeting of the Satellite Division of The Institute of Navigation*, September 1998.

[18] T. Fan, V. S. Lin, G. H. Wang, and P. A. Dafesh, "Study of signal combining methodologies for gps iii's flexible navigation payload (part ii)," *IEEE*, 2008.

[19] P. Dafesh, T. M. Nguyen, and S. Lazar, "Coherent adaptive subcarrier modulation (casm) for gps modernization," *Proceedings of ION National Technical Meeting*, January 1999.

[20] P. A. Dafesh and C. R. Cahn, "Phase-optimized constant-envelope transmission (pocet) modulation method for gnss signals," *22nd International Meeting of the Satellite Division of The Institute of Navigation*, September 2009.

[21] T. Stansell, K. Hudnut, and R. Keegan, "Gps l1c: Enhanced performance, receiver design suggestions, and key contributions," *23rd International Technical Meeting of the Satellite Division of The Institute of Navigation*, 2010.

[22] J. Langer, "Gps program update to 49th cgsic meeting." CGSIC, September 2009.

[23] J. J. Rushanan, "The spreading and overlay codes for the l1c signal," *NAVIGATION: Journal of The Institute of Navigation*, vol. 54, no. 1, pp. 43 – 51, 2007.

[24] J. W. Betz, "Binary offset carrier modulations for radionavigation," *Navigation: Journal of the Institute of Navigation*, vol. 48, pp. 227–246, March 2002.

[25] J. W. Betz, "On the power spectral density of gnss signals, with applications," *ION 2010 International Technical Meeting*, 2010.

[26] J. W. Betz, "Course 551: Advanced gnss receiver processing." NavtechGPS Short Course, March 2012.

[27] J. G. Proakis, *Digital Communications*. McGraw Hill, 2001.

[28] P. M. Fishman and J. W. Betz, "Predicting performance of direct acquisition for the m-code signal," *ION NTM 2000*, January 2000.

[29] F. Bastide, O. Julien, C. Macabiau, and B. Roturier, "Analysis of l5/e5 acquisition, tracking and data demodulation thresholds," *ION GPS 2002*, September 2002.

[30] C. Hegarty, M. Tran, and A. J. V. Dierendonck, "Acquisition algorithms for the gps l5 signal," *ION GPS/GNSS 2003*, September 2003.

[31] D. Borio, C. O'Driscoll, and G. Lachapelle, "Coherent, noncoherent, and differentially coherent combining techniques for acquisition of new composite gnss signals," *Aerospace and Electronic Systems, IEEE Transactions on*, vol. 45, pp. 1227 –1240, july 2009.

[32] A. J. V. Dierendonck and J. J. J. Spilker, "Proposed civil gps signal at 1176.45 mhz: In-phase/quadrature codes at 10.23 mhz chip rate," *ION 55th Annual Meeting*, June 1999.

[33] C. J. Hegarty, "Optimal and near-optimal detectors for acquisition of the gps l5 signal," *ION National Technical Meeting 2006*, January 2006.

[34] C. Yang, C. Hegarty, and M. Tran, "Acquisition of the gps l5 signal using coherent combining of i5 and q5," *ION GNSS 17th International Technical Meeting of the Satellite Division*, September 2004.

[35] P. G. Mattos, "Acquisition of the galileo oas l1b/c signal for the mass-market receiver," *ION GNSS 18th International Technical Meeting of the Satellite Division*, 2005.

[36] P. G. Mattos, "Galileo l1c - acquisition complexity: Cross correlation benefits, sensitivity discussions on the choice of pure pilot, seconday code, or something different," *IEEE*, 2006.

[37] D. Borio, C. O'Driscoll, and G. Lachapelle, "Composite gnss signal acquisition over multiple code periods," *Aerospace and Electronic Systems, IEEE Transactions on*, vol. 46, pp. 193 –206, jan. 2010.

[38] K. C. Seals, W. R. Michalson, P. F. Swaszek, and R. J. Hartnett, "Analysis of L1C acquisition by combining pilot and data components over multiple code periods," *ION International Technical Meeting 2013*, January 2013.

[39] M. H. Zarrabizadeh and E. S. Sousa, "A differentially coherent pn code acquisition receiver for cdma systems," *IEEE Transactions on Communications*, vol. 45, pp. 1456–1465, November 1997.

[40] J. A. A. Rodriguez, T. Pany, and B. Eissfeller, "A theoretical analysis of acquisition algorithms for indoor positioning," *Proceedings of the 2nd ESA Workshop on Satellite Navigation User Equipment Technologies*, December 2004.

[41] A. Schmid and A. Neubauer, "Performance evaluation of differential correlation for single shot measurement positioning," *ION GNSS 17th International Technical Meeting of the Satellite Division*, September 2004.

[42] H. Elders-Boll and U. Dettmar, "Efficient differentially coherent code/doppler acquisition of weak gps signals," *ISSSTA 2004 Sydney, Austrailia*, September 2004.

[43] C. O'Driscoll, *Performance Analysis of the Parallel Acquisition of Weak GPS Signals*. PhD thesis, National University of Ireland, 2007.

[44] F. Macchi, *Development and Testing of an L1 Combined GPS-Galileo Software Receiver*. PhD thesis, University of Calgary, 2010.

[45] F. Macchi-Gernot, M. G. Petovello, and G. Lachapelle, "Combined acquisition and tracking methods for gps l1 c/a and l1c signals," *International Journal of Navigation and Observation*, 2010.

[46] H. L. V. Trees, *Detection, Estimation, and Modulation Theory Part I*. Wiley, 1968.

[47] M. K. Simon, *Probability Distributions Involving Gaussian Random Variables*. Springer, 2002.

[48] K. C. Seals, W. R. Michalson, P. F. Swaszek, and R. J. Hartnett, "Analysis of coherent combining for gps l1c acquisition," *ION GNSS 2012*, September 2012.